EFFECT OF TUBE PASS RATIOS AND FLOW PASS CONFIGURATIONS ON THE THERMAL AND HYDRAULIC PERFORMANCE OF THE ALUMINIUM MINI-CHANNEL HEAT EXCHANGER

by

THOO KOK KEONG

A Thesis

Submitted to the Postgraduate Studies Programme

as a Requirement for the Degree of

MASTER OF SCIENCE

MECHANICAL ENGINEERING DEPARTMENT

UNIVERSITI TEKNOLOGI PETRONAS

BANDAR SERI ISKANDAR,

PERAK

NOVEMBER 2013

STATUS OF THESIS

Title of thesis	**Effect of Tube Pass Ratios and Flow Pass Configurations on the Thermal and Hydraulic Performance of the Aluminium Mini-Channel Heat Exchanger**

I **THOO KOK KEONG**

hereby allow my thesis to be placed at the Information Resource Center (IRC) of Universiti Teknologi PETRONAS (UTP) with the following conditions:

1. The thesis becomes the property of UTP

2. The IRC of UTP may make copies of the thesis for academic purposes only.

3. This thesis is classified as

[√] Confidential

[ ] Non-confidential

If this thesis is confidential, please state the reason:

The work is fully sponsored by and carried out in OYL Research & Development Centre Sdn. Bhd. where the student is a full time employee. The outcome of this work is deemed confidential as the methodology can be used for the design of mini-channel heat exchanger as condenser in the air-conditioner. This gives OYL an advantage over her competitors in coming out with competitive air conditioners in the HVAC market.

The contents of the thesis will remain confidential for 5 years.

Remarks on disclosure:
N/A

Endorsed by

M. R. Heikal

Signature of Author

Signature of Supervisor

Permanent address: No. 11, Jalan Permaisuri 21/6, Seksyen 6, Bandar Mahkota Cheras, 43200 Batu 9, Cheras, Selangor.

Name of Supervisor
Prof. Dr. Morgan R.Heikal

Date : 29/11/13

Date : 29/11/13

UNIVERSITI TEKNOLOGI PETRONAS

EFFECT OF TUBE PASS RATIOS AND FLOW PASS CONFIGURATIONS ON THE THERMAL AND HYDRAULIC PERFORMANCE OF THE ALUMINIUM MINI-CHANNEL HEAT EXCHANGER

by

THOO KOK KEONG

The undersigned certify that they have read, and recommend to the Postgraduate Studies Programme for acceptance this thesis for the fulfillment of the requirements for the degree stated.

M. R. Heikal

Signature:	
Main Supervisor:	Prof. Dr. Morgan R. Heikal
Signature:	
Co-Supervisor:	
Signature:	
Head of Department:	Ir. Dr. Masri Baharom
Date:	

EFFECT OF TUBE PASS RATIOS AND FLOW PASS CONFIGURATIONS ON THE THERMAL AND HYDRAULIC PERFORMANCE OF THE ALUMINIUM MINI-CHANNEL HEAT EXCHANGER

by

THOO KOK KEONG

A Thesis

Submitted to the Postgraduate Studies Programme

as a Requirement for the Degree of

MASTER OF SCIENCE

MECHANICAL ENGINEERING DEPARTMENT

UNIVERSITI TEKNOLOGI PETRONAS

BANDAR SERI ISKANDAR,

PERAK

NOVEMBER 2013

DECLARATION OF THESIS

Title of thesis	**Effect of Tube Pass Ratios and Flow Pass Configurations on the Thermal and Hydraulic Performance of the Aluminium Mini-Channel Heat Exchanger**

I **THOO KOK KEONG**

hereby declare that the thesis is based on my original work except for quotations and citations which have been duly acknowledged. I also declare that it has not been previously or concurrently submitted for any other degree at UTP or other institutions.

Witnessed by

M. R. Heikal

Signature of Author

Signature of Supervisor

Permanent address: No. 11, Jalan Permaisuri 21/6, Seksyen 6, Bandar Mahkota Cheras, 43200 Batu 9, Cheras, Selangor.

Name of Supervisor
Prof. Dr. Morgan R.Heikal

Date : 29/11/13

Date : 29/11/13

DEDICATION

To my dear wife Mei Sun who had been so understanding and patient with me while I spent long hours in both the research work and in the completion of this thesis. Throughout this time she has been my constant support and source of encouragement.

To my mother, sisters and auntie who had given me moral support all this while. To auntie Poh Kim who had shown much concern and support.

ACKNOWLEDGEMENTS

Firstly I would like to thank Mr Yeow Tee Siong the Operation Manager of OYL Research & Development Centre Sdn. Bhd. who has approved this project and also the use of OYL laboratories for all the experiment. The outcome of this research work will be useful to OYL design engineers in the selection of mini-channel heat exchangers as condensers.

I also would like to extend my gratitude to my field supervisor Dr. Chin Wai Meng and technical advisor Professor Dr. Vijay R. Raghavan for their relentless effort and invaluable inputs in guiding me throughout the entire research work. Others I wished to thank are Mohd Fadzil bin Ismail, Mohd Fadzli bin Zakaria, Muhammad Raimhy Bin Mohd Razali and Mohamad Fadhullah Bin Mohd Nor who have helped me in the set-up of the experiment.

Last but not least, I would like to thank my supervisor Professor Dr. Morgan R. Heikal who has been patient in guiding me and for his invaluable advice which helped tremendously in the progress and completion of this work.

ABSTRACT

Aluminium mini-channel heat exchanger or in short MCHX is gaining much popularity in the field of HVAC&R. MCHX is a suitable choice to replace conventional fin-tube condensers due to its high heat transfer area per unit volume, light weight and resistance to galvanic corrosion. Due to the high energy consumption of air conditioners, it has become almost mandatory for design engineers to come out with energy efficient equipment. In view of this, a research work has been carried out to determine the effect of different flow pass configurations and tube pass ratios to the thermal and hydraulic performance of MCHX and to come out with an optimum MCHX design. A numerical simulation using known correlations for condensing coefficient and pressure drop on the refrigerant side was carried out. A baseline MCHX configuration with equal number of tubes in each pass was used as comparison to other MCHX with the same flow passes but different tube pass ratios. In the simulation, it was discovered that refrigerant mass flux and the number of tubes in the flow pass are factors that could affect the thermal and hydraulic performance of the MCHX. In order to determine the optimum MCHX design, a ratio of thermal performance over pumping power of the MCHX, $Q_t/dP.V_r$ was calculated. The MCHX with the highest $Q_t/dP.V_r$ is the optimum MCHX design. The simulation was compared to experiment and good accuracies were found. Compared to experiment, the analysis over-predicts the thermal performance by about 1% and under-predicts the hydraulic performance by < 7%.

ABSTRAK

Alat pemindah haba yang dibuat daripada tiub aluminium yang leper atau "MCHX" semakin mendapat perhatian di dalam bidang HVAC&R. "MCHX" merupakan pengganti yang sesuai untuk alat pemindah haba yang lazim kerana ia mempunyai nisbah luas permukaan kepada isipadu yang tinggi untuk pemindahan haba, ringan dan tahan kakisan galvani. Oleh kerana alat pendingin hawa menggunakan banyak tenaga elektrik, jurutera reka bentuk mesti mengeluarkan ciptaan yang berkesan dari segi penggunaan tenaga electrik. Justeru itu, kerja penyelidikan telah dijalankan untuk mengetahui kesan pas aliran dan nisbah bilangan tiub pas-pas terhadap prestasi terma dan hidraulik MCHX dan untuk mencari reka cipta MCHX yang optimum. Simulasi berangka yang menggunakan korelasi-kolerasi yang umum untuk pemeluapan pekali dan kejatuhan tekanan untuk bahan penyejuk telah dilakukan. MCHX dengan bilangan tiub yang sama di dalam setiap aliran digunakan sebagai rujukan untuk dibandingkan dengan MCHX yand lain yang mempunyai bilangan pas aliran yang sama tetapi berbeza dari segi nisbah bilngan tiub pas-pas. Simulasi berangka menunjukkan fluks jisim bahan penyejuk dan bilangan tiub di dalam pas merupakan factor yang mepengaruhi prestasi terma dan hidraulik MCHX. Untuk menentukan MCHX yang optimum, nisbah prestasi haba kepada kuasa pam MCHX, $Q_t/dP.V_r$ dikira. MCHX dengan $Q_t/dP.V_r$ yang paling tinggi merupakan MCHX dengan reka cipta yang optimum. Keputusan simulasi ini dekat dengan keputusan ujikaji di mana dari segi prestasi haba simulasi tinggi lhampir 1% manakala dari segi prestasi hidraulik simulasi rendah < daripada 7% berbanding dengan ujikaji.

TABLE OF CONTENTS

LIST OF FIGURES

LIST OF TABLES

LIST OF SYMBOLS

The following list gives the meaning of symbols used in this thesis, unless otherwise defined in the text and appendices:

A_{ba}	Air-side flow area blocked by fins [m^2]
A_c	Total core face area [m^2]
A_{da}	Air-side direct heat transfer area [m^2]
A_{effa}	Air-side effective heat transfer area [m^2]
A_{fa}	Total air-side free flow area [m^2]
A_{ida}	Air-side indirect heat transfer area [m^2]
A_{bt}	Air-side flow area blocked by webs [m^2]
A_t	Total tube side cross section area [m^2]
A_{dt}	Tube-side direct heat transfer area [m^2]
A_{efft}	Tube-side effective heat transfer area [m^2]
A_{ft}	Total refrigerant free flow area [m^2]
A_{idt}	Tube-side indirect heat transfer area [m^2]
A_{sh}	Area for desuperheated process [m^2]
A_{tp}	Area for condensing process [m^2]
A_{sc}	Area for subcooling process [m^2]
A_m	Mean tube wall heat transfer area [m^2]
C	Heat capacity rate [W/K]
C_{ratio}	Heat capacity ratio [-]
C_p	Specific heat at constant pressure [Jkg^{-1}K^{-1}]
C_d	Coefficient of discharge [-]
CFM	Air flow measured in cubit feet per minute [-]
dP	Differential pressure [mmAq]
dh	Difference in enthalpy [kJ/kg]
d_n	Nozzle diameter [m]
$d_{h,a}$	Air-side hydraulic diameter [m]

$d_{h,t}$	Tube-side hydraulic diameter [m]
dT	Difference in temperature [°C]
F	Fin [-]
f	Friction factor [-]
F_h	Fin height [mm]
F_l	Fin length [mm]
F_p	Fin pitch [mm]
F_{thk}	Fin thickness [mm]
Fr	Froude number [-]
G	Mass flux [kg/m^2.s]
g	Function, or acceleration due to gravity [ms^{-2}]
h_i	Refrigerant-side heat transfer coefficient [W/m^2.K]
$h_{i,avg}$	Average refrigerant h/t coefficient (condensing) [W/m^2.K]
h_o	Air-side heat transfer coefficient [W/m^2.K]
h_f	Enthalpy of saturated fluid [kJ/kg]
h_g	Enthalpy of saturated vapor [kJ/kg]
j	Colburn j-factor [-]
k	Thermal conductivity [W/m.K]
k_a	Thermal conductivity of air [W/m.K]
k_t	Thermal conductivity of aluminium tube [W/m.K]
L_t	Total length of tube [m]
L_L	Louver length [mm]
L_H	Louver height [mm]
L_p	Louver pitch [mm]
L_{seg}	Segment length [m]
L_{sh}	Tube length for desuperheating process [m]
L_{sc}	Tube length for subcooling process [m]

L_{cond}	Tube length for condensing process [m]
$LMTD$	Log-mean temperature difference [^{o}C]
m_a	Air mass flow rate [kg/s]
m_r	Refrigerant mass flow rate [kg/s]
NTU	Number of heat transfer units [-]
Nu	Nusselt number [-]
N_t	Number of tubes [-]
N_w	Number of webs [-]
N_l	Number of tube at 1st pass [-]
N_p	Number of portion (for condensing) [-]
P	Pressure [Pa]
P_{ratio}	Pressure ratio [-]
per_a	Air-side perimeter [m]
per_t	Refrigerant side wetted perimeter [m]
Pr	Prandtl number [-]
Q_{total}	Total heat transfer rate of PFC [W]
Q_{sh}	Heat transfer rate of superheat region [W]
Q_{cond}	Heat transfer rate of condensing region [W]
Q_{sc}	Heat transfer rate of subcool region [W]
$R_{w'}$	Thermal resistance of the wall [m^2.K/W]
Re	Reynolds number [-]
Re_{cri}	Critical Reynolds number [-]
Re_L	Reynolds number based on louver pitch [-]
SpV	Specific volume [m^3/kg]
$T_{a,i}$	Air inlet temperature [°C]
$T_{a,o}$	Air outlet temperature [°C]
T_s	Tube surface temperature [°C]
T_{wo}	Water out temperature [°C]
T_{wi}	Water inlet temperature [°C]
T_{ao}	Air outlet temperature [°C]
T_{ai}	Air inlet temperature [°C]

t_{ih} Tube inner height [mm]

t_{thk} Tube wall thickness [mm]

t_{oh} Tube outer height [mm]

t_p Tube pitch [mm]

t_{iw} Tube inner width [mm]

t_{ow} Tube outer width [mm]

$t_{w'}$ Tube wall thickness [mm]

U Overall heat transfer coefficient [W/m^2.K]

V_{max} Maximum air velocity [m/s]

V_r Refrigerant volumetric flow rate [m^3/hr]

V_{ratio} Velocity ratio [-]

W Absolute Humidity [kg/kg]

We Weber number [-]

w_t Web thickness [mm]

w_{sp} Web spacing [mm]

X_{tt} Martinelli parameter

x Quality [-]

Greek Symbols

α_L Louver angle

α Aspect ratio of mini-channel tube

η_f Fin efficiency

ε Efficiency of heat exchanger

@ At temperature

β The fall-off rate of air flow angle

$\eta_{f,a}$ Air side fin efficiency

μ Kinematic viscosity

ρ Density

ΔL_c Length of 1 step for condensing

Subscripts

a	Air
t	Tube
cf	crossflow
F	Fanning
avg	average
dec	deceleration
fric	friction
sat	Saturated
cond	Condenser
in	Inlet
out	Outlet
liq	Liquid
eff	Effective
sh	Superheat
sc	Subcool
max	Maximum
min	Minimum
cal	Calculated
ΔL	1 step for condensing
vap	vapour
lo	liquid only
go	gas only
t	total
TP	Two phase
w	water

CHAPTER 1

INTRODUCTION

1.1 Chapter overview

A general description of mini-channel heat exchanger (MCHX) is given in this chapter. The effects of different tube pass ratios and flow pass configurations on the thermal and hydraulic performance of the MCHX are also briefly described. The objective of this study is to ultimately obtain an optimum design of the MCHX as condenser in air conditioning systems.

1.2 Description of mini-channel heat exchanger

Mini-channel heat exchangers are made of aluminium and commonly used in automotive industries as heat transfer elements to transport energy from a heat source or to a heat sink. In recent years, due to the high price of copper, mini-channel heat exchangers are gaining popularity as heat exchangers in air-conditioning to replace the conventional copper-aluminium construction. MCHXs are made from extruded aluminium tubes brazed to aluminium louvered fins in a temperature controlled environment such as the Nocolok oven. The tubes are brazed at both ends to aluminium manifolds or headers. The entire construction is from aluminium. Figure 1.1 shows an overview of the mini-channel heat exchanger.

Air is drawn in by a blower and passes through the matrix of the fins and tubes of the MCHX while the refrigerant passes through the tubes. The advantages of MCHX are high specific surface area (m^2/m^3), i.e., heat transfer area per unit volume, light weight and resistance to galvanic corrosion.

The mini-channel flow as shown in Fig. 1.1 is divided into 2 passes. It can also be further subdivided into 3, 4 etc. Each pass is made up of a number of tubes. The tube pass ratio is the number of tubes in each pass divided by the total number of tubes in the mini-channel heat exchanger. Figure 1.2 shows an example of a 2 flow pass heat exchanger with different tube pass ratios while Figure 1.3 shows heat exchangers with 2, 3 and 4 flow passes used in this research work.

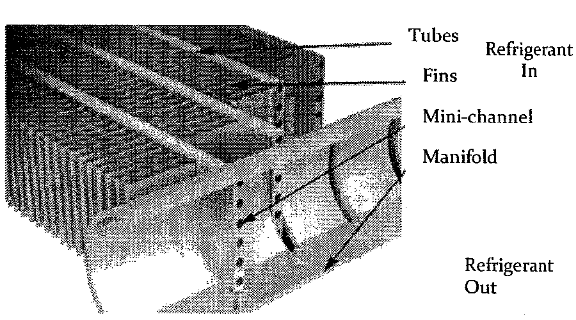

Picture of MCHX Inner Structure

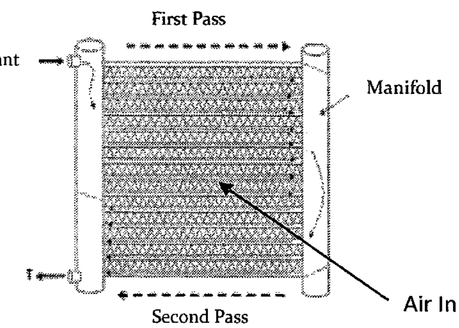

Picture of MCHX showing refrigerant and air flow direction

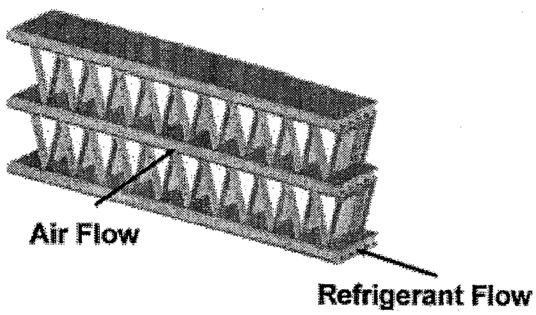

The tubes are flattened and the fins are welded to the flattened tubes so that contact resistance can be completely eliminated.

Fig. 1.1: Overview of a Mini-Channel Heat Exchanger

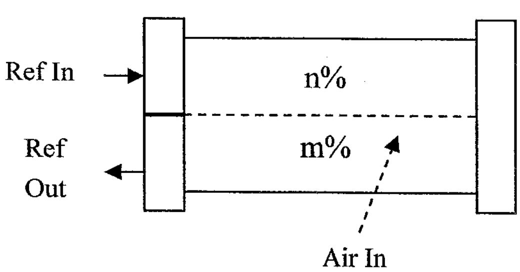

n%	m%
95	5
90	10
85	15
80	20
70	30
60	40
50	50

Fig. 1.2: Example of Tube Pass Ratio in a Mini-Channel Heat Exchanger

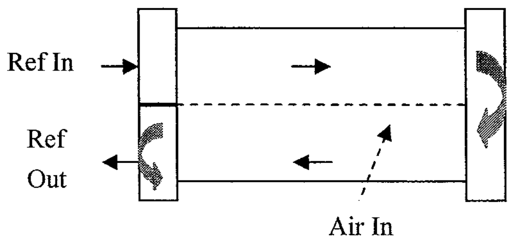

2-Pass Flow Configuration

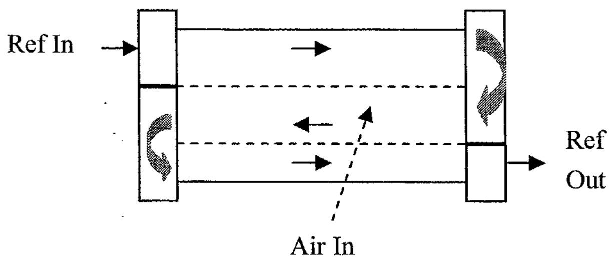

3-Pass Flow Configuration

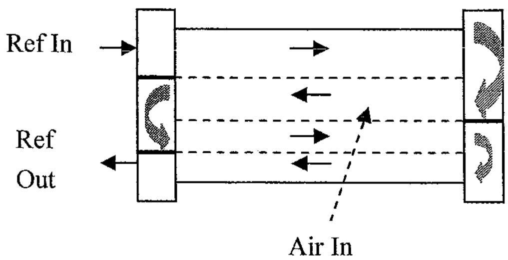

4-Pass Flow Configuration

Fig. 1.3: Different number of Flow Passes

1.3 Problem Statement

In the MCHX condenser, refrigerant vapor enters at a quality of 1.0 and exits after complete condensation. Due to the difference in densities between the vapor and the liquid, velocities at the entrance to MCHX are high and the exit velocities are low. High velocities contribute to a high pressure drop while low velocities contribute to poor heat transfer coefficients. Often the vapor enters in superheated condition and is required to leave in a sub-cooled state, which makes the situation more severe. A good compromise requires that the number of flow passes and the number of tubes per pass be so chosen as to get an optimum thermal and hydraulic performance. This is the focus of the study.

1.4 Justification for the research

A study [1] has shown that Malaysia consumed approximately 89 billion kWh of electrical energy in 2008, where well over one-third was used in commercial buildings [2]. Perez-Lombard et al. [3] have shown that approximately 40 to 50% of the energy used in buildings is due to the installed refrigeration and HVAC systems which employ fin-tube heat exchangers extensively. If the cost of electricity is taken as RM0.27 per kWh, and if the energy consumption of these HVAC&R systems could be reduced by just 1%, energy cost reduction of at least RM32 million per annum could be realized. Such a saving would be significant in view of the current global energy crisis which is seeing a potential reduction of world crude oil production [4]. Dwindling resources have also caused escalation of crude oil prices which had reached a record high of US$146 per barrel in July 2008 [5].

It is because of the realization that HVAC&R systems are among the main consumers of energy that many countries have implemented regulatory controls to ensure that this type of equipment operates at high energy efficiency levels. For example, the European Union has implemented an Energy Labeling programme for air-conditioning equipment with cooling capacity less than 12 kW, following the EU Council directive 92/75/EEC [6]. Similar programmes are also in place in Australia and New Zealand (Regulation AS/NZS 3823.2) [7], Hong Kong (Energy Labeling Ordinance 2009) [8] and Singapore (Mandatory Energy Labeling Scheme 2008) [9]. Closer to home, Malaysia has recently implemented a similar voluntary energy labeling in 2009 for air-conditioning products with cooling capacity up to 7.32 kW (25,000 Btu/hr) [10]. Consumers are continuously being educated and encouraged to purchase equipment which has the highest energy efficiency.

As a result of the demand for high energy efficiency, various design strategies have been used to increase the heat transfer performance while reducing the electrical power input of HVAC&R equipment. Some examples of these include using high efficiency compressors, improving the heat transfer characteristics of the heat exchanger and implementing frequency-inverter control systems. Another approach to reduce high energy consumption is to use mini-channel heat exchangers to replace conventional fin-tube heat exchangers. In order to use mini-channel heat exchanger as HVAC&R equipment, their design must be optimized in terms of tube pass ratio and flow pass configuration to yield optimum thermal and hydraulic performance.

1.5 Objectives of research

The objectives of this work are twofold. Firstly, it is to investigate the effect of tube pass ratio and flow pass configuration on the thermal and hydraulic performance of mini-channel heat exchangers. Secondly, an optimum mini-channel heat exchanger in terms of tube pass ratio and flow pass configuration is proposed for design work.

1.6 Scope of research

The research conducted in this work has investigated the effect of tube pass ratio and flow pass configuration on the thermal and hydraulic performance of the mini-channel heat exchangers. The tube pass ratio and flow pass configuration are summarized in Table 1.1.

Table 1.1: Mini-channel Heat Exchangers used in this Research

No. of Flow Passes	Tube Pass Ratio
2	95-5, 90-10, 85-15, 80-20, 75-25, 70-30, 60-40, **50-50**
3	70-20-10, 60-30-10, 55-30-15, 50-30-20, 40-30-20, **33-33-33**
4	40-30-20-10, 45-25-18-12, **25-25-25-25**

For each flow pass, the mini-channel heat exchanger with equal number of tubes in each pass, shown in bold, was used as a base case for comparison with other heat exchangers having the same flow pass but with different tube pass ratio. In varying the tube pass ratio, the thermal performance changed due to the change in available tubes for heat transfer in each flow pass while the hydraulic performance changed due to the change in mass flux. In order to find the optimum heat exchanger design, a balance-point between the thermal and hydraulic performances was sought. For each heat exchanger, a ratio of the thermal performance over the hydraulic performance, $Q_t/dP.V_r$ was calculated. The heat exchanger with the highest $Q_t/dP.V_r$ is recommended as the optimum heat exchanger design.

1.7 Thesis outline

The presentation of the thesis has been divided into a number of chapters. After the present introductory Chapter 1, the literature in the area of mini-channel is reviewed in Chapter 2. A detailed numerical analysis in terms of thermal and hydraulic performance of each heat exchanger mentioned in Table 1.1 is reported in Chapter 3. Chapter 4 describes the experimental work carried out to determine the air side heat transfer coefficient of the mini-channel heat exchanger and the thermal and hydraulic performance of one type of mini-channel heat exchanger. Chapter 5 shows the results of the numerical analysis and gives a detail discussion on the results. The conclusions of the work are given in Chapter 6.

1.8 Chapter summary

A general description of the mini-channel heat exchanger has been given in this chapter together with its advantages when used as HVAC&R equipment. This research work is carried out to ensure the mini-channel heat exchanger design is optimized in terms of tube pass ratio and flow pass configuration. In this way, an optimum heat exchanger design could be arrived at, to help reduce energy consumption.

CHAPTER 2

LITERATURE REVIEW

2.1 Chapter overview

This chapter documents the findings of the literature review on various design considerations for heat exchangers that cause degradation of their performance, with focus given to mini-channel heat exchangers. The outcome of this survey showed that the proposed work has not been carried out earlier by any researcher. The Wilson Plot method used in one of the experiments is also discussed here.

2.2 Review findings

2.2.1 Study on Mini-Channel

In the past fifteen years, mini-channels have gained much application in various fields such as in the electronic cooling, automotive and air conditioning industries. In fact, the art of the utilization of mini-channels is much farther ahead than the science of obtaining a comprehensive understanding of them.

Due to the many potential enhancements of mini-channel and its wide application, many research efforts have been carried out. These research studies focus on single mini-channel tubes, mini-channel evaporators and condensers.

Webb and Ermis [11] studied condensation of refrigerant R134a in extruded aluminium tubes with multiple parallel micro-channels with and without fins. They found that the heat transfer coefficients and pressure gradients increase with decreasing hydraulic diameter.

Webb and Lee [12] studied the use of micro-channel condensers as replacements for 2-row, round-tube with 7 mm diameter tubes conventional air conditioning heat exchangers. They discovered that up to 55% material cost reductions over the conventional heat exchanger was possible due to a combination of air side and tube side improvements in mini-channel heat exchangers.

Jiang and Garimella [13] compared micro-channel tube with conventional round tube systems using refrigerant R22. They discovered that the volume of the micro-channel heat exchangers can be reduced by at least one third of the volume of the conventional round tube. Refrigerant charge in the micro-channel system also reduced at least 20% compared to the conventional round tube system.

In another study, Kim and Bullard [14] compared the performance of the micro-channel condenser with a finned-tube condenser for a window room air conditioner using refrigerant R22. They found that the heat transfer rates per unit volume are higher for micro-channel condensers compared to the conventional finned round-tube condensers. The refrigerant charge, condenser volume and mass also reduced for the micro-channel condenser compared to the conventional finned round-tube condenser.

Dang et al. [15] studied experimentally the effects of gravity on the behaviour of heat transfer and pressure drop of a micro-channel heat exchanger. The results showed that the influence of gravity on this behaviour is negligibly small.

Kandlikar et al. [16] stated that the pressure drop penalty needs to be carefully evaluated when selecting the channel size. The pressure gradient (pressure drop per unit length) increases drastically with channel size reduction [17] and therefore mini-channel heat exchangers need to be suitably designed to provide short flow lengths to limit the overall pressure drop.

Cavallini et al. [18] studied condensation heat transfer and pressure drop in a horizontal smooth tube using a new HFC refrigerant. The effects of vapour quality, mass velocity, saturation temperature, driving temperature difference and reduced pressure were also discussed. It was discovered that low-pressure and mid-pressure refrigerants such as R22 perform better than high pressure refrigerants such as R410A while on the other hand, at the same mass velocity and vapor quality low pressure fluids such as R22 show a higher pressure drop penalty than R410A.

Del Col et al. [19] studied the effect of the cross sectional shape on the condensation behaviour in a single square mini-channel and compared it to the circular mini-channel. It was discovered that at lower mass fluxes the square channel yielded higher heat transfer coefficients than that of a circular channel. This was thought to be due to the effect of surface tension pulling the liquid towards the corners and reducing the average thermal resistance.

Kandlikar and Schmitt [20] studied the effect of surface roughness on the pressure drop in single phase flow in a mini-channel pipe and found that the average relative roughness value ε / D_h was greater than the threshold value of 0.05 used in the Moody diagram. They introduced three surface characterization parameters together with equivalent roughness and constricted hydraulic diameter. Brackbill and Kandlikar [21] proved that using these parameters, the relationship between the critical Reynolds value and $\varepsilon / D_{h,\,cf}$ agree theoretically and experimentally.

Using known correlations and computer software, Subramaniam and Garimella [22] studied the parameters that influence the performance of R410A micro-channel condensers and suggested an optimum condenser design from a baseline design.

2.2.2 Condensation in Mini-Channel

Yang and Webb [23] studied heat transfer in single and two phase flow of refrigerant R12 in rectangular plain and microfin tubes with d_h = 2.64 and 1.56 mm, respectively, using modified Wilson plot technique. The measurements were conducted at mass fluxes between 400 to 1400 kg/m^2.s. They found that the heat transfer coefficients for the microfinned tube showed steeper slopes than those for plain tubes when plotted against quality. The heat transfer coefficients also showed a heat flux dependence ($h \alpha q^{0.2}$). Their results also showed that the heat transfer enhancement due to microfins decreased when mass flux increased.

Yang and Webb [24] also developed a heat transfer model for condensation of refrigerant R12 and R134a in extruded micro-channels with d_h = 1.41 and 1.56 mm and with microfins 0.2 and 0.3 mm deep. They found that the surface tension contribution to heat transfer coefficient could equal or exceed the vapor shear term at low mass flux of 400 kg/m^2.s and $x > 0.5$ while at high mass flux of say 1400 kg/m^2.s the surface tension contribution was very small. They also found that a small fin tip radius enhanced the heat transfer and a large inter-fin drainage area allowed the surface tension effect to be activated at lower qualities.

Kim et al.[25] conducted a similar study to that of Yang and Webb [24] on similar tube with d_h = 1.41 mm but with 1.56 mm microfin (with 39% greater surface area than the smooth tube) and using refrigerant R22 and R410A for mass flux between 200 to 600 kg/m^2.s at 45°C. They found that microfin tubes yielded higher heat transfer coefficients than the smooth tube when refrigerant R22 is used. For R410A, the microfin tube heat transfer coefficients were higher than smooth tubes at low mass fluxes, but became lower than smooth tube at a mass flux of 600 kg/m^2.s. They explained it using the rationale of Carvanos [26,27] that for a single phase performance in finned tubes, the fins reduce the inter-fin velocity, thus decreasing heat transfer. In condensing flows, the surface tension drainage force is prominent at low mass fluxes and thus compensates for the decrease in velocity, whereas at high mass flux, the velocity reduction effect became dominant. They also found that for R410A, the heat transfer coefficients were slightly higher than for R22 in smooth tubes while the opposite was true for microfin tubes. In smooth tubes, the higher heat transfer coefficients for R410A were due to its larger thermal conductivity and smaller viscosity compared to R22. In microfin tubes, the Weber number of R22 was 2.7 times lower than that of R410A leading to greater surface tension drainage and heat transfer. Besides this, the vapor-to-liquid volume ratio for R22 is twice compared to R410A which led to a larger fraction of the fin surface being exposed to the vapor, thus enhancing the heat transfer.

Wang et al. [28] studied rectangular channels with d_h = 1.46 mm for the condensation of R134a at 61.5-66 °C over the mass flux range 75-750 kg/m^2.s. Tests were conducted in 610 mm long tubes with finned 10 multi-port channels cooled by air in crossflow. They found that the heat transfer coefficients were insensitive to quality at the low mass fluxes but more sensitive to quality at high mass fluxes where the heat transfer coefficients increased as mass fluxes increased.

Koyama et al. [29] studied condensation of R134a in two multi-port extruded aluminium tubes with eight 1.11 mm channels and nineteen 0.80 mm channels, respectively. Local heat transfer coefficients were measured using heat flux sensors. They recognized that it is difficult to measure local heat transfer coefficients in small channels using temperature rise in the coolant due to inaccuracies in the measurement of low heat transfer rates and small temperature differences.

Wang and Rose [30,31] developed analytical models to address condensation heat transfer in triangular and square micro-channels. They developed a model for film condensation taking into account surface tension, shear stress and gravity. They were able to predict the various condensate flow patterns across both the cross section and the length of the channel. Wang et al. [32] developed another model for film condensation in a square, horizontal, 1 mm micro-channel. As these papers account for three primary governing influences in micro-channel condensation, they provide an avenue for the modeling of phenomena specific to micro-channels.

In another study, Cavallini et al. [18] studied the heat transfer coefficient and pressure drop during condensation of R134a and R410A inside multiple parallel 1.4 mm d_h channels. They found good agreement between data for R134a and the correlations of Friedel [33], Zhang and Webb [34], Mishima and Hibiki [35] and Mueller-Steinhagen and Heck [36]. However all these correlations overpredicted the R410A data.

Shin and Kim [37] used the outlet temperature of an electrically heated air stream and matched it with that of a similar air stream heated by condensing refrigerant R134a to measure small, local condensation heat transfer rates. They tested circular and square channels for the mass flux range of $100 < G < 600$ kg/m^2.s at 40°C and with $0.5 < d_h < 1$ mm. They found that most of the available models namely Akers et al. [38], Soliman et al. [39], Traviss et al. [40], Cavallini and Zecchin [41], Shah [42], Dobson [43] and Moser et al [44] under predicted their data at low mass fluxes. The agreement improved at the higher mass fluxes. They also found that square channels had higher heat transfer coefficients than those for circular channels at lower mass fluxes, whereas the reverse was true for high mass fluxes.

Traviss et al. [40] used the heat-momentum analogy and the von Karman universal velocity distribution in the liquid film to develop a correlation for the Nusselt number in annular flow condensation. The results were compared with experiments on R12 and R22 condensing in an 8 mm tube for $161 < G < 1533$ kg/m^2.s. Agreement with the experiment data was good for qualities as low as 0.1. When the turbulent Martinelli parameters was below 0.155, the correlation produced good results. Above 0.155, the experimental data were under predicted by the correlation.

Shah [42] developed a general purpose condensation correlation from a large database of 21 investigators. The mean deviation between the predictions and the 474 data points used for correlation development was 17%. However there is some under prediction of the data at high qualities (0.85-1.0) which could be due to entrance or entrainment effects. The operating conditions included $11 < G < 211$ kg/m^2.s, 21°C <

$T_{sat} < 310°C$, $3 < U_v < 300m/s$, reduced pressure from 0.002 to 0.44, and $1 < Pr_l < 13$, for tube diameters between 7 and 40 mm. The correlation should be used only for $Re_l > 350$ due to lack of lower Re_l data used during development of the correlation.

Soliman [45] developed a heat transfer correlation for condensation in annular-mist flow. The study took into account the wall stress as a combination of friction, momentum and gravity contributions and used the resulting expression to evaluate the heat transfer coefficient.

Chitti and Anand [46] developed an analytical model for annular flow condensation in smooth horizontal round tubes. The results were compared with data for condensation of R22 inside an 8 mm tube. This model showed reasonable agreement with a mean deviation of 15.3%, about the same as Traviss et al. [40] and Shah correlations [42]. Chitti and Anand [47] later extended the experiments to R32/R125 mixtures (50/50 by weight) with oil and condensation of R22 in an 8 mm horizontal tube. Heat transfer coefficients for R32/R125 mixtures were about 15% higher than those for R22, and the effect of polyolester oil was also found to be minimal, within uncertainty estimates.

2.2.3 Maldistribution Effects

As in the conventional heat exchangers, MCHX is also subject to air and refrigerant side flow maldistribution. Hwang et al. [48] studied the refrigerant inlet location in the manifold and compared the behavior of side-inlet and end-inlet locations. The side-inlet location showed better liquid refrigerant flow distribution than the end-inlet location by more effectively mixing the liquid and vapor refrigerant from the inlet. They found that by improving refrigerant maldistribution through the manifold inlet, the mini-channel evaporator performance could be improved.

An example of air side maldistribution in conventional finned-heat exchangers had been studied by Chin and Raghavan [49]. Various factors contribute to refrigerant flow maldistribution. They include the heat exchanger geometry, operating conditions, multiphase flow and fouling [50]. Maldistribution causes degradation in the heat exchanger performance which would mean less efficient heat exchange or more energy required to overcome the pumping losses.

2.2.4 Pressure Drop in the Mini-Channel

In the study of pressure drop in the mini-channel, classical correlations such as those of Lockhart-Martinelli [51], Chisholm [52] and Friedel [53] were used. The Lockhart-Martinelli correlation was based on adiabatic flow of air and benzene, kerosene, water, and various oils flowing through 1.5-26 mm pipes, and the pressure drops were correlated based on whether the individual liquid and gas phases were considered to be in laminar or turbulent flow. The two-phase pressure drop is expressed in terms of two-phase multipliers corresponding to the pressure drop of single phase liquid or gas phase.

Chisholm [54] developed correlations for the two-phase multipliers of Lockhart and Martinelli. He also modified the procedure and equations developed by Baroczy [55,56] that account for fluid properties, quality and mass flux based on steam, water/air and mercury/nitrogen.

Friedel [34,53] developed a correlation based on a database of 25,000 points for adiabatic flow through channels with d > 1mm. It is more widely used for vertical upward and horizontal flow, and is recommended by Hewitt et al. [57] for situations where surface tension data are available, and by Hetsroni [58] for $\mu_l/\mu_v > 1000$.

Cavallini et al. [18] investigated condensation heat transfer and pressure drop of new HFC refrigerants such as R410A in an 8 mm horizontal smooth tube. Experiments were run at a saturation temperature range of 30 to 50°C, mass flux between 100 to 750 kg/m^2.s and vapour quality range of 0.15 to 0.85. In order to compute the frictional pressure drop, they modified the two-phase multiplier in the Friedel correlation. For vapour mass velocity $J_G > 2.5$ the modified two-phase multiplier is used while for $J_G < 2.5$, the original two-phase multiplier proposed by Friedel is used.

Garimella et al. [59,60] developed experimentally validated models for pressure drops during condensation of refrigerant R134a in intermittent flow through circular and non circular micro-channels. The predicted pressure drops are on average within ±13.5% and ±16.5% from measured values for circular and non circular passages respectively. Besides that they developed a model for condensation pressure drop in annular flow [61] and then a comprehensive multi-regime pressure drop model [62] for micro-channels for the mass flux range $150 < G < 750$ kg/m^2.s. The experiment was first conducted by measuring the single-phase pressure drop for each tube in the laminar and turbulent regimes for both superheated vapor and sub-cooled liquid cases. The single phase pressure drops were in good agreement with values predicted by Churchill [63].

2.2.5 Wilson Plot Method

The original Wilson Plot Method developed by Wilson [64] in 1915 is often used to evaluate the convection coefficients in shell and tube condensers. The overall thermal resistance is a sum of inside tube convective thermal resistance, the tube wall resistance and the external shell convection thermal resistance. According to Wilson, when the mass flow rate of the cooling liquid inside the tube changes the overall thermal resistance, the change would be mainly due to the variation of the in-tube convection coefficient with the external shell convective thermal and tube wall resistance remaining nearly constant. The overall thermal resistance and the cooling liquid velocity were determined experimentally. With the overall thermal resistance determined from experiment and either the internal or external convective thermal resistance predicted from known correlations, the other convective thermal resistance is determined. The Wilson Plot Method requires the assumption of the exponents of the Reynolds and the Prandtl dimensionless numbers.

Williams and Katz [65] analyzed the performance of six plain and fin-tube bundles forming a shell and tube heat exchanger using Wilson Plot method. Experiments were conducted using water, lubricating oil and glycerin in the shell side and cooling water inside the tubes. The outside convection coefficient was obtained.

Hasim et al. [66,67] studied the heat transfer enhancement by combining ribbed tubes with wire and twisted tape inserts. Water was used as both cooling and heating fluids in a double pipe heat exchanger. The experimental convective coefficients were reported in these papers.

The modified Wilson Plot Method is based on the described Wilson Plot Method but takes into account a second linear equation obtained by applying logarithms to both sides of the thermal resistance equation plus an iteration procedure. The modified Wilson Plot Method is used when there is not a dominant resistance and one of the coefficients is unknown. This modified method requires only the assumption of the exponent of Prandtl dimensionless numbers.

Young and Wall [68] modified the Wilson Plot Method in which several correlations were proposed for both internal and external thermal resistances. The method used is like repeating several basic Wilson plots for several levels of constant shell-side resistance while the second side varies. Each step has its own coefficients.

Ribatski and Thome [69] used the modified method to estimate internal heat transfer performance for of smooth and enhanced tubes, while the outside tube was operating under pool boiling conditions. Wilson plots were obtained by varying the water mass flow rate for a constant heat flux (for each heat flux, a new constant was calculated).

Briggs and Young [70] used the modified method to calculate three unknowns. They calculated the heat transfer coefficient of the annulus side in a simple tube-in-tube heat exchanger.

Kartabil [71] developed a method to determine three resistances with up to five unknown parameters. Three complete sets of experimental data were used (each with a different dominant resistance).

2.2.6 Application of Artificial Neural Network (ANN) and Generic Algorithm (GA) to determining heat transfer coefficients.

ANN has gained much popularity due to its wide application in many fields such as thermal engineering, engineering mechanics, optimization, system control and pattern recognition. Jambunathan et al. [72] and Alvarez et al. [73] used ANN-based methodology to estimate the convective heat transfer coefficients using crystal thermography and mass transfer coefficients in bubble columns with Newtonian and non-Newtonians fluids respectively. Mazzola [74] used a combined approach of ANNs and standard correlations to investigate the critical heat flux in water-cooled flow boiling. ANN has been used in the modeling of thermal devices such as solar receivers by Fowler [75], in thermosyphon water heaters by Kalogirou [76] and in HVAC systems by Mistry and Nair [77]. Zhao [78] and Diaz [79] reported the prediction of heat transfer rates in heat exchangers without condensation using ANN.

Jeannette et al. [80] and Diaz [81] used the ANN technique to study control problems in heat exchangers and HVAC systems.

The use of GA has increased at a fast pace in its use in statistics, electromagnetics, optimization, engineering and machine learning. GA was used to find the optimum shape in cooling channels by Von Wolfersdorf et al. [82] and in fin profiles by Fabbri [83]. The analysis of high heat flux flow boiling systems by Castrogiovanni and Sforza [84] , the study of inverse heat transfer problems by Raudensky et al. [85], Okamoto et al. [86] and Li and Yang [87] and the numerical solution of the conduction equation by Davalos and Rubinsky [88] are other problems that had been approached with this technique. Schmit et al. [89] and Tayal et al. [90] had also used this method in the design of thermal equipment. Arturo et al. [91] proposed a method of data reduction that improves the prediction of correlations obtained from heat exchanger measurements. An ideal heat exchanger was defined on the basis of commonly made assumptions so that the two heat transfer correlations corresponding to both sides of the heat transfer surface can be simultaneously determined. The predictions were further improved by correlating the error that is introduced by the assumptions of the ideal heat exchanger.

2.3 Chapter summary

A comprehensive literature review has been done to determine the *status quo* of research to determine the effect of different tube pass and flow pass configurations on the thermal and hydraulic performance in mini-channels. The outcome of the review showed that past research focused on studies of single mini-channel tube, mini-channel evaporators and mini-channel condensers. Study of single mini-channel tube includes pressure drop versus channel size, condensation heat transfer coefficient and pressure drop for various types of refrigerant, comparison of condensation behavior between square and circular channel and effect of surface roughness to pressure drop. Study of mini-channel evaporator focused on refrigerant distribution and header designs while study of mini-channel condenser focused on design parameter study, performance comparison between mini-channel and conventional fin-tube condenser, condensation coefficients and pressure drops. No study has been carried out on the effect of different tube pass ratios and flow pass configurations and their relationship to thermal and hydraulic performance of the mini-channel heat exchanger. Therefore this study was undertaken and the outcome of it is to find out the optimum mini-channel heat exchanger arrangement in terms of tube pass ratio and flow pass configuration. As a result, the objectives of the present research have been identified and a set of methodology steps have been laid down to carry out the research. Besides this, literature review on the use of Wilson Plot method to determine the heat transfer coefficient showed that this method has been used extensively and successfully. Wilson Plot method is used in this study to determine the air side heat transfer coefficient which is the dominant resistance while the refrigerant side heat transfer coefficient is determined from known correlation. Other alternative methods to Wilson Plot method which can be used to determine heat transfer coefficients are ANN and GA.

CHAPTER 3

NUMERICAL SIMULATION STUDIES

3.1 Chapter overview

In this chapter, numerical simulation was used to compare the thermal and hydraulic performance of an air-cooled condenser with mini-channels on the refrigerant side, with different tube pass ratios and flow pass configurations. The simulation is based on well-known correlations for condensing coefficient and pressure drop on the refrigerant side.

3.2 Methodology

The approach taken for this study is to determine the thermal and hydraulic performance of a mini-channel heat exchanger for a given geometry and inlet fluid temperatures (air and refrigerant). The mass flow rates of both streams are also known. The geometric parameters of the mini-channel are shown in Table 3.1 while the air and refrigerant inlet temperatures and flow rates are shown in Table 3.2.

Table 3.1: Geometric Parameters of the Mini-Channel Heat Exchanger

Geometric Specification	Length / Quantity	Unit
MCHX Length	0.457	m
MCHX Height	0.457	m
Tube width(inner), t_{iw}	15.21	mm
Tube width (outer), t_{ow}	16.01	mm
Tube height (outer), t_{oh}	1.9	mm
Tube height (inner), t_{ih}	1.1	mm
Tube thickness, t_{thk}	0.40	mm
Web thickness, W_t	0.43	mm
No. of webs, N_w	6	-
Web spacing, W_{sp}	2.304	mm
Fin pitch, F_p	1.4	mm
Fin height, F_h	9.1	mm
Fin thickness, F_{thk}	0.115	mm
Fin depth, F_{depth}	16.01	mm
No. of tubes, N_t	39	-

Total tube length, L_t	17.82	m
Tube pitch T_p	11.0	mm
Louver pitch L_p	1.3	mm
Louver length L_l	1.383	mm
Louver height L_h	0.473	mm
Louver angle, L_α	20.0	degrees
Aspect ratio	0.4774	-

Table 3.2: Air and Refrigerant Inlet Temperature and Flow Rate

Air Stream		**Refrigerant Side**	
Coil Inlet Temperature, °C	**Volumetric Flow Rate, m^3/s**	**Condenser Inlet Temperature, °C**	**Mass Flow Rate, kg/s**
35.0	0.318	81.8	0.018

The air side heat transfer coefficient, h_o which is determined from the Wilson Plot experiment, is used to calculate *j-factor* using equation (3.1)

$$j = \frac{h_o \, \mathrm{Pr}_a^{2/3}}{\rho_a V_{\max} C_{pa}} \tag{3.1}$$

Corresponding *j-factor* and Reynolds number, Re_a were calculated and shown in Chapter 4.

As shown in Table 3.2 air enters the mini-channel heat exchanger at an ambient temperature of 35°C and a frontal air velocity of 1.52 m/s. The airside heat transfer coefficient at 35°C, $h_{o@35°C}$ calculated from Fig. 4.11 is 142 $W/m^2.K$. This value will be used in the numerical simulation.

Mathematical models and empirical relations are used to calculate the heat transfer and pressure drop of the mini-channel heat exchanger and are explained in the following sequence:

3.2.1 Geometry (Air side heat transfer area & tube internal heat transfer area)
3.2.2 Air side heat transfer coefficient
3.2.3 Refrigerant side condensing coefficient

3.2.4 Total heat transfer capacity

3.2.5 Pressure drop calculation

3.2.1 Geometry

3.2.1.1 Air Side Heat Transfer Area

Subramaniam [96] has developed the calculation model for the air side area which simplifies the geometry of the multi-louvered fins. Figure 3.1 shows a cross section of the tube outer surface after the simplification. The fins are assumed to be perfectly rectangular and at right angles to the tube outer surface. The air flow is normal to the plane of the paper and in cross flow with the refrigerant.

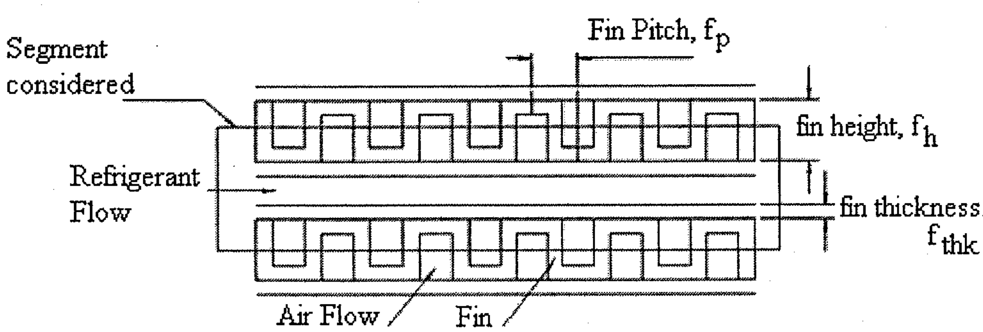

Fig. 3.1: Segment of MCHX and Parameters of Louvered Fin

The face area of one tube and fin set in one segment is given by:

$$A_c = (t_{oh} + F_h)L_{seg} \tag{3.2}$$

Of this, the area blocked by the fins is given by:

$$A_{ba} = \frac{L_{seg}}{F_p}\left(F_h F_{thk} + \left(F_p - 2F_{thk}\right)F_{thk}\right) \tag{3.3}$$

The area available for air flow is the total area less the area blocked by the fins and the area occupied by the tube for refrigerant flow.

$$A_{fa} = A_c - (A_{ba} + t_{oh}L_{seg}) \tag{3.4}$$

The perimeter of the tube directly in contact with air is:

$$per_a = 2\left[\frac{L_{seg}}{F_p}(F_h - F_{thk}) + L_{seg} - L_{seg}\frac{F_{thk}}{F_p}\right] \quad (3.5)$$

The hydraulic diameter is given by:

$$d_{h,a} = \frac{4A_{fa}}{per_a} \quad (3.6)$$

Part of the tube wall, which is in contact with the refrigerant on the inside surface and with air on the outside surface directly transfers heat from the refrigerant to the outside air. This constitutes the direct heat transfer area.

$$A_{da} = \left[2(t_{ow} - t_{oh})\left(1 - \frac{F_{thk}}{F_p}\right) + \pi t_{oh}\right]L_{seg} \quad (3.7)$$

The fins also help in transferring heat from the refrigerant to the outside air. This constitutes the indirect heat transfer area.

$$A_{ida} = 2F_l\frac{1}{F_p}(F_h - F_{thk})L_{seg} \quad (3.8)$$

It is known that the fin surface which extends outward from the tubes will not have a uniform temperature equal to the temperature of the tube surface. Therefore, it is necessary to account for this "inefficiency" of the fin in transferring heat, as there will be a varying temperature gradient along the fin length. By definition:

$$\eta_{fa} = \frac{\textit{Actual heat transfer for fin and base}}{\textit{Heat transfer for fin and base when the fin is at tube surface temperature}}$$

According to Subramaniam [96], the fin efficiency is given by:

$$\eta_{fa} = \frac{\tanh\left[\sqrt{\frac{2h_o(F_l + F_{thk})}{k_t F_{thk} F_l}}\left(\frac{F_h}{2}\right)\right]}{\sqrt{\frac{2h_o(F_l + F_{thk})}{k_t F_{thk} F_l}}\left(\frac{F_h}{2}\right)} \quad (3.9)$$

By using the values obtained in equation (3.7), (3.8) and (3.9), we are now able to calculate the air side effective heat transfer area of a segment with the following equation:

$$A_{eff,a} = A_{da} + \eta_{fa} A_{ida} \tag{3.10}$$

3.2.1.2 Tube Internal Heat Transfer Area

The calculation model for the tube side area which was developed by Subramaniam [96] simplifies the geometry of the tube cross section area. Figure 3.2 shows a cross section of the tube after the simplification. The two end passages are assumed to be perfectly semi-circular.

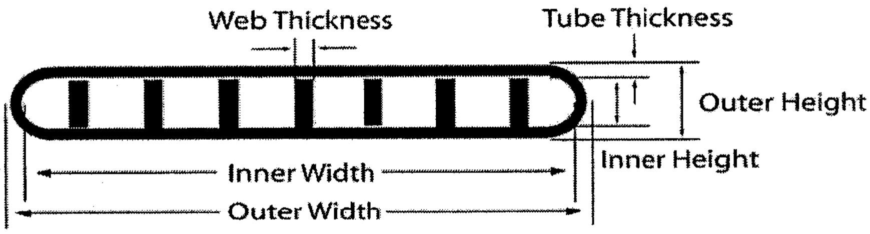

Fig. 3.2: Cross Section of Mini-Channel Extrusion Tubes

Hence, the total tube side cross section area is given by:

$$A_t = t_{ih}(t_{iw} - t_{ih}) + \frac{\pi}{4} t_{ih}^2 \tag{3.11}$$

The tube free-flow area is obtained by:

$$A_{ft} = A_t - N_w t_{ih} w_t \tag{3.12}$$

The tube wetted perimeter is the total tube perimeter in contact with the refrigerant which is given by:

$$per_t = \pi t_{ih} + 2(t_{iw} - t_{ih} - N_w w_t) + 2t_{ih} N_w \tag{3.13}$$

The hydraulic diameter is given by:

$$d_{ht} = \frac{4A_{ft}}{per_t} \tag{3.14}$$

The tube wall wetted directly by the refrigerant directly transfers heat from the refrigerant to the outside air. This constitutes the direct heat transfer area.

$$A_{dt} = 2(t_{iw} - t_{ih})L_t + \pi t_{ih} L_t - 2N_w w_t L_t \tag{3.15}$$

The webs act as fins and assist in transferring heat from the refrigerant to the outside air.

This constitutes the indirect heat transfer area.

$$A_{idt} = 2N_w t_{ih} L_t \tag{3.16}$$

The total heat transfer area is given by:

$$A_{efft} = A_{dt} + \eta_{ft} A_{idt} \tag{3.17}$$

The fin efficiency is given as follows:

$$\eta_{ft} = \frac{\tanh\left[\sqrt{\frac{2h_i(L_{seg}+w_t)}{k_t w_t L_{seg}}}\left(\frac{t_{hi}}{2}\right)\right]}{\sqrt{\frac{2h_i(L_{seg}+w_t)}{k_t w_t L_{seg}}}\left(\frac{t_{hi}}{2}\right)} \tag{3.18}$$

3.2.2 Air Side Heat Transfer Coefficient

With the *j-factor* determined from Wilson Plot test, we can then obtain the air side heat transfer coefficient as:

$$h_o = \frac{j\rho V_{\max} C_{p,a}}{\Pr^{2/3}} \tag{3.19}$$

where

$$\Pr = \frac{C_{p,a}\mu}{k} \tag{3.20}$$

3.2.3 Refrigerant Side Heat Transfer Coefficient

Refrigerant enters the condenser as superheated vapor and goes through the condensation process before leaving the condenser as subcooled liquid. Superheated vapor and subcooled liquid are in one-phase region and condensing mixture is in two-phase region.

For both the superheated and subcooled regions, the correlations for the heat transfer coefficients are different for laminar flow and turbulent flow. The critical Reynolds number that determines the transition is found from the following equation developed by Bhatti and Shah [97].

$$\mathrm{Re}_{cri} = \frac{4650}{V_{ratio}} \tag{3.21}$$

The velocity ratio is given by the equation developed by Purday [98]:

$$V_{ratio} = \left(\frac{m+1}{m}\right)\left(\frac{n+1}{n}\right) \tag{3.22}$$

The equations for m and n have been developed by Natarajan and Lakshmanan [99]:

$$m = 1.7 + 0.5\alpha^{-1.4} \tag{3.23}$$

If $\alpha < \frac{1}{3}$ then $\mathrm{n} = 2$

else $n = 2 + 0.3\left(\alpha - \frac{1}{3}\right)$ (3.24)

where α is the aspect ratio, defined as

$$\alpha = \frac{t_{ih}}{w_{sp}} \tag{3.25}$$

The value of the refrigerant mass flux can be calculated by:

$$G = \frac{m_r}{A_{fi}} \tag{3.26}$$

With this, the internal flow Reynolds number can then be obtained by:

$$\mathrm{Re} = \frac{Gd_{ht}}{\mu_{avg}} \tag{3.27}$$

This is then compared with the critical Reynolds number, Re_{cri} to determine the flow regime. If the Reynolds number is higher than Re_{cri}, the flow is turbulent, otherwise it is laminar.

The Nusselt number for single phase laminar flow refrigerant is provided by Bhatti and Shah [97]:

$$Nu = 8.325\left(1 - 2.0241\alpha + 3.0853\alpha^2 - 2.4765\alpha^3 + 1.0578\alpha^4 - 0.1861\alpha^5\right) \tag{3.28}$$

For single phase turbulent flow refrigerant, the equation developed by Churchill [63] is used:

$$Nu = \left[4.364^{10} + \left[\frac{e^{\frac{2200-\mathrm{Re}}{365}}}{4.364^2} + \frac{1}{\left(6.3 + \frac{0.079(f/8)^{0.5}\,\mathrm{Re}\,\mathrm{Pr}}{(1+\mathrm{Pr}^{0.8})^{5/6}} \right)^2} \right]^{-5} \right]^{1/10} \tag{3.29}$$

where f is the friction factor, expressed as:

$$f = 8\left[\left(\frac{8}{\mathrm{Re}} \right)^{12} + \frac{1}{\left[\left(2.457 \ln\left(\frac{1}{(7/\mathrm{Re})^{0.9} + (0.27r/d_{ht})} \right) \right)^{16} + \left(\frac{37530}{\mathrm{Re}} \right)^{16} \right]^{1.5}} \right]^{1/12} \tag{3.30}$$

Once the value of the Nusselt number is obtained, the heat transfer coefficient of each region (superheated and subcooled) can be calculated by:

$$h_i = \frac{Nu \cdot k_{avg}}{d_{ht}} \tag{3.31}$$

where $k_{avg} = 0.5(k_{g@sat} + k_{@cond,in})$ for superheated region

or $k_{avg} = 0.5(k_{f@sat} + k_{@cond,out})$ for subcooled region

For the condensing two phase region, the heat transfer coefficient is calculated by the equation developed by Shah [42]:

$$h_i = 0.023 \frac{k_{liq}}{d_{ht}} \mathrm{Re}_{liq}^{0.8} \mathrm{Pr}_{liq}^{0.4} \left[(1-x)^{0.8} + \frac{3.8x^{0.76}(1-x)^{0.04}}{P_{ratio}^{0.38}} \right] \tag{3.32}$$

where k_{liq}, Re_{liq} and Pr_{liq} are evaluated at the saturated liquid temperature. A curve fitting procedure of the refrigerant saturation properties is used to obtain these values. Other than that, $P_{ratio} = \frac{P_{cond,out}}{P_{cri}}$ and $d_{h,t}$ can be determined from the MCHX geometry. However, the refrigerant quality x is changing from 1 to 0 during the condensation process. Thus, the local heat transfer coefficient will also be changing as the refrigerant flows through. Nevertheless, it is possible to obtain an average heat transfer coefficient by integrating Equation (3.32):

$$h_{i,avg} = -\int_{x=1}^{x=0} h_i dx \tag{3.33}$$

For comparison purposes, the heat transfer coefficient calculated from equation (3.32) were replaced with the equation developed by Traviss et al. [41] and also Dobson and Chato [100]

For Traviss et al,

$$h_i = \frac{k_{avg}}{d_{h,t}}\left(\frac{1}{X_{tt}} + \frac{2.85}{X_{tt}^{0.476}}\right)\left(\frac{0.15 * \Pr * \mathrm{Re}^{0.9}}{F}\right) \tag{3.34}$$

where

$$X_{tt} = \left(\frac{1-x}{x}\right)^{0.9}\left(\frac{\rho_{go}}{\rho_{lo}}\right)^{0.5}\left(\frac{\mu_{lo}}{\mu_{go}}\right)^{0.1} \tag{3.35}$$

$$F = 0.707 * \Pr * \mathrm{Re}^{0.5} \qquad \text{for Re} < 50$$

$$F = 5\Pr + 5\ln\left(1 + \Pr\left(0.09636\,\mathrm{Re}^{0.585} - 1\right)\right) * \Pr * \mathrm{Re}^{0.5} \qquad \text{for } 50 <= \text{Re} <= 1125$$

$$F = 5\Pr + 5\ln\left(1 + 5\Pr\right) + 2.5\ln\left(0.00313\,\mathrm{Re}^{0.812}\right) \qquad \text{for Re} > 1125$$

(3.36)

For Dobson and Chato,

$$h_i = \frac{k_{avg}}{d_{ht}} * 0.023 * \mathrm{Re}^{0.8} * \Pr^{0.4}\left(1 + \frac{2.22}{X_{tt}^{0.89}}\right) \tag{3.37}$$

3.2.4 *Total heat transfer capacity*

With the heat transfer coefficients known, it is now possible to calculate the total heat transfer capacity of the MCHX coil. However, to do this, we will first need to know the heat transfer surface areas for the superheated region, two-phase region and subcooled region.

To help in the analysis, the MCHX coil is considered as consisting of three distinct coils, as shown in the Figure 3.3. Each coil will have its corresponding external surface area, i.e. A_{sh}, A_{tp} and A_{sc}.

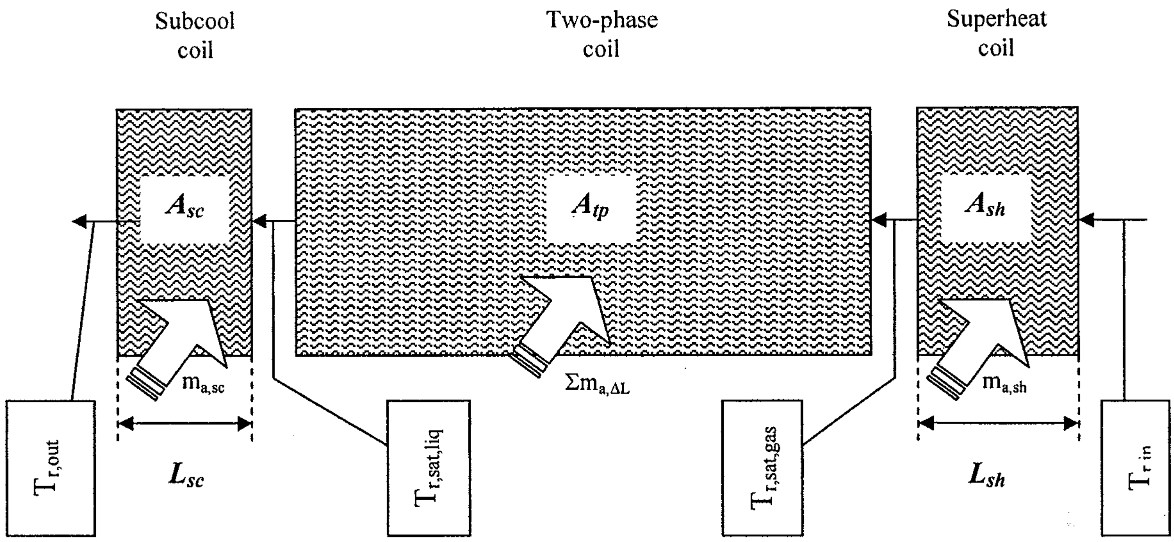

Fig. 3.3: Three distinct regions of the MCHX coil

The assumptions used for the analysis are:

1. The air side heat transfer coefficient, h_o, calculated from equation (3.19), is the same throughout the entire coil.
2. The air flow is uniform over the entire coil surface.

3.2.4.1 Superheat coil

The governing equation describing the heat transfer process at this portion of the coil is given as:

$$\frac{1}{UA_{sh}} = \frac{1}{h_{i,sh}A_{efft,sh}} + \frac{1}{h_o A_{effa,sh}} \tag{3.38}$$

In this equation, the resistance of the aluminum tube wall is ignored as it contributes only a small percentage, the convective resistances being dominant.

We can express the effective areas in this superheated region by using an area ratio of the total coil surface area. If L_{sh} is the total tube length of the superheated region, we will then have:

$$A_{effi,sh} = \left(\frac{L_{sh}N_{t,sh}}{L_t}\right)A_{effi} \tag{3.39}$$

$$A_{effa,sh} = \left(\frac{L_{sh}N_{t,sh}}{L_t}\right)A_{effa} \tag{3.40}$$

Equation (4.38) will then yield:

$$\frac{1}{UA_{sh}} = \left(\frac{L_t}{L_{sh}N_{t,sh}}\right)\left[\frac{1}{h_{i,sh}A_{effi}} + \frac{1}{h_o A_{effa}}\right] \tag{3.41}$$

With the assumption of a uniform air distribution, the air mass flow rate over this coil is calculated as:

$$m_{a,sh} = \left(\frac{L_{sh}N_{t,sh}}{L_t}\right)m_a \tag{3.42}$$

Next, the NTU is calculated as follows:

$$NTU = \frac{UA_{sh}}{C_{\min}} \tag{3.43}$$

where C_{min} is C_r $(= m_r C_{pr})$ or C_a $(= m_{a,sh}C_{pa})$ whichever value is smaller. The values of the specific heats can be obtained from known property tables.

The effectiveness of coil is then evaluated (cross flow, both fluids unmixed):

$$\varepsilon_{sh} = 1 - \exp\left\{\frac{NTU^{0.22}}{C_{ratio}}\left[\exp\left(-C_{ratio}NTU^{0.78}\right) - 1\right]\right\} \tag{3.44}$$

where

$$C_{ratio} = \frac{C_{\min}}{C_{\max}} \tag{3.45}$$

The heat transfer rate of the mini-channel heat exchanger in the superheated region is thus given as:

$$Q_{sh} = \varepsilon_{sh}C_{\min}(T_{r,in} - T_{a,in}) \tag{3.46}$$

If the refrigerant inlet temperature is known, the temperature at the superheat coil outlet can then be calculated as:

$$T_{r,out,sh} = T_{r,in} - \frac{Q_{sh}}{m_r C_{p,r}} \tag{3.47}$$

To obtain the value of L_{sh}, an iterative method is used where the length is increased incrementally until $T_{r,out,sh}$ converges on $T_{r,sat,gas}$ which corresponds to the location where two-phase flow begins.

3.2.4.2 Two-phase condensing coil

To calculate the condensing area, the coil is discretized into smaller sections, each with length ΔL_c. Each section is treated as an individual coil, with its own fluid stream properties. By using the same proportional method as mentioned above, the effective surface area and mass flow rate of each section is calculated:

$$A_{effi,\Delta L} = A_{eff,i}\left(\frac{\Delta L_c N_{t,\Delta L}}{L_t}\right) \tag{3.48}$$

$$A_{effa,\Delta L} = A_{eff,a}\left(\frac{\Delta L_c N_{t,\Delta L}}{L_t}\right) \tag{3.49}$$

$$m_{a,\Delta L} = m_a\left(\frac{\Delta L_c N_{t,\Delta L}}{L_t}\right) \tag{3.50}$$

The local internal heat transfer coefficient (3.32) is then used to calculate the UA value for each section:

$$\frac{1}{U_{\Delta L} A_{\Delta L}} = \frac{1}{h_i A_{effi,\Delta L}} + \frac{1}{h_o A_{effa,\Delta L}} \tag{3.51}$$

The heat exchanger effectiveness in this two-phase region is given as:

$$\varepsilon_{cond} = 1 - \exp(-NTU) \tag{3.52}$$

where NTU is expressed as:

$$NTU = \frac{U_{\Delta L} A_{\Delta L}}{C_a} \tag{3.53}$$

In the condensing region, the heat capacity rate of the refrigerant is infinite. Therefore, the minimum heat capacity rate will be on the air side

With this, the heat transfer rate of each section is given as:

$$Q_{cond,\Delta L} = \varepsilon_{cond} C_a (T_{r,sat.liq} - T_{a,in}) \tag{3.54}$$

The change of enthalpy for the refrigerant in this section is thus:

$$\Delta h = \frac{Q_{cond,\Delta L}}{m_r} \tag{3.55}$$

By knowing the entering refrigerant enthalpy, we can then calculate the leaving enthalpy:

$$h_{r,\Delta L,out} = h_{r,\Delta L,in} - \Delta h \tag{3.56}$$

The refrigerant quality at the outlet is then given as:

$$x = \frac{h_{r,\Delta L,out} - h_f}{h_g - h_f} \tag{3.57}$$

Equations (3.48) to (3.57) are then repeated iteratively to cover a quality range from 1 to 0.

The summation of $Q_{p,cond,\Delta L}$ for all the sections will then be the total heat transfer rate for the condensation region

$$Q_{cond} = \sum Q_{p,cond,\Delta L} \tag{3.58}$$

3.2.4.3 Subcool coil

Upon completion of the calculation for the superheat and condensing coils, we can then determine the remaining available area for subcooling:

$$A_{effa,sc} = A_{effa} - A_{effa,sh} - \sum A_{effa,\Delta L} \tag{3.59}$$

The heat transfer rate in the subcooled region, Q_{sc} and the tube length of subcool region, $L_{sc,}$ can be determined by the same iterative method for the superheat coil. The relevant equations will thus be:

$$\frac{1}{UA_{sc}} = \left(\frac{L_t}{L_{sc} N_{t,sc}}\right)\left[\frac{1}{h_{i,sc} A_{efft}} + \frac{1}{h_o A_{effa}}\right] \tag{3.60}$$

$$Q_{sc} = \varepsilon_{sc} C_{\min} (T_{r,sat,liq} - T_{a,in}) \tag{3.61}$$

$$T_{r,out,sc} = T_{r,sat,liq} - \frac{Q_{sc}}{m_r C_{p,r}} \tag{3.62}$$

However, the convergence criterion for the iteration is when the coil effective area reaches $A_{effa,sc}$ as determined from Equation (3.59). Note also that the inlet temperature to this portion of the coil is the refrigerant saturated liquid temperature.

Finally, the total heat transfer rate of the mini-channel heat exchanger is:

$$Q_t = Q_{sh} + Q_{cond} + Q_{sc} \tag{3.63}$$

3.2.5 *Pressure Drop Calculation*

For the analysis of the refrigerant pressure drop in the mini-channel, the following equations are used.

For single phase pressure drop in the laminar region, Shah and London [101] equation developed for rectangular ducts is used.

$$f = \frac{96}{\mathrm{Re}}\left[1 - 1.3553\alpha + 1.9476\alpha^2 - 1.7012\alpha^3 + 0.9564\alpha^4 - 0.2537\alpha^5\right] \tag{3.64}$$

For turbulent flow, the following equation developed by Bhatti and Shah [97] is used.

$$f=(1.0875-0.1125)8\left[\left(\frac{8}{\mathrm{Re}}\right)^{12}+\frac{1}{\left[\left(2.457\ln\left(\frac{1}{(7/\mathrm{Re})^{0.9}+(0.27r/d_h)}\right)\right)^{16}+\left(\frac{37530}{\mathrm{Re}}\right)^{16}\right]^{1.5}}\right]^{1/12}$$

(3.65)

The pressure drop in the two phase region consists of the frictional pressure drop and the deceleration pressure drop. The frictional pressure drop is calculated using the following equation developed by Friedel [34]

$$\left(\frac{dp}{dx}\right)_{fric}=\phi_{lo}^2\left(\frac{dp}{dx}\right)_{lo} \tag{3.66}$$

where,

$$\phi_{lo}^2=E+\frac{3.25FH}{Fr^{0.045}We^{0.035}} \tag{3.67}$$

$$We=\frac{G^2d_h}{\rho_{TP}\sigma} \tag{3.68}$$

$$Fr=\frac{G^2}{gd_h\rho_{TP}^2} \tag{3.69}$$

$$\rho_{TP}=\left[\frac{x}{\rho_{vap}}+\frac{1-x}{\rho_{liq}}\right]^{-1} \tag{3.70}$$

$$H=\left(\frac{\rho_{liq}}{\rho_{vap}}\right)^{0.91}\left(\frac{\mu_{vap}}{\mu_{liq}}\right)^{0.19}\left(1-\frac{\mu_{vap}}{\mu_{liq}}\right)^{0.7} \tag{3.71}$$

$$F = x^{0.78}(1-x)^{0.24} \tag{3.72}$$

$$E = (1-x^2) + x^2\left(\frac{\rho_{liq} f_{go}}{\rho_{vap} f_{lo}}\right) \tag{3.73}$$

where f_{go} and f_{lo} are the vapor only and liquid only Darcy friction factors calculated using Churchill correlation [63] as follows:

$$\left[\frac{dp}{dx}\right]_{lo} = \frac{f_{lo} G^2}{2 d_h \rho_{liq}} \tag{3.74}$$

$$\left[\frac{dp}{dx}\right]_{go} = \frac{f_{go} G^2}{2 d_h \rho_{vap}} \tag{3.75}$$

The deceleration pressure drop is given by

$$\left(\frac{dp}{dx}\right)_{dec} = G^2\left[\frac{x_{out}{}^2}{\alpha_v \rho_{vap}} + \frac{(1-x_{out})^2}{(1-\alpha_v)\rho_{liq}}\right] - G^2\left[\frac{x_{in}^2}{\alpha_v \rho_{vap}} + \frac{(1-x_{in})^2}{(1-\alpha_v)\rho_{liq}}\right] \tag{3.76}$$

where α_v is the void fraction given by Butterworth [102]

$$\alpha_v = \left[1 + 0.28\left(\frac{1-x}{x}\right)^{0.64}\left(\frac{\rho_{vap}}{\rho_{liq}}\right)^{0.36}\left(\frac{\mu_{liq}}{\mu_{vap}}\right)^{0.07}\right]^{-1} \tag{3.77}$$

The pressure drop across the mini-channel heat exchanger is summed up as follows:

$$dP_t = \int_{0.001}^{Lsh}\left(\frac{dp}{dx}\right)_{go} .dx + \int_{L_{sh}}^{Lc}\left(\frac{dp}{dx}\right)_{fric} .dx + \int_{L_{sh}}^{L_c}\left(\frac{dp}{dx}\right)_{dec} .dx + \int_{L_c}^{Lsc}\left(\frac{dp}{dx}\right)_{lo} .dx \tag{3.78}$$

The entrance and exit losses are not considered as they contribute very little to the overall pressure drop.

For comparison purpose, the pressure drop in the two phase region calculated using Friedel correlation is replaced by correlation developed by Cavallini et al. [19,103,104]. This correlation is actually a modification to Friedel correlation. The parameter E shown in equation (3.73) is maintained while parameters F & H are modified.

$$F = x^{0.6978} \tag{3.79}$$

$$H = \left(\frac{\rho_{liq}}{\rho_{vap}}\right)^{0..3278}\left(\frac{\mu_{vap}}{\mu_{liq}}\right)^{-1.181}\left(1-\frac{\mu_{vap}}{\mu_{liq}}\right)^{3.477} \tag{3.80}$$

The Weber number is defined in terms of the gas-phase density as follows:

$$We = \frac{G^2 d_h}{\rho_{go}\sigma} \tag{3.81}$$

The two-phase multiplier is calculated as follows:

$$\phi_{lo}^2 = E + \frac{1.262FH}{We^{0.1458}} \tag{3.82}$$

Table 3.3 summarized the analysis method used to determine the total heat transfer (thermal performance) and pressure drop (hydraulic performance) in the mini-channel heat exchanger.

Table 3.3: Heat Transfer and Pressure Drop Analysis Method

Heat Transfer Analysis Method			
1-Phase Superheated Region	Σ-NTU	Σ-NTU	Σ-NTU
2-Phase Condensing region	Shah	Traviss	Dobson & Chato
1-Phase Subcooled Region	Σ-NTU	Σ-NTU	Σ-NTU
Pressure Drop Analysis Method			
1-Phase Superheated Region	Churchill	Churchill	-
2-Phase Condensing region	Friedel	Cavallini	-
1-Phase Subcooled Region	Churchill	Churchill	-

3.3 Chapter summary

The numerical simulation was successfully carried out using well-known correlations for condensing coefficient and pressure drop on the refrigerant side. In order to calculate heat transfer in the two phase condensing region, three different correlations namely Shah, Traviss and Dobson and Chato were used for comparison purposes. For calculation of pressure drop in the two phase region, two different correlations namely Friedel and Cavallini were used. The results from the simulation are shown, compared with the experimental results and discussed in detail in Chapter Five.

CHAPTER 4

EXPERIMENTAL STUDIES

4.1 Chapter overview

This chapter reports the details of three kinds of experimental studies conducted in support of this research.

In the first experiment, a hydraulic test is conducted on a single mini-channel tube. The purpose of this experiment is to determine the Reynolds Number Re_t, required for turbulent flow to initiate inside the tube. The Re_t is used as a reference value to conduct the second experiment.

In the second experiment, a Wilson Plot test is conducted on a mini-channel heat exchanger. The purpose of this experiment is to determine the air side heat transfer coefficient, h_o of the mini-channel. The internal tube heat transfer coefficient h_i is calculated using known correlations. The thermal performance of both the air side and water inside the tube are determined from the experiment.

In the third experiment, a psychrometric test is conducted on an air-conditioning unit which uses a mini-channel condenser. The thermal performance of the mini-channel condenser is measured on the air side while the pressure drop of the refrigerant is measured across the mini-channel condenser. These results are used to validate the numerical simulation result conducted on the corresponding tube pass ratio and flow pass configuration of the mini-channel heat exchanger.

4.2 Mini-Channel Single Tube Hydraulic Experiment

4.2.1 Set-up and test procedure

For the hydraulic test conducted on a single mini-channel tube, an experimental rig shown in Fig. 4.1 is set-up and water is used as the fluid flowing inside the mini-channel tube. A water pump MOT MG 132SC2-38FF265-D1 5.5kW 3 Phase 50/60Hz (Grundfos) is used to pump water through the circuit. The temperature of water at tube entry and exit is measured using Pt-100 resistance temperature detectors (RTD). The water pressure at tube entry and exit is measured using pressure transmitters EJX430A (Yokogawa) while the flow rate is measured using a magnetic flow meter AXF015G (Yokogawa). The temperature T1 of the water entering the tube is controlled via a water heater rated at 7kW which heats up the water. The temperature control works in a feedback loop. The entering water temperature is fedback to a temperature controller UT 37(Yokogawa) which is used to control a voltage controller RSC-AAM 60 (Carlo Gavazzi) which in turn regulates the supply voltage to the heater to obtain the desired temperature set in the controller.

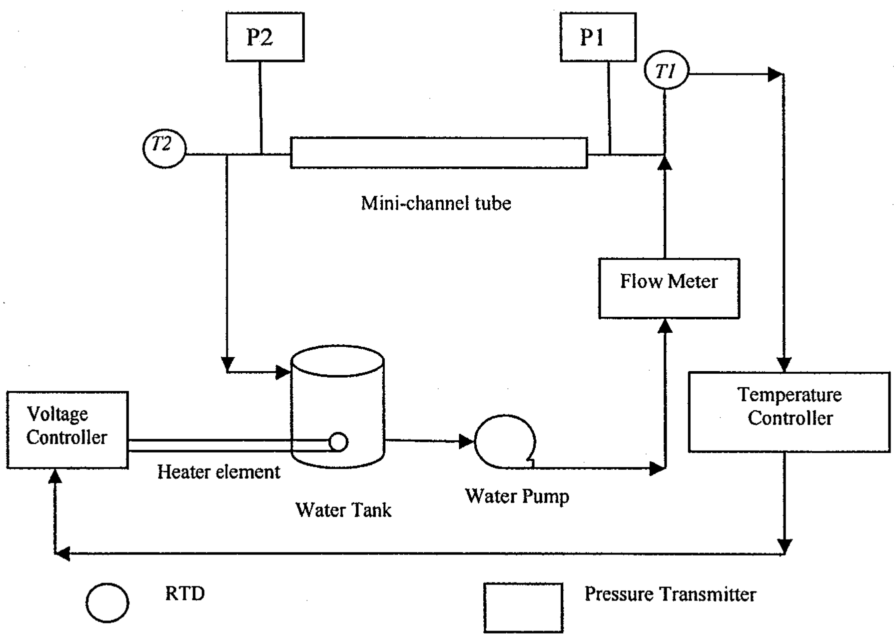

Fig. 4.1: Schematic of Experimental Rig for Hydraulic Test to Determine Re_t

After running for 30 minutes, the data are collected every second for a duration of one minute. The average readings are calculated and tabulated in Appendix A. Data collected from this experiment are used to calculate the Reynolds Number and Fanning friction factor, f_F using the following equations.

$$\mathrm{Re} = \frac{\rho v d_h}{\mu} \tag{4.1}$$

$$f_F = dP\left(\frac{d_h}{L_t}\right)\left(\frac{1}{2\rho v^2}\right) \tag{4.2}$$

The f_F and Re values are then used to plot a f_F vs. Re chart from which Re_t is determined.

4.2.2 Test results and discussion

As observed from Fig. 4.2, the Reynolds numbers for turbulent flow to initiate in the mini-channel tube is 830. Hence the Wilson Plot test are run at Re above 1000.

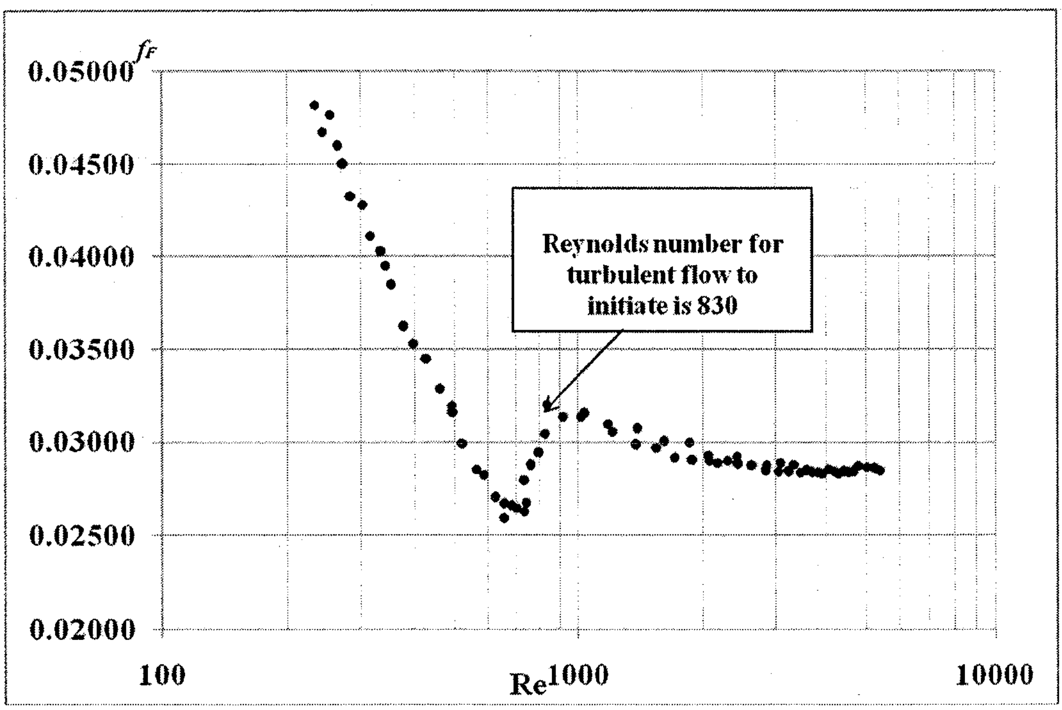

Fig. 4.2: Friction factor vs. Reynolds Number in Single Mini-Channel Tube

4.3 Wilson Plot Experiment

4.3.1 Set-Up and Test Procedure

A Wilson plot experiment set-up is done according to Fig. 4.3. The mini-channel heat exchanger or coil as shown in Fig. 4.3 is placed inside an air nozzle chamber. The air that passes through the external fin and tube side of the coil is pre-conditioned upstream. The air is pre-cooled by a fan coil unit ADB100BW. The fan coil unit is supplied with chilled water from a mini chiller. The water that enters from the chiller is set at a temperature of 7°C. An additional blower FSA315C-CW360 (Kruger) is used to help channel the air through the air nozzle to achieve the required air flow rate. The blower is driven by a 3kW 1500rpm 50Hz motor (Dong Guan).

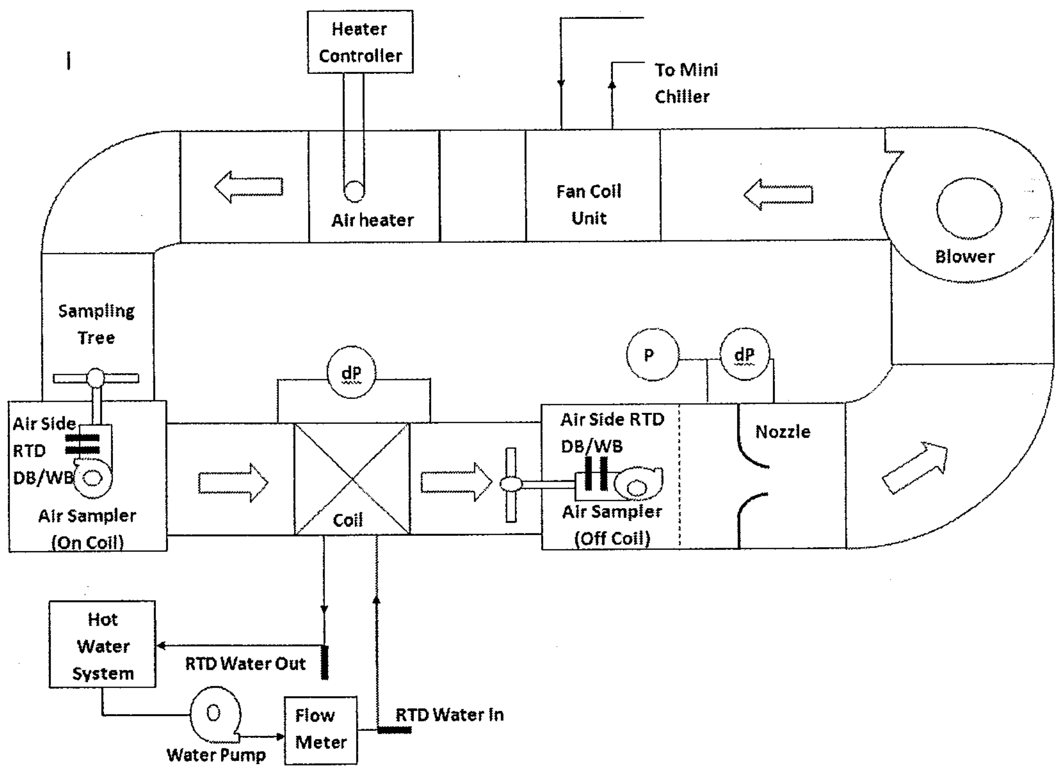

Fig. 4.3: Wilson Plot Test Rig

An air heater is used to reheat the air leaving the fan coil unit to a dry bulb temperature of 20.0±0.1°C. The heater voltage is regulated by a PID controller in order to maintain the air temperature that enters the coil. The air that enters the coil is heated up and leaves the coil at a higher temperature, and then enters the fan coil unit and the process is repeated. The dry bulb and wet bulb temperatures of the air that enters and leaves the coil are measured by RTDs that are placed inside an air sampler. To get an average air temperature, a sampling device as shown in Fig.4.4 is placed upstream of the air sampler to draw air coming in from different locations in the chamber. The mixed air is then drawn by a fan and passed through the RTD placed inside a box. Air pressure drop across the nozzle is measured using a differential pressure transmitter EJX110A (Yokogawa) while air pressure that enters the nozzle is also measured using a differential pressure transmitter only this time it is with reference to the atmospheric pressure. The air flow rate is calculated using equation (4.3)

$$Q = A_n * V' * 60 \tag{4.3}$$

where

$$V' = V * C_d \tag{4.4}$$

Air velocity $V = \sqrt{(2g * dP * SpV)}$ (4.5)

Area of the nozzle $A_n = \pi d_n^2/4$ (4.6)

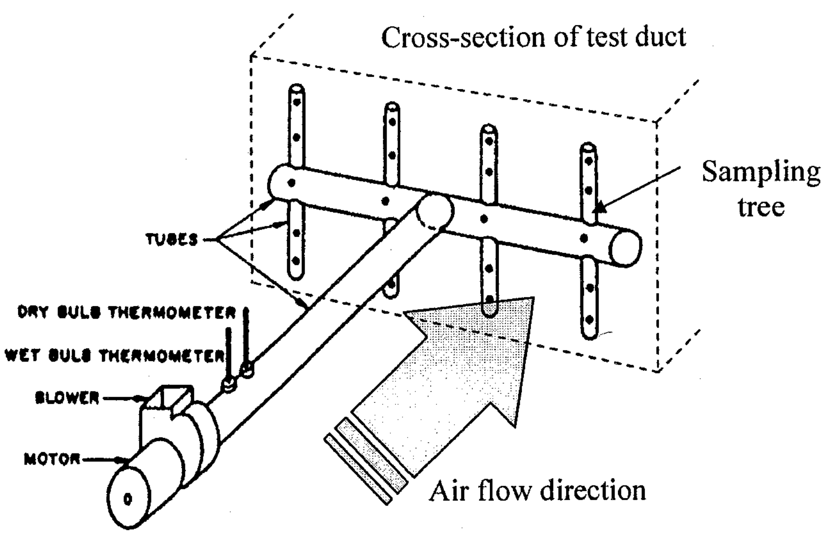

Fig. 4.4: Example of aspirating sampling device [92]

The fluid that flows inside the tube side of the coil is water. The temperature of the water that enters the coil is pre-heated by a 7kW water heater immersed inside a water tank. The same test procedure mentioned in 4.2.1 is used. In this test, the water that enters the coil is set at 50.0±0.1°C.

The air side performance of the coil, Q_a is calculated by the difference between the air enthalpy at coil inlet and exit multiplied by the mass flow rate of the air that passes through the coil. The water side performance of the coil, Q_w is calculated by the difference between the temperature of the water at coil inlet and exit multiplied by the volumetric flow rate of the water in the coil. The average performance of the coil, Q_{ave} is the average value between Q_a and Q_w.

$$Q_a = 14.333 * CFM * C_p * dT / SpV / 35.3 \tag{4.7}$$

$$Q_w = \dot{m} C_p dT \tag{4.8}$$

Readings are taken after running the experiment for 30 minutes to ensure the temperature and pressure readings are stable. The data are taken every five seconds over a 5 minutes duration. Each set of readings is taken three times. The readings are tabulated in Appendix B.

To prevent heat exchange with the ambient, the air duct and water pipes in the test rig are insulated. With careful experiments, the air-side heating capacity of the test coil agreed with the water-side within ±5%, as prescribed in [93].

All the data from the instruments are acquired with a YOKOGAWA MX-100 recorder. A customized LabView programme is used to communicate and transfer data from the recorder to a computer, which are then displayed on the monitor screen. The temperature and air flow rate readings are monitored and controlled for stabilization before readings are taken. The criteria for deciding this steady state condition include:

1. A continuous operation for at least 30 minutes

2. Air and water temperatures to be within ±0.1°C of set-point

3. Water flow rate to be within ±0.01 m^3hr^{-1} of set-point

4. Air flow rate to be within ±0.0014 m^3hr^{-1} (±3 ft^3min^{-1}) of set-point

5. Difference between air-side and water-side heating capacity to be lower than ±5%

Upon stabilization, an averaging process is initiated where the acquired data are downloaded and saved onto a Microsoft EXCEL template spreadsheet at 5 seconds interval for duration of 5 minutes, i.e. a total of 60 data points.

The photographs in Fig. 4.5 to 4.8 show the actual test rig used in the experiment.

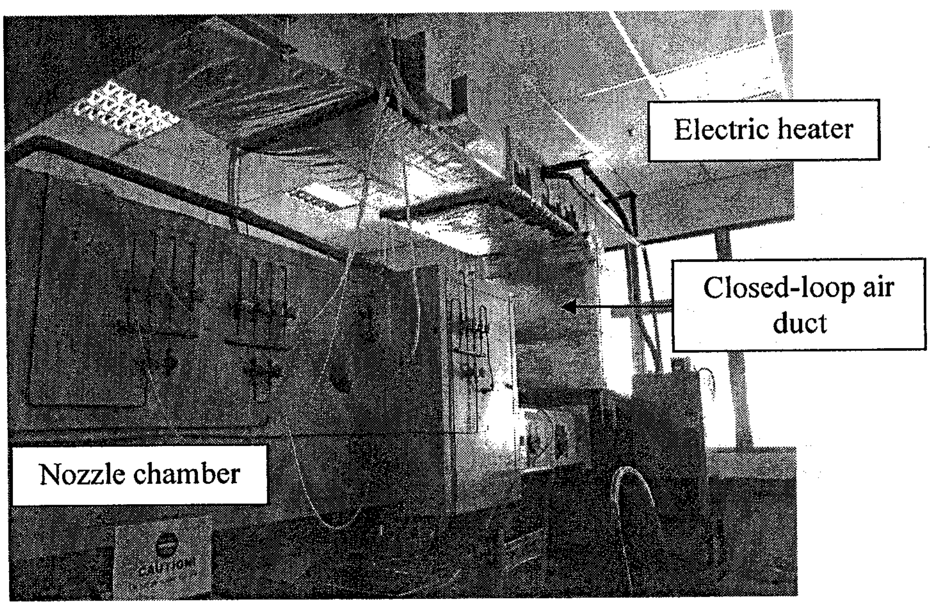

Fig. 4.5: Overall view of air loop in test rig

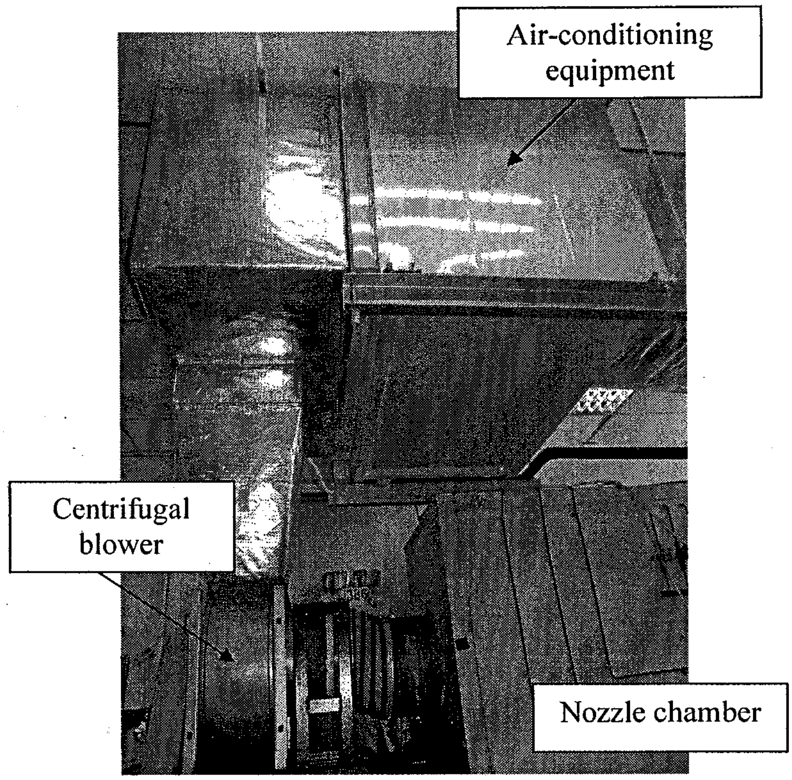

Fig. 4.6: Centrifugal blower and air-conditioning equipment

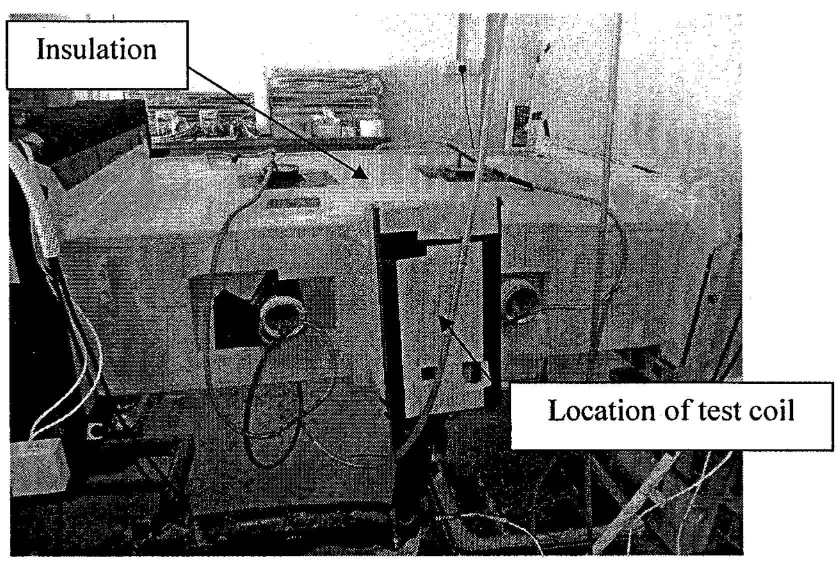

Fig. 4.7: Test duct with polyurethane insulation

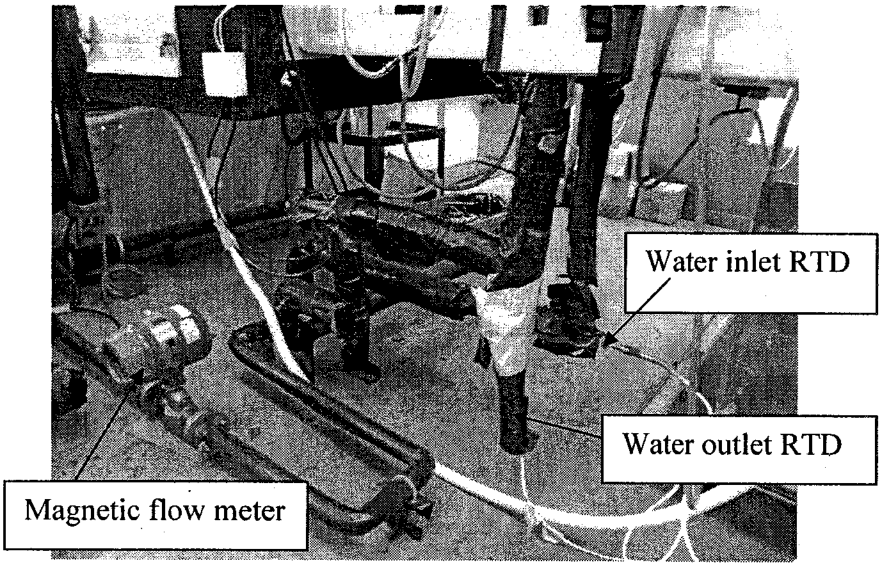

Fig. 4.8: Water inlet and outlet to test coil

$A_{eff,a}$ is the air-side effective heat transfer area of external fin and tube which is calculated according to equation (4.9). The heat exchanger log mean temperature difference (LMTD) is calculated according to equation (4.10)

$$A_{eff,a} = A_{da} + \eta_{f,a} A_{ida} \tag{4.9}$$

$$LMTD = \frac{(T_{wo} - T_{ai}) - (T_{wi} - T_{ao})}{\ln\left(\dfrac{T_{wo} - T_{ai}}{T_{wi} - T_{ao}}\right)} \tag{4.10}$$

and for two-pass cross flow heat exchanger, fluid A mixed, fluid B unmixed except between passes,

$$F = \frac{r(crossflow)}{r_o} \tag{4.11}$$

$$r_o = \frac{p - q}{\ln\left(\dfrac{1-q}{1-p}\right)} \tag{4.12}$$

$$r(crossflow) = \frac{q}{2\ln\left(\dfrac{1}{1-\dfrac{q}{r}\ln\left(\sqrt{\dfrac{1-q}{1-p}}-\dfrac{q}{p}\Big/\left\{1-\dfrac{q}{p}\right\}\right)}\right)} \tag{4.13}$$

$$p = \frac{T_{wi} - T_{ao}}{T_{wi} - T_{ai}} \tag{4.14}$$

$$q = \frac{T_{ao} - T_{ai}}{T_{wi} - T_{ai}} \tag{4.15}$$

$$\Delta t_m = F \times \frac{(T_{wo} - T_{ai}) - (T_{wi} - T_{ao})}{\ln\left(\dfrac{T_{wo} - T_{ai}}{T_{wi} - T_{ao}}\right)} \tag{4.16}$$

The air side overall heat transfer coefficient is given by equation (4.17)

$$U_o = \frac{Q_{ave}}{A_{eff,a} \Delta t_{m,cf}} \tag{4.17}$$

Q_{ave} and $\Delta t_{m,cf}$ are determined from the Wilson Plot test and $A_{eff,a}$ is calculated from the geometric parameter.

$$Q_{ave} = \left(\frac{Q_a + Q_w}{2}\right) \tag{4.18}$$

The water side heat transfer coefficient h_i is calculated using the Dittus-Boelter equation.

$$h_i = 0.023 * \mathrm{Re}^{0.8}\,\mathrm{Pr}^{0.4} \tag{4.19}$$

$$h_i = 0.023 * \left(\frac{\rho v d_h}{\mu}\right)^{0.8} \mathrm{Pr}^{0.4} \tag{4.20}$$

The relationships between U_o, $A_{eff,a}$, h_o, $A_{eff,t}$ and h_i are shown in equation (4.21)

$$\frac{1}{U_o} = \frac{1}{n_{f,a} h_o} + R_w + \frac{A_{eff,a}}{h_i A_{eff,t}} \tag{4.21}$$

where

$$R_{w'} = \frac{t_w A_{eff,a}}{k_w A_m}$$

$R_{w'}$ is neglected as its value is small.

$A_{eff,t}$ is calculated from equation (4.22)

See $A_{eff,t}$ in Eq. 4.22

$$A_{eff,t} = A_{dt} + \eta_{ft} A_{idt} \tag{4.22}$$

Equation (4.21) is then compared to the following form

$y = mx + c$

$$y = \frac{1}{U_o} \tag{4.23}$$

$$\frac{1}{n_{f,a} h_o} + R_w = c \tag{4.24}$$

$$\frac{A_{eff,a}}{0.023 * \left(\frac{\rho d_h}{\mu}\right)^{0.8} \mathrm{Pr}^{0.4} A_{eff,t}} = m \tag{4.25}$$

$$\frac{1}{V_w^{0.8}} = x \tag{4.26}$$

Figure (4.9) shows how equation (4.21) can be represented graphically

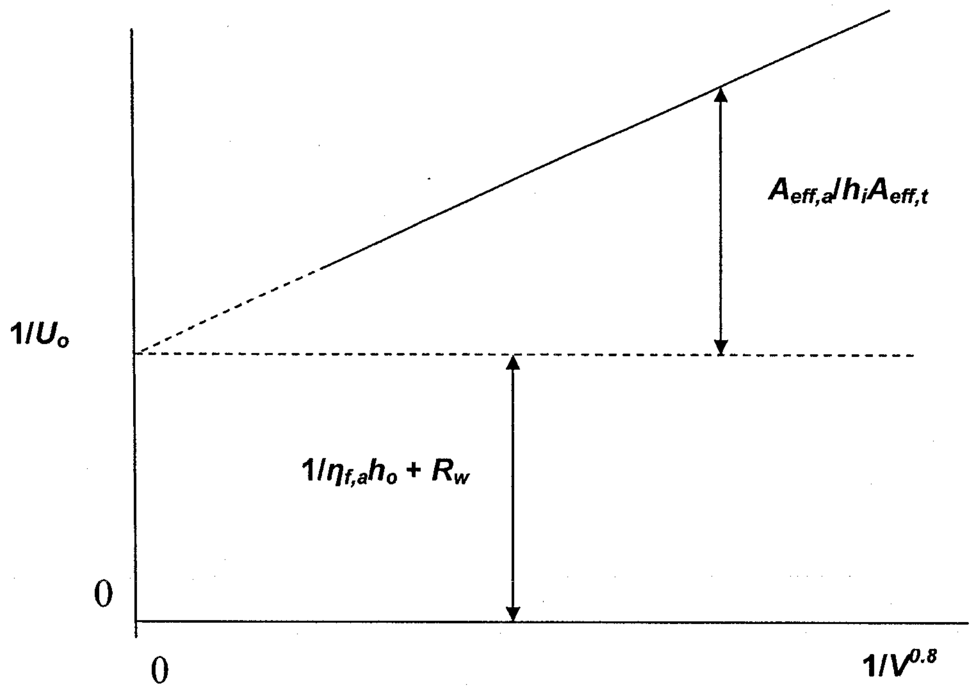

Fig. 4.9: $1/U_o$ versus $1/V^{0.8}$ determined from Wilson Plot Experiment

A straight line is obtained from the Wilson Plot experiment and is extended until it meets the $1/U_o$-axis. This takes place when the water velocity is infinite and hence h_i is infinite. Ao/h_iA_i becomes zero and ignoring R_w, $1/n_{f,a}h_o$ = c. h_o is easily calculated. Each straight line represents one air flow rate. The experiment is conducted under five air flow rates namely 0.12, 0.19, 0.26, 0.33 and 0.40 m^3/s and five water flow rates 0.8, 0.9, 1.0, 1.1 and 1.2 m^3/hr.

A $\eta_{f,a}ho$ versus v_a curve is shown in Figure 4.10

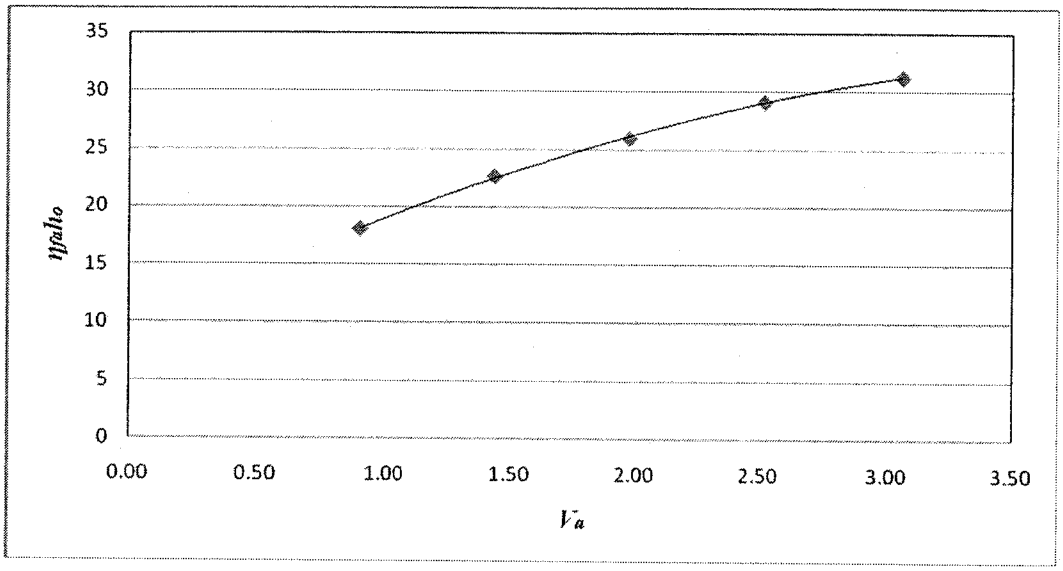

Fig. 4.10: Air Side Heat Transfer Coefficient $\eta_{f,a}h_o$ vs. Frontal Air Velocity v_a

The h_o values are used to calculate *j-factor* using equation (4.27)

$$j = \frac{h_o \mathrm{Pr}_a^{2/3}}{\rho_a V_{\max} C_{pa}} \tag{4.27}$$

Corresponding *j-factor* and Reynolds number, Re_a are calculated and are shown in Table 4.1.

Table 4.1: Air Side Re_a versus *j-factor*

Re_a	179	285	392	500	607
j-factor	0.05808	0.04562	0.03783	0.03379	0.02949

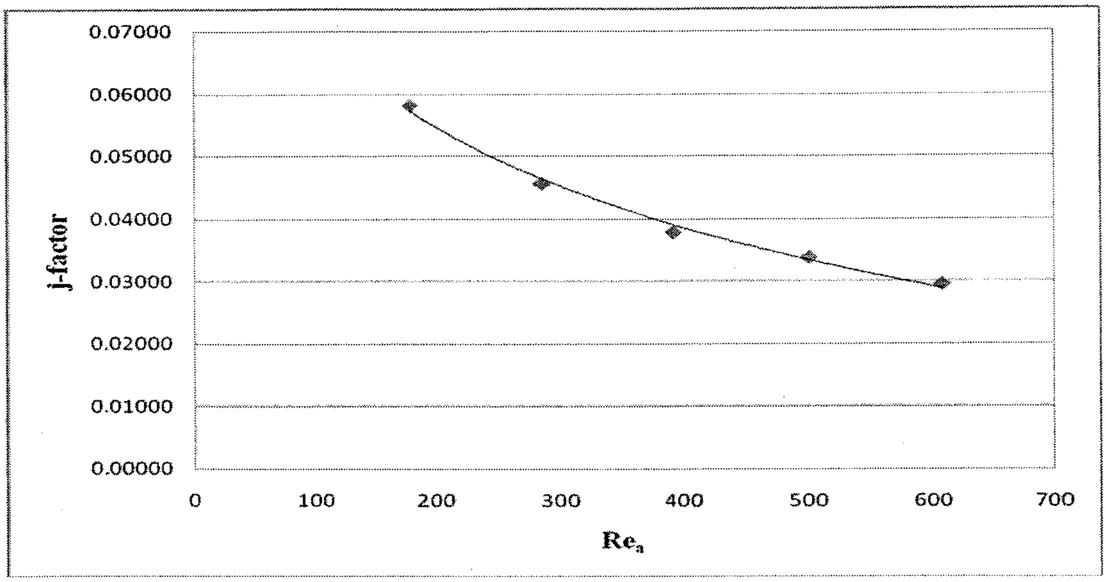

Fig. 4.11: Air Side *j-factor* versus Re_a

Using the plot in Fig. 4.11 we can calculate the actual $h_{o@35°C}$ for the mini-channel condenser to operate which is at an ambient of 35°C and a frontal air velocity of 1.52 m/s. This h_o value will then be used in the numerical simulation to determine the effect of different tube pass and flow pass configurations of the mini-channel on its thermal and hydraulic performance. This will reduce the error in the analysis.

4.3.2 Test results and discussion

The airside heat transfer coefficient at 35°C, $h_{o@35°C}$ and a frontal air velocity of 1.52 m/s calculated from Fig. 4.11 is 142 W/m^2.K.

4.4 Psychrometric Experiment

4.4.1 Set-Up and test procedure

The psychrometric test is conducted on an air-conditioner unit in a psychrometric test laboratory. The test is conducted with an air nozzle chamber in accordance with ANSI/ASHRAE Standard 40 [94]. The fan coil unit is coupled with copper pipes to the corresponding outdoor condensing unit where the mini-channel condenser is placed. The outdoor condensing unit is connected to the nozzle chamber by using a rectangular duct adapter which channels the discharged air. The duct is constructed in accordance with ANSI/ASHRAE Standard 37 [95] as shown in Fig. 4.12. The final assembly of the test system is as shown in Fig. 4.13. The external static pressure is tapped on the duct adapter and measured by a pressure transmitter P1. The transmitter sends a signal to a single loop controller (SLC) UT 550 (Yokogawa), which in turn sends a control signal to drive the inverter fan motor. The inverter fan motor draws air through the air nozzle chamber to achieve and maintain the required external static pressure set on the SLC. Another differential pressure transmitter P2 measures the differential pressure drop before and after the nozzle. This differential pressure reading is used to calculate the air flow rate. The air that enters and leaves the mini-channel condenser is measured using RTD. Both the dry bulb and wet bulb temperatures are measured. The total cooling performance of the mini-channel condenser are calculated from the air enthalpy difference between inlet and exit of the mini-channel condenser multiplied by the air flow rate that passes through the mini-channel condenser and is shown in equation (4.28) while the sensible cooling performance of the mini-channel condenser are calculated from the air temperature difference between inlet and exit of the mini-channel condenser multiplied by the air flow rate and is shown in equation (4.29). The pressure drop across the mini-channel heat exchanger is determined by measuring the refrigerant inlet and outlet pressure using pressure transmitters.

$$Q_T = 14.333 * CFM * dh/(SpV * 0.252 * (1+W))/35.3 \tag{4.28}$$

$$Q_s = 14.333 * CFM * C_p * dT/SpV/35.3 \tag{4.29}$$

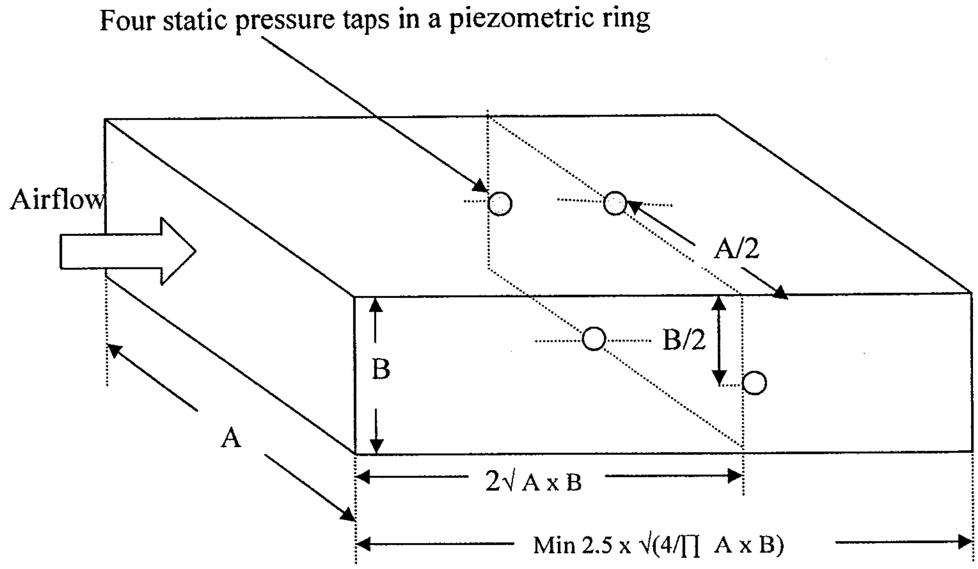

Fig. 4.12: Static Pressure Tapping Point on a duct adapter

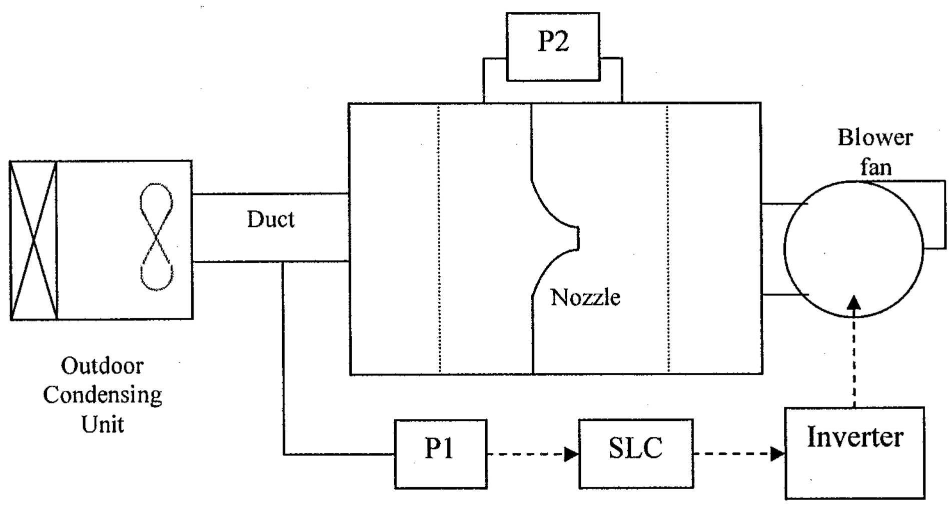

Fig. 4.13: Test Set-Up for Air Flow Measurement (Nozzle Chamber Method)

After the air conditioner has run for 30 minutes to ensure the air conditioner is operating at a stable condition, readings are taken once every seven minutes until seven readings are taken. An average reading is calculated from these seven readings.

4.4.2 Test results and discussion

The test results for a mini-channel condenser with tube pass ratio 70-30 and two flow pass configuration is shown in Table 4.2.

Table 4.2: Total Tested Cooling Performance of a Mini-Channel Heat Exchanger

Parameter	**Reading**	**Unit**
Temperature at condenser inlet	81.80	°C
Pressure at condenser outlet	3040	kPa
Pressure at condenser inlet	3055	kPa
Net pressure drop across the condenser	15	kPa
Outdoor air temperature (entering)	35.03	°C
Volumetric Air Flow Rate	0.318	m^3/s
Mini-Channel Performance	3522	W

4.5 Measurement Uncertainty

Test equipment used in the measurement exhibit uncertainty. There are two types of uncertainty namely type A and type B. Type A is caused by uncertainty due to repeatability in data collection while type B is caused by equipment and calibrator measurement uncertainties. Type A uncertainty is calculated statistically while type B is calculated from equipment measurement uncertainty from calibration certificates or manufacturer's specifications.

In order to determine type A uncertainty the following method is used. The number of readings is taken to be n while the average $\bar{x}$ is the sum of all the reading, Σx_i divided by the number of readings, n.

The estimated standard deviation S_n is calculated as follows:

$$S_n = \sqrt{\left(\frac{\sum_{i=1}^{n}(x_i - \bar{x})^2}{n-1}\right)} \tag{4.30}$$

and the estimated standard uncertainty U_A is given by

$$U_A = \frac{S_n}{\sqrt{n}} \tag{4.31}$$

As for type B uncertainty, the measurement uncertainty of each equipment and calibrator is obtained from the calibration certificate or manufacturer's specification.

In order to calculate the standard uncertainty, the normal distribution is used where

$$U_B = \frac{MU}{2} \tag{4.32}$$

If more than uncertainty is considered, Type B standard deviation can be calculated as shown in Table 4.3:

Table 4.3: List of uncertainty relationships

Expression for parameter Ω	Uncertainty relationship
$\Omega = A \pm B \pm C$	$U_\Omega^2 = U_A^2 + U_B^2 + U_c^2$
$\Omega = \frac{A \cdot B}{C}$	$\left(\frac{U_\Omega}{\Omega}\right)^2 = \left(\frac{U_A}{A}\right)^2 + \left(\frac{U_B}{B}\right)^2 + \left(\frac{U_c}{C}\right)^2$
$\Omega = \ln A$	$U_\Omega = \frac{U_A}{A}$
$\Omega = A^n$	$\frac{U_\Omega}{\Omega} = n\frac{U_A}{A}$

Each standard deviation calculated using type A and type B can be summed up in summation in quadrature or root sum of the squares. The result is called the combined standard uncertainty shown by U_c.

$$U_C = \sqrt{(U_{1A}^2 + U_{2A}^2 + ...U_{1B}^2 + U_{2B}^2 ...} \tag{4.33}$$

The calculated expanded uncertainties from the experimental data, for a 95% confidence level, are shown in Sections 4.5.1 to 4.5.3.

4.5.1 Hydraulic Experiment

Table 4.4: Measurement uncertainties (M.U.) of the instruments

Water side	
	M.U.
Flow meter	± 0.11%
$RTD_{w,i}$	± 0.06°C
$RTD_{w,o}$	± 0.06°C

Pressure transmitter	±0.1psig

Table 4.5: Measurement uncertainties of friction factor and Reynolds number

	M.U.
Friction factor	± 2.00%
Reynolds number	± 1.47%

4.5.2 Wilson Plot Experiment

Table 4.6: Measurement uncertainties of the instruments

Water side		Air side	
	M.U.		M.U.
Flow meter	± 0.11%	Differential pressure transmitter (across nozzle)	± 0.016 mmAq
		Different pressure transmitter (for heat exchanger)	± 0.040 mmAq
$RTD_{w,i}$	± 0.06°C	$RTD_{a,db,i}$	± 0.06°C
$RTD_{w,o}$	± 0.06°C	$RTD_{a,db,o}$	± 0.06°C
		$RTD_{a,wb,i}$	± 0.06°C
		$RTD_{a,wb,o}$	± 0.06°C

Table 4.7: Measurement uncertainties of heat duty

	M.U.
Water side capacity, Q_w	± 0.98%
Air side capacity, Q_a	± 0.31%

4.5.3 Psychrometric Experiment

Table 4.8: Measurement uncertainties of the instruments

Testing Equipment (Ref Std)	M.U	U_B	Unit
Dry Bulb Air Entering RTD	0.06	0.03	°C
Wet Bulb Air Entering RTD	0.06	0.03	°C
Dry Bulb Air Leaving RTD	0.06	0.03	°C
Wet Bulb Air Leaving RTD	0.06	0.03	°C
DP Transmitter	0.03	0.015	mm H_2O
DP Transmitter 2 (Before Nozzle)	0.03	0.015	mm H_2O
Barometric Pressure Transmitter	0.01	0.005	inHg
Thermocouple	0.5	0.25	°C
Caliper	0.01	0.005	mm
Static Pressure Transmitter	0.03		
SLC 1	0.073		
SLC 2	0.043		
Temperature Recorder	0.073		

Table 4.9: Measurement uncertainty of heating capacity

	M.U.
Air side capacity, Q_a	± 2.64%

4.6 Chapter summary

The hydraulic test result showed that the Reynolds number for turbulent flow to initiate in the mini-channel tube is 830. Hence the Wilson Plot test is run at Reynolds number above 1000. The Wilson Plot test result yielded an air side heat transfer coefficient, h_o as 142 W/m^2.K. This h_o value is used to analyse the performance of the mini-channel heat exchangers with different tube pass ratios and flow pass configurations. The psychrometric test result showed that the mini-channel condenser with tube pass ratio 70-30 and two-pass flow configuration yielded a performance of 3522W and pressure drop of 15kPa.

CHAPTER 5

NUMERICAL SIMULATION RESULTS AND DISCUSSION

5.1 Chapter overview

In this chapter, numerical simulation results on the thermal and hydraulic performance of an air-cooled condenser with mini-channels on the refrigerant side, with different tube pass ratios and flow pass configurations are shown and compared in detail. The optimum mini-channel heat exchanger configuration in terms of $Q_t/dP.V_r$ is proposed.

5.2 Results and discussion

The results for the thermal and hydraulic analysis are shown in Appendix C. Another comparison is made by calculating the ratio of $Q_t/dP.V_r$. This is the ratio of heat duty and pumping power and is non-dimensional. It is an index of how well the expended pressure drop is utilized for heat transfer. A summary of the comparison is shown in Appendix C and represented in graphical form in the following figures.

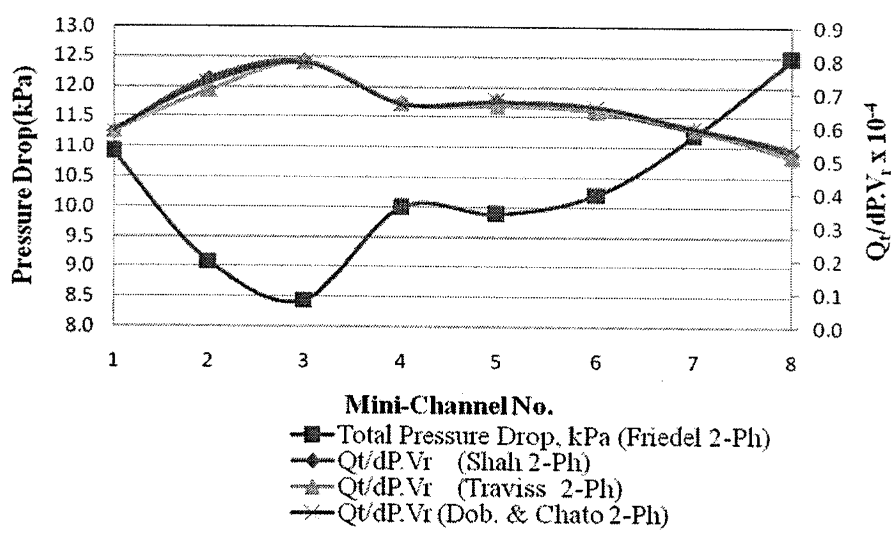

Fig. 5.1: Comparison of $Q_t/dP.V_r$ for Mini-Channel Heat Exchanger with 2-Pass Flow Configuration and Various Tube Passes.

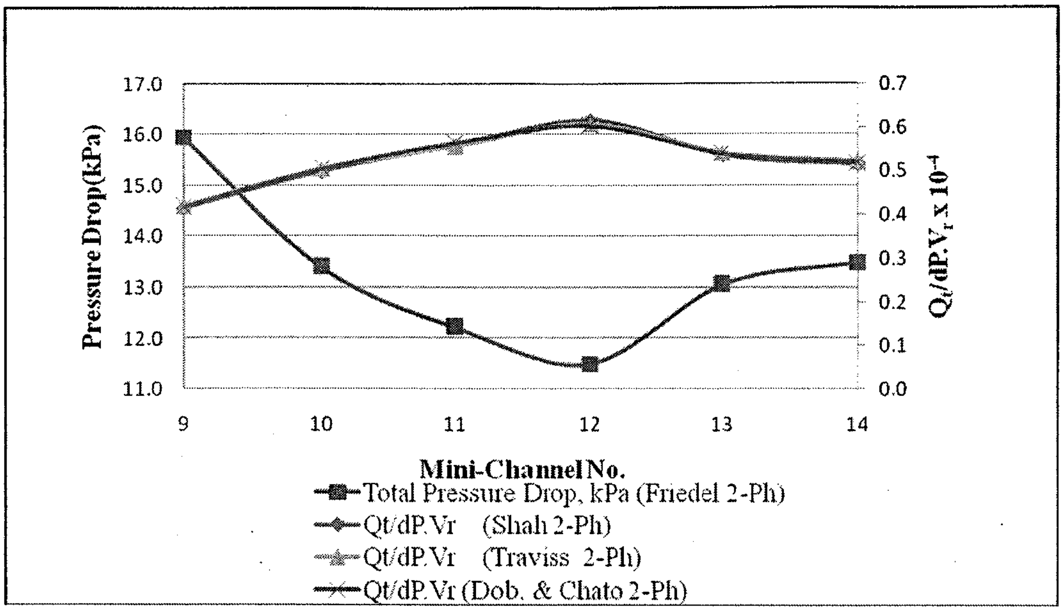

Fig. 5.2: Comparison of $Q_t/dP.V_r$ for Mini-Channel Heat Exchanger with 3-Pass Flow Configuration and Various Tube Passes.

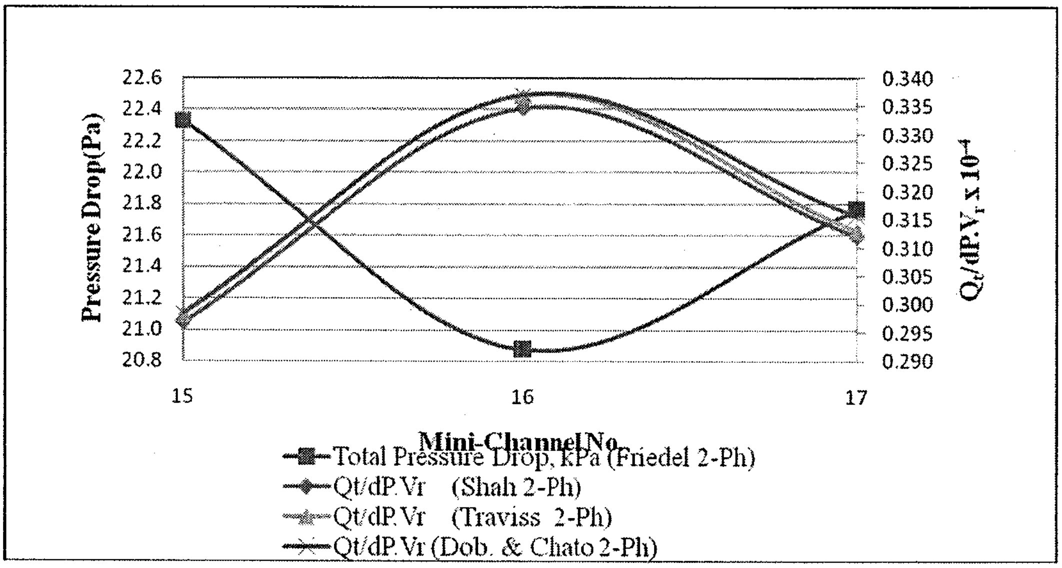

Fig. 5.3: Comparison of $Q_t/dP.V_r$ for Mini-Channel Heat Exchanger with 4-Pass Flow Configuration and Various Tube Passes.

Figures 5.1 to 5.3 show the ratio of $Q_t/dP.V_r$ and pressure drop for 2-pass , 3-pass and 4-pass flow configurations at various tube pass ratios. Figure 5.1 shows that mini-channel heat exchanger number 3 with a configuration of 2-pass flow and tube pass ratio of 85-15 yields the highest $Q_t/dP.V_r$ compared to the other heat exchangers with 2-pass flow. This heat exchanger also yields the lowest pressure drop compared with the others. Figure 5.2 shows that mini-channel heat exchanger number 12 with a configuration of 3-pass flow and tube pass ratio of 70-20-10 yields the highest $Q_t/dP.V_r$ compared to the other heat exchangers with 3 flow pass. This heat exchanger also yields the lowest pressure drop compared with the others. Figure 5.3 shows that mini-channel heat exchanger number 16 with a configuration of 4-pass flow and tube pass ratio of 45-25-18-12 yields the highest $Q_t/dP.V_r$ compared to the other heat exchangers with 4-pass flow. This heat exchanger also yields the lowest pressure drop compared with the others. These results showed that pressure drop is a more dominant factor compared to heat transfer in order to determine the optimum mini-channel heat exchanger.

It can be seen that the mini-channel with the highest $Q_t/dP.V_r$ is the mini-channel with 85-15 tube pass ratio and 2-pass flow configuration. Comparing the same flow pass configuration, mini-channels with equal tube pass ratio is found to be with the lowest $Q_t/dP.V_r$.

For comparison purpose, the heat transfer in the two phase condensing region are calculated using Shah, Traviss and Dobson and Chato correlations while the heat transfer in the superheated and subcooled region are calculated using the Σ-NTU method. The results obtained are very close to each other. The total variation in heat transfer among results of different correlations was less than ±5%.

Table 5.1: Comparison of Length Required for Different Region of Heat Transfer in Mini-Channel Heat Exchanger

No of Passes	No	Tube Pass Ratio	Tube Pass No.	Region of Heat Transfer in Mini-Channel Heat Exchanger		
				Superheated Region, Lsh(m) [*hi*]	Two Phase Condensing, Ltp (m) [exit quality, *x*]	Subcooled Region, Lsc(m) [*hi*]
2-Pass	1	95-5	One	0.132 [199]	0.325 [0.10]	-
			Two	-	0.016 [0.03]	0.441[3360]
	2	90-10	One	0.126 [232]	0.332 [0.11]	-
			Two	-	0.033 [0.03]	0.424[1995]
	3	85-15	One	0.122 [268]	0.336 [0.13]	-
			Two	-	0.034 [0.03]	0.423[1096]
	4	80-20	One	0.120 [307]	0.338 [0.17]	-
			Two	-	0.051 [0.03]	0.406 [442]
	5	75-25	One	0.120 [326]	0.338 [0.19]	-
			Two	-	0.068 [0.03]	0.389 [266]
	6	70-30	One	0.123 [377]	0.335 [0.25]	-
			Two	-	0.084 [0.03]	0.373 [266]
	7	60-40	One	0.134 [437]	0.324[0. 36]	-
			Two	-	0.162 [0.03]	0.295 [266]
	8	50-50	One	0.149 [490]	0.309 [0.47]	-
			Two	-	0.263 [0.03]	0.194 [266]
3-Pass	9	33-33-33	One	0.197 [651]	0.260[0.69]	
			Two		0.457[0.13]	
			Three		0.091 [0.03]	0.366 [266]
	10	40-30-30	One	0.178 [588]	0.279 [0.62]	
			Two		0.419 [0.03]	0.039 [266]
			Three			0.457 [266]
	11	50-30-20	One	0.151 [499]	0.306 [0.49]	
			Two		0.260 [0.03]	0.197 [442]
			Three			0.457 [442]
	12	70-20-10	One	0.122 [378]	0.335 [0.25]	
			Two		0.101 [0.03]	0.357 [1995]
			Three			0.457 [1995]
	13	60-30-10	One	0.133 [437]	0.324 [0.36]	
			Two		0.162 [0.03]	0.295 [1995]
			Three			0.457 [1995]
	14	55-30-15	One	0.141 [466]	0.316 [0.42]	
			Two	0.214 [0.80]	0.205 [0.03]	0.252 [1096]
			Three			0.457 [1096]

No of Passes	No	Tube Pass Ratio	Tube Pass No.	Region of Heat Transfer in Mini-Channel Heat Exchanger		
				Superheated Region, Lsh(m) [*hi*]	Two Phase Condensing, Ltp (m) [exit quality, *x*]	Subcooled Region, Lsc(m) [*hi*]
4-Pass	15	25-25-25-25	One	0.243 [806]	0.214 [0.80]	-
			Two	-	0.457 [0.37]	-
			Three	-	0.375 [0.03]	0.083 [266]
			Four	-	-	0.457 [266]
	16	45-25-18-12	One	0.157 [518]	0.300 [0.52]	-
			Two	-	0.285 [0.03]	0.172 [266]
			Three	-	-	0.457 [689]
			Four	-	-	0.457 [1995]
	17	40-30-20-10	One	0.178 [588]	0.279 [0.62]	-
			Two	-	0.419 [0.03]	0.039 [266]
			Three	-	-	0.457 [442]
			Four	-	-	0.457 [1995]

The heat transfer region and the corresponding number of tubes and tube length required for each region are tabulated in Table 5.1. The following observations are made from Table 5.1.

a) In the superheated region, the refrigerant mass flux is inversely proportional to the number of tubes in the pass. When the number of tubes in the pass is high as in the 2-pass flow and 95-5 tube pass ratio the refrigerant mass flux is low, which resulted in a low refrigerant heat transfer coefficient. In order to achieve the required heat transfer in this region, more tubes' surface area will be needed. When the number of tubes in the pass reduces as in the 2-pass flow and 85-15 tube pass ratio the refrigerant mass flux is higher, which resulted in a higher heat transfer coefficient. The required tube surface area now reduces. When considering only the 2-pass flow heat exchangers, the number of tubes in the first pass is the least in the 50-50 tube pass ratio but the refrigerant mass flux is the highest. However since the number of tubes is the least here, the heat exchange takes place over a longer tube length.

b) In the two phase region, the number of tubes is proportional to the difference in refrigerant quality between the entering and exit refrigerant in each segment. The more tubes in the pass, the larger is the difference in refrigerant quality. This results in quicker achievement of exit quality of zero where the two phase heat transfer region ends. In turn the remaining tubes can be utilized for subcooling in the subcool region.

c) In the subcooled region, the more the available area for heat transfer, the higher is the subcooling. This in turn results in higher heat transfer rate in the subcool region on account of a higher ΔT. Another factor that affects the heat transfer is the heat transfer coefficient. Refrigerant which flows through a pass with less number of tubes has higher mass flux compared to a pass with more tubes.

The above consideration is true, if heat transfer rate is the only design criterion for the mini-channel heat exchanger. However the refrigerant pressure drop is another design criterion which must be considered in order to come out with an optimum mini-channel design.

The pressure drop calculation for superheated and subcooled region are based on the Churchill correlation while the two-phase condensing pressure drop is based on the Friedel correlation. A summary of pressure drop calculations in each region is shown in Table 5.2.

Table 5.2: Comparison of Pressure Drop in Different Regions of Heat Transfer in Mini-Channel Heat Exchanger (using Friedel correlation)

No of Passes	No	Tube Pass Ratio	Pressure Drop, Pa			
			Superheated Region	2 phase Condensing Region (Friedel)	Subcooled Region	Total
2-Pass	1	95-5	889	5,186	4,841	10,916
	2	90-10	902	5,360	2,823	9,085
	3	85-15	912	5,513	2,023	8,448
	4	80-20	946	7,773	1,274	9,993
	5	75-25	967	8,024	897	9,888
	6	70-30	1,062	8,402	752	10,216
	7	60-40	1,301	9,299	594	11,194
	8	50-50	1,642	10,438	393	12,473
3-Pass	9	33-33-33	2,941	12,285	736	15,962
	10	40-30-30	2,385	10,319	696	13,400
	11	50-30-20	1,698	8,196	2,330	12,224
	12	70-20-10	1,064	6,543	3,892	11,499
	13	60-30-10	1,301	6,953	4,814	13,068
	14	55-30-15	1,473	7,490	4,533	13,496
4-Pass	15	25-25-25-25	4,525	16,705	1,101	22,331
	16	45-25-18-12	1,836	8,554	10,483	20,873
	17	40-30-20-10	2,385	10,317	9,061	21,763

It can be observed from Fig. 5.1 to 5.3, that there is a pressure drop trend. They are summarized as follows:

1) The less the number of tubes in the pass, the higher is the refrigerant mass flux. This in turn will result in a higher pressure drop. This is observed in the superheated and subcooled regions.
2) In the mini-channel with 2-pass flow configuration, the two phase heat transfer takes place in both passes. The dominant factors that affect pressure drop are the refrigerant mass flux to the power of two, G^2 and the number of tubes in each pass. In the 2-pass flow configuration, the pass with more number of tubes has lower mass flux while the pass with less number of tubes has higher mass flux. Refrigerant that flows through each tube experiences pressure drop so that the greater the number of tubes in a pass the higher is the sum of the pressure drop across that pass. This explains the lowest pressure drop calculated in the two phase region in the mini-channel with tube pass ratio 95-5. In the same way, for 3-pass flow configuration the lowest pressure drop in the two phase region is found in the mini-channel with tube pass ratio 70-20-10 while for 4-pass flow configuration is found in the mini-channel with tube pass ratio 45-25-18-12.
3) However when the total pressure drops of all three regions are taken into account, the 2-pass flow mini-channel with tube pass ratio 85-15 has the lowest pressure drop.

   For calculation of pressure drop in the two phase condensing region, the Friedel correlation is replaced with Cavallini correlation. The results are shown in Table 5.3.

Table 5.3: Comparison of Pressure Drop in Different Regions of Heat Transfer in Mini-Channel Heat Exchanger (using Cavallini correlation)

No of Passes	No	Tube Pass Ratio	Pressure Drop, Pa (Cavallini 2-Ph)			
			Desuperheating	2 phase cond	Subcooling	Total
2-Pass	1	95-5	889	7,831	4,841	13,561
	2	90-10	902	8,036	2,823	11,761
	3	85-15	912	8,179	2,023	11,114
	4	80-20	946	11,961	1,274	14,181
	5	75-25	967	12,201	897	14,065
	6	70-30	1,062	12,706	752	14,520
	7	60-40	1,301	13,662	594	15,557
	8	50-50	1,642	14,978	393	17,013
3-Pass	9	33-33-33	2,941	15,687	736	19,364
	10	40-30-30	2,385	13,469	696	16,550
	11	50-30-20	1,698	11,147	2,330	15,175
	12	70-20-10	1,064	9,384	3,892	14,340
	13	60-30-10	1,301	9,815	4,814	15,930
	14	55-30-15	1,473	10,390	4,533	16,396
4-Pass	15	25-25-25-25	4,525	22,437	1,101	28,063
	16	45-25-18-12	1,836	11,470	10,483	23,789
	17	40-30-20-10	2,385	12,700	9,061	24,146

The results showed that calculated pressure drop using Cavallini correlation are higher than using Friedel correlation. However the trend of pressure drop is the same as seen in Fig. 5.4 to 5.6. Hence, the Cavallini results are used in further comparisons.

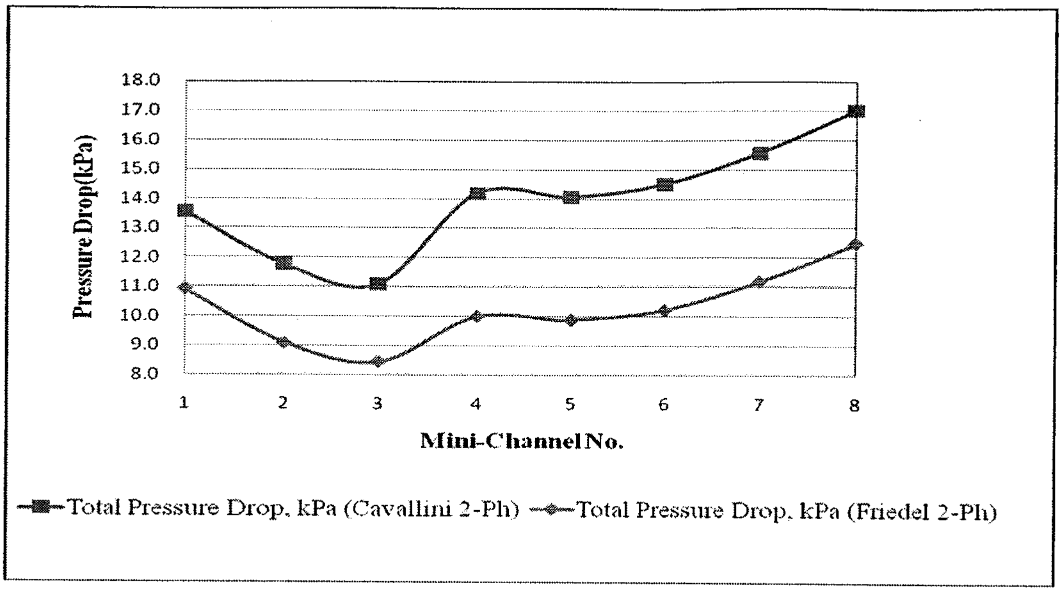

Fig. 5.4: Comparison of Pressure Drop for Mini-Channel Heat Exchanger with 2-Pass Flow Configuration and Various Tube Passes.

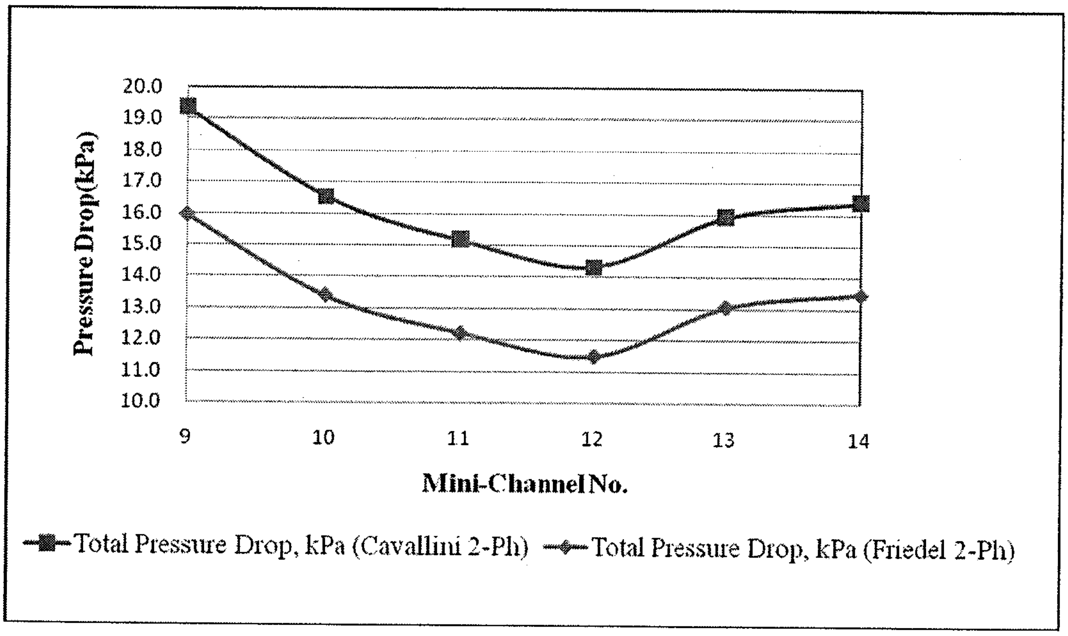

Fig. 5.5: Comparison of Pressure Drop for Mini-Channel Heat Exchanger with 3-Pass Flow Configuration and Various Tube Passes.

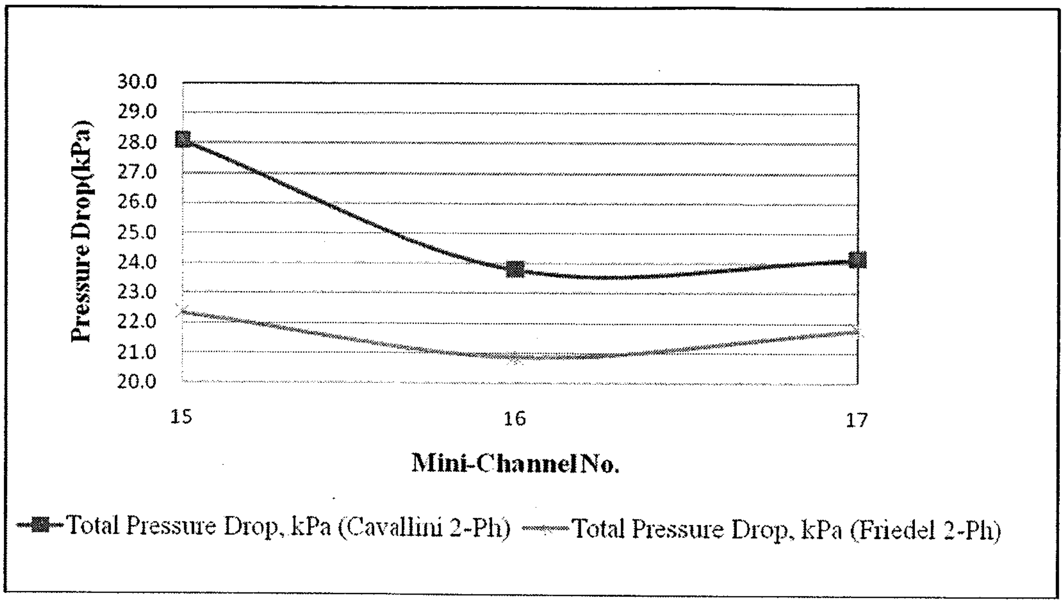

Fig. 5.6: Comparison of Pressure Drop for Mini-Channel Heat Exchanger with 4-Pass Flow Configuration and Various Tube Passes.

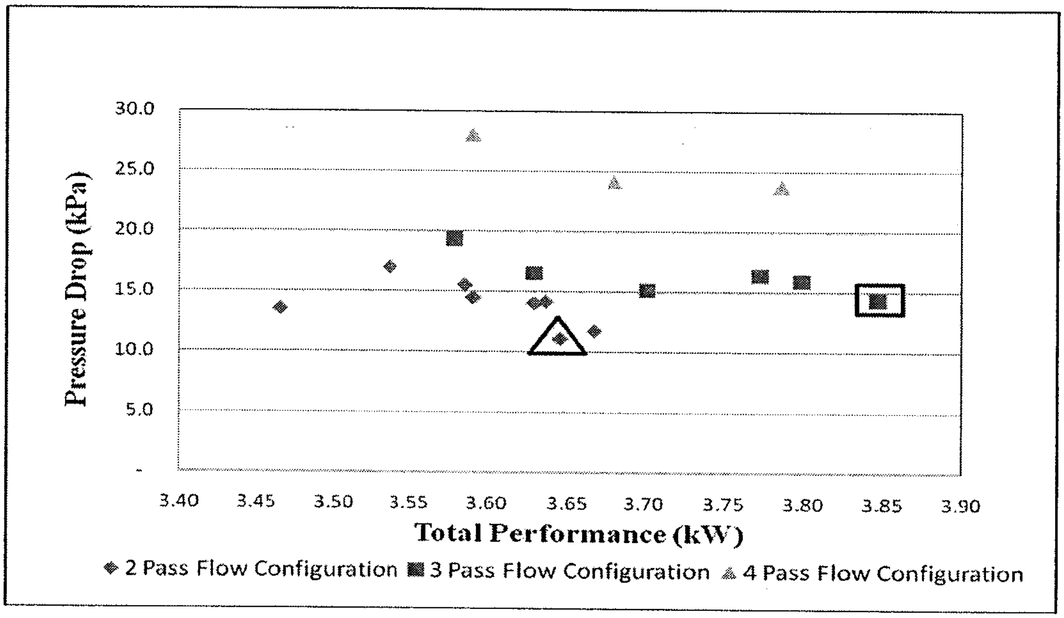

Fig. 5.7: Comparison between Mini-Channel with Different Tube Pass Ratios and Flow Pass Configurations in terms of Thermal and Hydraulic Performance

In combining the total heat transfer and pressure drop performance of the various mini-channels under study, it can be seen from Figure 5.7 that the mini-channel with 2-pass flow and tube pass ratio 85-15 yields the lowest pressure drop (shown by diamond symbol) while the mini-channel with 3-pass flow and tube pass ratio 70-20-10 yields the highest heating performance (shown by square symbol).

The analysis for the mini-channel mentioned above is compared to test results. For comparison, results calculated using the Shah correlation for two phase heat transfer and Cavallini correlation for two phase pressure drop are used. The results are as shown in Table 5.4. Compared to test results for a MCHX with 70-30 tube pass ratio and 2 pass flow configuration, the analysis over-predicts the thermal performance by about 1% and under-predicts the hydraulic performance by < 7%.

Table 5.4: Psychrometric Test Results of Mini-Channel with 2-Pass Flow Configuration and 70-30 Tube Pass Ratio

Measured Parameter	**Unit**	Value
Condenser Inlet Pressure	kPa	3055
Condenser Inlet Temperature	°C	81.80
Condenser Outlet Pressure	kPa	3040
Condenser Outlet Temperature	°C	44.4
Measured Condenser Heating Performance	W	**3522**
Measured Pressure Drop Across Condenser	kPa	**15**

Calculated Parameter	**Unit**	**Value**
Calculated Heating Performance	W	**3563**
Calculated Pressure Drop Across Condenser	kPa	**14**
Deviation between measured and calculated heating performance	%	**+ 1.16**
Deviation between measured and calculated pressure drop	%	**- 6.67**

5.3 Chapter summary

From this study, it is concluded that the optimum design in terms of tube pass ratio and flow pass configuration is the mini-channel with 85-15 tube pass ratio and 2 pass flow configuration. Pressure drop predictions by the Cavallini correlation were higher and much closer to experiments. Hence only the Cavalini results were considered in the validation of the simulation results. Compared to test results for a MCHX with 70-30 tube pass ratio and 2 pass flow configuration, the analysis over-predicts the thermal performance by about 1% and under-predicts the hydraulic performance by < 7%. This is satisfactory, considering that two-phase flow and condensation heat transfer in mini-channels is still an evolving art. Mini-channel design with equal tube pass ratio is not recommended due to low thermal performance and high pressure drop.

CHAPTER 6

CONCLUSION

6.1 Chapter overview

The main findings from this research are reviewed in this chapter. The objectives achieved in this research are also discussed. Numerical simulation using known correlations for condensing coefficient and refrigerant side pressure drop is used to predict the thermal and hydraulic performance of mini-channel heat exchangers respectively and a good accuracy has been obtained. Finally, recommendations for future work arising from this research are given.

6.2 Review of findings

Mini-channel heat exchangers with different tube pass ratios and flow pass configurations have been compared using numerical simulation. The simulation showed that an optimum mini-channel heat exchanger design is a balance between good thermal performance and reasonable refrigerant side pressure drop. The factors which govern the thermal performance are the mass flux and the number of tubes in each pass. The more the number of tubes per pass, the lower is the mass flux. When the mass flux is low, a longer tube length is needed for heat transfer to take place in the superheated region. In the two-phase region, the more the number of tubes the quicker it will be for the refrigerant to achieve an exit quality of zero and this would result in more area being available in the subsequent tubes for subcooling to take place. This in turn contributes to good thermal performance. However pressure drops are influenced by the square of mass flux and number of tubes in each flow pass. This is obvious when we look at a two flow pass heat exchanger and the pressure drop in two-phase region which takes place in both passes. Refrigerant which flows through the first pass with more number of tubes has lower mass flux while refrigerant which flows through the second pass with less number of tubes has higher mass flux. The pressure drop in each pass is dependent on whether mass flux or number of tubes is the dominant factor. Another point to consider is when there is more tube length for subcooling, the pressure drop in the subcool region increases compared to when there is less tube length. In the desuperheating region where there are more tubes, the mass flux is lower compared to a region where there are less number of tubes. This in turn contributes to lower pressure drop in the desuperheating region. In summing up, the pressure drop in all these three regions and comparing them one with one another, we have a pressure trend. The right way to analyse these results for each heat exchanger is to calculate $Q_t/ dP.V_r$ which is dimensionless. The heat exchanger with the highest $Q_t/ dP.V_r$ is chosen as the optimum MCHX. In this study, the optimum MCHX is the one with 2-pass flow and tube pass ratio of 85-15.

6.3 Recommendations for future research

The heat exchanger with 2-pass flow configuration and 70-30 tube pass ratio is chosen for the psychrometric test and for validation of the simulation as it is a standard manufactured product and is easily available. Future work can be extended for example, to test other MCHXs with different tube pass ratios but with the same flow pass configuration.

The Wilson Plot tests were conducted with an assumption that the air entering the heat exchanger is uniform. The air side maldistribution has not been considered and future studies can be carried out to understand this problem.

This study has been on mini-channel heat exchanger as condenser. Future study can focus on mini-channel as evaporator. The process is similar except that the refrigerant enters the evaporator at a vapor quality between 0.1- 0.2 and exits at a quality greater than 1.0, i.e., in superheated state. Simulations of heat transfer and pressure drop in evaporator also require a different set of specific correlations for evaporation.

This study focused on one particular size of mini-channel condenser. Different sizes of mini-channel condenser require different refrigerant mass fluxes and the optimum heat exchanger may not be the same as discovered in this study. However, the methodology developed in the present study is directly applicable in every other case.

6.4 Chapter summary

The objectives of this research work were mentioned in Section 1.5 and from the research findings it can be concluded that both objectives had been met satisfactorily. The numerical simulation method used in this study was successfully used to predict the thermal and hydraulic performance of MCHXs with different flow pass configurations and tube pass ratios. The numerical simulation method was also used to predict an optimum MCHX design, which is the MCHX with the highest $Q_t / dP.V_r$. The benefit of this work to air conditioner designers is to help them to reduce tremendous and time-consuming experimental work. An optimum MCHX design will ensure that the air conditioner is designed to operate efficiently.

APPENDIX A-1

Hydraulic Experiment Data

Test No	Q, m3/hr	dP, Pa	V, m/s	*Re*	f_F
1	0.01380	95	0.26	233	0.0482
2	0.01440	99	0.27	243	0.0467
3	0.01500	103	0.28	253	0.0476
4	0.01560	108	0.29	264	0.0460
5	0.01620	112	0.30	273	0.0450
6	0.01680	116	0.31	285	0.0433
7	0.01800	124	0.34	303	0.0428
8	0.01860	128	0.35	315	0.0411
9	0.01980	137	0.37	336	0.0402
10	0.02040	141	0.38	344	0.0395
11	0.02100	145	0.39	354	0.0384
12	0.02220	153	0.41	377	0.0362
13	0.02340	161	0.44	398	0.0353
14	0.02520	174	0.47	429	0.0345
15	0.02700	186	0.50	460	0.0329
16	0.02880	199	0.54	491	0.0319
17	0.02940	203	0.55	495	0.0316
18	0.03060	211	0.57	523	0.0299
19	0.03300	228	0.62	564	0.0285
20	0.03420	236	0.64	588	0.0282
21	0.03660	252	0.68	627	0.0270
22	0.03840	265	0.72	658	0.0259
23	0.03840	265	0.72	657	0.0267
24	0.03900	269	0.73	686	0.0265
25	0.04020	277	0.75	706	0.0265
26	0.04200	290	0.78	736	0.0263
27	0.04320	298	0.81	743	0.0267
28	0.04380	302	0.82	739	0.0280
29	0.04440	306	0.83	763	0.0287
30	0.04620	319	0.86	794	0.0295
31	0.04800	331	0.90	825	0.0304
32	0.04920	339	0.92	833	0.0320
33	0.05160	356	0.96	1017	0.0314
34	0.05460	376	1.02	917	0.0314
35	0.05760	397	1.07	1177	0.0310
36	0.06180	426	1.15	1033	0.0315

APPENDIX A-2

Hydraulic Experiment Data

Test No	Q, m3/hr	dP, Pa	V, m/s	*Re*	f_F
37	0.06720	463	1.25	1382	0.0307
38	0.07260	501	1.35	1207	0.0306
39	0.07740	534	1.44	1606	0.0300
40	0.08340	575	1.56	1380	0.0298
41	0.08880	612	1.66	1854	0.0300
42	0.09360	645	1.75	1545	0.0297
43	0.09840	678	1.83	2059	0.0292
44	0.10440	720	1.95	1706	0.0292
45	0.10980	757	2.05	2299	0.0290
46	0.11460	790	2.14	1890	0.0291
47	0.11940	823	2.23	2425	0.0292
48	0.12480	860	2.33	2070	0.0290
49	0.12960	894	2.42	2862	0.0287
50	0.13020	898	2.43	2184	0.0289
51	0.13920	960	2.60	3089	0.0289
52	0.14520	1001	2.71	2446	0.0288
53	0.15000	1034	2.80	3348	0.0288
54	0.15540	1071	2.90	2642	0.0288
55	0.16020	1105	2.99	3591	0.0285
56	0.16620	1146	3.10	2842	0.0285
57	0.17040	1175	3.18	3828	0.0284
58	0.17640	1216	3.29	3050	0.0284
59	0.18120	1249	3.38	4074	0.0286
60	0.18660	1287	3.48	3249	0.0284
61	0.19080	1316	3.56	4302	0.0283
62	0.19680	1357	3.67	3462	0.0284
63	0.20100	1386	3.75	4535	0.0283
64	0.20700	1427	3.86	3692	0.0283
65	0.21060	1452	3.93	4666	0.0284
66	0.21720	1498	4.05	3932	0.0283
67	0.22080	1522	4.12	4820	0.0287
68	0.22680	1564	4.23	4196	0.0284
69	0.23040	1589	4.30	5002	0.0286
70	0.23700	1634	4.42	4414	0.0284
71	0.24180	1667	4.51	5230	0.0286
72	0.24720	1704	4.61	4659	0.0284

APPENDIX A-3

Hydraulic Experiment Data

Test No	Q, m3/hr	dP, Pa	V, m/s	*Re*	f_F
73	0.25140	1733	4.69	5387	0.0285

APPENDIX B-1

Wilson Plot Experiment Data

		250CFM & 0.80 m^3/hr			250CFM & 0.90 m^3/hr		
Parameter	Unit	Average 1	Average 2	Average 3	Average 1	Average 2	Average 3
Ta,in DB :	°C	20.05	20.00	20.04	19.97	19.95	19.99
Ta,in WB :	°C	13.16	13.52	13.10	13.15	13.09	13.12
Ta,out DB :	°C	44.39	44.37	44.34	44.59	44.64	44.64
Ta,out WB :	°C	21.50	21.79	21.52	21.56	21.54	21.57
Taout WB Calc:	°C	21.50	21.79	21.52	21.56	21.54	21.57
Tw,in :	°C	50.00	50.00	49.95	49.96	49.96	49.96
Tw,out :	°C	46.61	46.59	46.55	46.90	46.91	46.92
Water Flow Rate :	m^3/hr	0.80	0.80	0.80	0.90	0.90	0.90
P Barometric :	inHg	29.53	29.55	29.64	29.58	29.53	29.51
DP Nozzle :	mmAq	25.28	25.29	25.39	25.30	25.26	25.24
PS before Nozzle :	mmAq	-1.93	-1.96	-1.89	-1.90	-1.89	-1.85
DP Coil :	mmAq	0.82	0.80	0.83	0.82	0.83	0.86
T before Nozzle :	°C	43.45	43.44	43.19	43.60	43.70	43.71
Air Flow	CFM	250.01	250.02	249.97	249.97	250.02	250.02
Air Side Capacity:	Btu/hr	10929.74	10958.30	10959.35	11067.25	11078.69	11050.64
Water Side Capacity:	Btu/hr	10750.94	10796.01	10772.02	10920.25	10881.53	10855.49
Heat Balance:	%	1.64	1.48	1.71	1.33	1.78	1.77
Log Mean Temp	°C	34.83	34.79	34.79	35.05	35.10	35.12

APPENDIX B-2

Wilson Plot Experiment Data

		250CFM & 1.00 m^3/hr			250CFM & 1.10 m^3/hr		
Parameter	Unit	Average 1	Average 2	Average 3	Average 1	Average 2	Average 3
Ta,in DB :	°C	19.95	19.97	19.99	20.01	19.99	19.95
Ta,in WB :	°C	13.26	13.28	13.30	13.13	13.13	13.23
Ta,out DB :	°C	44.87	44.90	44.89	45.00	45.05	45.05
Ta,out WB :	°C	21.85	21.88	21.87	21.80	21.82	21.88
Taout WB Calc:	°C	21.85	21.88	21.87	21.80	21.82	21.88
Tw,in :	°C	49.95	49.99	49.98	49.95	50.02	50.00
Tw,out :	°C	47.21	47.24	47.23	47.45	47.52	47.49
Water Flow Rate :	m^3/hr	1.00	1.00	1.00	1.10	1.10	1.10
P Barometric :	inHg	29.49	29.48	29.48	29.60	29.60	29.53
DP Nozzle :	mmAq	25.19	25.19	25.20	25.29	25.29	25.23
PS before Nozzle :	mmAq	-1.83	-1.83	-1.82	-1.85	-1.85	-1.89
DP Coil :	mmAq	0.86	0.86	0.87	0.85	0.85	0.83
T before Nozzle :	°C	43.95	43.99	43.96	43.99	44.01	44.10
Air Flow	CFM	249.97	249.99	250.04	249.98	250.00	250.03
Air Side Capacity:	Btu/hr	11158.81	11159.66	11144.20	11226.60	11260.43	11249.53
Water Side Capacity:	Btu/hr	10890.56	10914.96	10907.47	10901.93	10940.34	10962.05
Heat Balance:	%	2.40	2.19	2.12	2.89	2.84	2.56
Log Mean Temp	°C	35.38	35.40	35.40	35.57	35.59	35.58

APPENDIX B-3

Wilson Plot Experiment Data

		250CFM & 1.20 m^3/hr		
Parameter	Unit	Average 1	Average 2	Average 3
Ta,in DB :	°C	20.04	20.00	19.97
Ta,in WB :	°C	13.12	13.10	13.10
Ta,out DB :	°C	45.15	45.11	45.15
Ta,out WB :	°C	21.70	21.67	21.69
Taout WB Calc:	°C	21.70	21.67	21.69
Tw,in :	°C	50.02	49.98	50.03
Tw,out :	°C	47.72	47.68	47.72
Water Flow Rate :	m^3/hr	1.20	1.20	1.20
P Barometric :	inHg	29.55	29.54	29.54
DP Nozzle :	mmAq	25.24	25.24	25.23
PS before Nozzle :	mmAq	-1.98	-1.99	-1.98
DP Coil :	mmAq	0.79	0.78	0.79
T before Nozzle :	°C	44.09	44.04	44.10
Air Flow	CFM	250.01	250.00	250.00
Air Side Capacity:	Btu/hr	11258.78	11254.97	11281.50
Water Side Capacity:	Btu/hr	10989.15	10990.05	11001.62
Heat Balance:	%	2.39	2.35	2.48
Log Mean Temp	°C	35.74	35.70	35.72

APPENDIX B-4

Wilson Plot Experiment Data

		400CFM & 0.80 m^3/hr			400CFM & 0.90 m^3/hr		
Parameter	Unit	Average 1	Average 2	Average 3	Average 1	Average 2	Average 3
Ta,in DB :	°C	19.96	20.03	20.02	19.98	20.01	20.00
Ta,in WB :	°C	15.42	15.59	15.63	13.11	13.70	13.72
Ta,out DB :	°C	41.47	41.44	41.41	41.83	41.84	41.85
Ta,out WB :	°C	22.45	22.56	22.59	20.87	21.30	21.31
Taout WB Calc:	°C	22.45	22.56	22.59	20.87	21.30	21.31
Tw,in :	°C	50.00	50.00	49.96	49.99	49.98	49.99
Tw,out :	°C	45.19	45.19	45.14	45.69	45.68	45.69
Water Flow Rate :	m^3/hr	0.80	0.80	0.80	0.90	0.90	0.90
P Barometric :	inHg	29.59	29.60	29.61	29.62	29.57	29.57
DP Nozzle :	mmAq	16.54	16.55	16.56	16.56	16.53	16.53
PS before Nozzle :	mmAq	-5.33	-5.40	-5.42	-5.24	-5.25	-5.23
DP Coil :	mmAq	1.60	1.57	1.56	1.61	1.61	1.61
T before Nozzle :	°C	40.71	40.67	40.62	41.10	41.17	41.19
Air Flow	CFM	400.00	400.00	399.98	399.97	400.02	400.03
Air Side Capacity:	Btu/hr	15659.62	15601.63	15587.55	15852.58	15826.99	15840.99
Water Side Capacity:	Btu/hr	15181.63	15204.58	15200.86	15283.91	15288.52	15268.10
Heat Balance:	%	3.05	2.54	2.48	3.59	3.40	3.62
Log Mean Temp	°C	32.19	32.20	32.17	32.55	32.57	32.57

APPENDIX B-5

Wilson Plot Experiment Data

		400CFM & 1.00 m^3/hr			400CFM & 1.10 m^3/hr		
Parameter	Unit	Average 1	Average 2	Average 3	Average 1	Average 2	Average 3
Ta,in DB :	°C	20.05	19.96	19.97	20.01	20.01	20.04
Ta,in WB :	°C	13.12	13.07	13.08	13.34	13.28	13.29
Ta,out DB :	°C	42.07	42.06	42.02	42.28	42.31	42.35
Ta,out WB :	°C	20.84	20.82	20.82	21.23	21.19	21.21
Taout WB Calc:	°C	20.84	20.82	20.82	21.23	21.19	21.21
Tw,in :	°C	49.95	50.02	49.95	49.98	49.99	50.01
Tw,out :	°C	46.05	46.10	46.04	46.39	46.40	46.43
Water Flow Rate :	m^3/hr	1.00	1.00	1.00	1.10	1.10	1.10
P Barometric :	inHg	29.62	29.59	29.59	29.52	29.54	29.54
DP Nozzle :	mmAq	16.55	16.54	16.54	16.49	16.50	16.50
PS before Nozzle :	mmAq	-5.37	-5.40	-5.41	-5.36	-5.30	-5.28
DP Coil :	mmAq	1.57	1.57	1.56	1.57	1.59	1.60
T before Nozzle :	°C	41.39	41.20	41.20	41.44	41.50	41.52
Air Flow	CFM	399.98	399.98	399.99	399.99	400.03	400.01
Air Side Capacity:	Btu/hr	15965.08	16007.91	15977.13	16089.67	16120.67	16126.76
Water Side Capacity:	Btu/hr	15423.98	15521.07	15461.06	15605.93	15609.02	15560.14
Heat Balance:	%	3.39	3.04	3.23	3.01	3.17	3.51
Log Mean Temp	°C	32.82	32.77	32.76	33.02	33.03	33.08

APPENDIX B-6

Wilson Plot Experiment Data

		400CFM & 1.20 m^3/hr		
Parameter	Unit	Average 1	Average 2	Average 3
Ta,in DB :	°C	19.97	19.99	20.05
Ta,in WB :	°C	13.14	13.19	13.27
Ta,out DB :	°C	42.47	42.50	42.58
Ta,out WB :	°C	21.15	21.20	21.27
Taout WB Calc:	°C	21.15	21.20	21.27
Tw,in :	°C	49.96	49.96	50.03
Tw,out :	°C	46.67	46.68	46.75
Water Flow Rate :	m^3/hr	1.20	1.20	1.20
P Barometric :	inHg	29.53	29.52	29.51
DP Nozzle :	mmAq	16.48	16.48	16.47
PS before Nozzle :	mmAq	-5.28	-5.27	-5.22
DP Coil :	mmAq	1.60	1.61	1.62
T before Nozzle :	°C	41.69	41.70	41.76
Air Flow	CFM	399.97	400.04	400.01
Air Side Capacity:	Btu/hr	16251.16	16255.51	16257.52
Water Side Capacity:	Btu/hr	15654.01	15610.78	15591.21
Heat Balance:	%	3.67	3.97	4.10
Log Mean Temp	°C	33.20	33.23	33.31

APPENDIX B-7

Wilson Plot Experiment Data

		550CFM & 0.80 m^3/hr			550CFM & 0.90 m^3/hr		
Parameter	Unit	Average 1	Average 2	Average 3	Average 1	Average 2	Average 3
Ta,in DB :	°C	19.97	20.00	19.99	20.01	20.00	20.01
Ta,in WB :	°C	13.34	13.35	13.36	12.86	13.25	13.23
Ta,out DB :	°C	39.14	39.19	39.17	39.46	39.49	39.51
Ta,out WB :	°C	20.16	20.16	20.17	19.83	20.14	20.13
Taout WB Calc:	°C	20.16	20.16	20.17	19.83	20.14	20.13
Tw,in :	°C	49.97	50.05	50.00	49.96	49.96	49.97
Tw,out :	°C	44.07	44.14	44.12	44.66	44.67	44.68
Water Flow Rate :	m^3/hr	0.80	0.80	0.80	0.90	0.90	0.90
P Barometric :	inHg	29.59	29.59	29.57	29.70	29.67	29.66
DP Nozzle :	mmAq	30.88	30.89	30.86	31.00	30.95	30.94
PS before Nozzle :	mmAq	-9.55	-9.54	-9.52	-9.62	-9.63	-9.62
DP Coil :	mmAq	2.55	2.56	2.57	2.54	2.53	2.53
T before Nozzle :	°C	38.60	38.63	38.62	38.73	38.85	38.86
Air Flow	CFM	549.99	550.05	550.01	549.98	550.00	549.99
Air Side Capacity:	Btu/hr	19263.65	19284.97	19262.02	19591.95	19611.26	19611.63
Water Side Capacity:	Btu/hr	18582.39	18612.42	18574.52	18896.05	18871.30	18863.24
Heat Balance:	%	3.54	3.49	3.57	3.55	3.77	3.82
Log Mean Temp	°C	30.43	30.47	30.46	30.73	30.75	30.76

APPENDIX B-8

Wilson Plot Experiment Data

		550CFM & 1.00 m^3/hr			550CFM & 1.10 m^3/hr		
Parameter	Unit	Average 1	Average 2	Average 3	Average 1	Average 2	Average 3
Ta,in DB :	°C	20.04	20.02	19.97	19.99	19.98	19.97
Ta,in WB :	°C	13.20	13.22	13.23	14.12	13.09	13.16
Ta,out DB :	°C	39.80	39.81	39.82	40.06	40.00	40.03
Ta,out WB :	°C	20.24	20.30	20.32	21.12	20.21	20.31
Taout WB Calc:	°C	20.24	20.30	20.32	21.12	20.21	20.31
Tw,in :	°C	49.98	49.97	49.98	50.02	49.98	50.00
Tw,out :	°C	45.14	45.13	45.14	45.56	45.51	45.54
Water Flow Rate :	m^3/hr	1.00	1.00	1.00	1.10	1.10	1.10
P Barometric :	inHg	29.55	29.53	29.53	29.52	29.61	29.60
DP Nozzle :	mmAq	13.90	13.90	13.89	13.87	13.93	13.92
PS before Nozzle :	mmAq	-9.92	-9.92	-9.90	-10.00	-9.98	-10.01
DP Coil :	mmAq	2.56	2.56	2.56	2.54	2.55	2.54
T before Nozzle :	°C	39.11	39.14	39.18	39.31	39.20	39.28
Air Flow	CFM	549.97	550.08	550.00	550.00	549.98	550.01
Air Side Capacity:	Btu/hr	19791.66	19812.35	19866.43	20088.73	20084.52	20108.70
Water Side Capacity:	Btu/hr	19102.12	19074.86	19113.61	19345.61	19388.21	19388.68
Heat Balance:	%	3.48	3.72	3.79	3.70	3.47	3.58
Log Mean Temp	°C	31.03	31.03	31.02	31.23	31.19	31.21

APPENDIX B-9

Wilson Plot Experiment Data

		550CFM & 1.20 m^3/hr		
Parameter	Unit	Average 1	Average 2	Average 3
Ta,in DB :	°C	20.01	19.96	20.00
Ta,in WB :	°C	14.21	14.12	14.13
Ta,out DB :	°C	40.26	40.24	40.25
Ta,out WB :	°C	21.27	21.19	21.18
Taout WB Calc:	°C	21.27	21.19	21.18
Tw,in :	°C	49.96	49.96	49.98
Tw,out :	°C	45.86	45.85	45.88
Water Flow Rate :	m^3/hr	1.20	1.20	1.20
P Barometric :	inHg	29.52	29.52	29.52
DP Nozzle :	mmAq	13.86	13.86	13.87
PS before Nozzle :	mmAq	-9.92	-9.98	-9.99
DP Coil :	mmAq	2.57	2.55	2.54
T before Nozzle :	°C	39.52	39.48	39.48
Air Flow	CFM	549.97	549.91	550.01
Air Side Capacity:	Btu/hr	20262.67	20279.95	20259.47
Water Side Capacity:	Btu/hr	19444.26	19449.98	19466.70
Heat Balance:	%	4.04	4.09	3.91
Log Mean Temp	°C	31.43	31.40	31.42

APPENDIX B-10

Wilson Plot Experiment Data

		700CFM & 0.80 m^3/hr			700CFM & 0.90 m^3/hr		
Parameter	Unit	Average 1	Average 2	Average 3	Average 1	Average 2	Average 3
Ta,in DB :	°C	20.00	20.00	19.97	20.03	20.01	19.99
Ta,in WB :	°C	13.52	13.54	13.48	13.53	13.50	13.50
Ta,out DB :	°C	37.09	37.08	37.07	37.61	37.53	37.52
Ta,out WB :	°C	19.60	19.63	19.58	19.79	19.71	19.72
Taout WB Calc:	°C	19.60	19.63	19.58	19.79	19.71	19.72
Tw,in :	°C	49.97	49.95	49.97	49.96	49.97	49.95
Tw,out :	°C	43.15	43.13	43.13	43.85	43.83	43.80
Water Flow Rate :	m^3/hr	0.80	0.80	0.80	0.90	0.90	0.90
P Barometric :	inHg	29.60	29.60	29.60	29.56	29.58	29.59
DP Nozzle :	mmAq	22.74	22.73	22.74	22.66	22.69	22.70
PS before Nozzle :	mmAq	-16.09	-16.13	-16.12	-15.82	-15.94	-15.96
DP Coil :	mmAq	3.65	3.63	3.64	3.71	3.67	3.66
T before Nozzle :	°C	36.50	36.50	36.44	37.02	36.88	36.85
Air Flow	CFM	700.04	699.98	699.98	700.00	699.96	699.96
Air Side Capacity:	Btu/hr	22006.35	21985.37	22013.20	22554.82	22513.16	22526.04
Water Side Capacity:	Btu/hr	21505.67	21497.98	21537.40	21704.72	21786.92	21806.56
Heat Balance:	%	2.28	2.22	2.16	3.77	3.23	3.19
Log Mean Temp	°C	29.04	29.04	29.02	29.44	29.38	29.37

APPENDIX B-11

Wilson Plot Experiment Data

		700CFM & 1.00 m^3/hr			700CFM & 1.10 m^3/hr		
Parameter	Unit	Average 1	Average 2	Average 3	Average 1	Average 2	Average 3
Ta,in DB :	°C	19.98	20.01	19.99	20.00	19.98	20.00
Ta,in WB :	°C	13.27	13.72	13.92	13.59	13.58	13.30
Ta,out DB :	°C	37.89	37.91	37.88	38.24	38.19	38.19
Ta,out WB :	°C	19.66	20.01	20.14	20.08	20.06	19.80
Taout WB Calc:	°C	19.66	20.01	20.14	20.08	20.06	19.80
Tw,in :	°C	50.01	50.02	49.99	50.01	49.93	50.01
Tw,out :	°C	44.39	44.40	44.37	44.84	44.77	44.83
Water Flow Rate :	m^3/hr	1.00	1.00	1.00	1.10	1.10	1.10
P Barometric :	inHg	29.65	29.62	29.61	29.49	29.49	29.67
DP Nozzle :	mmAq	22.72	22.68	22.68	22.56	22.57	22.71
PS before Nozzle :	mmAq	-15.85	-15.89	-15.89	-15.68	-15.66	-15.74
DP Coil :	mmAq	3.69	3.66	3.66	3.68	3.68	3.68
T before Nozzle :	°C	37.29	37.33	37.29	37.69	37.61	37.60
Air Flow	CFM	700.01	699.97	700.02	700.02	700.00	700.03
Air Side Capacity:	Btu/hr	23032.16	22995.56	22994.79	23303.17	23266.19	23384.68
Water Side Capacity:	Btu/hr	22171.65	22161.95	22177.94	22420.45	22379.66	22504.59
Heat Balance:	%	3.74	3.63	3.55	3.79	3.81	3.76
Log Mean Temp	°C	29.65	29.67	29.65	29.93	29.89	29.89

APPENDIX B-12

Wilson Plot Experiment Data

		700CFM & 1.20 m^3/hr		
Parameter	Unit	Average 1	Average 2	Average 3
Ta,in DB :	°C	20.02	20.00	20.03
Ta,in WB :	°C	13.58	13.56	13.57
Ta,out DB :	°C	38.45	38.44	38.50
Ta,out WB :	°C	20.13	20.10	20.12
Taout WB Calc:	°C	20.13	20.10	20.12
Tw,in :	°C	49.96	49.97	50.05
Tw,out :	°C	45.21	45.22	45.29
Water Flow Rate :	m^3/hr	1.20	1.20	1.20
P Barometric :	inHg	29.49	29.49	29.49
DP Nozzle :	mmAq	22.55	22.55	22.55
PS before Nozzle :	mmAq	-15.72	-15.66	-15.66
DP Coil :	mmAq	3.66	3.67	3.67
T before Nozzle :	°C	37.80	37.81	37.83
Air Flow	CFM	700.02	700.02	700.01
Air Side Capacity:	Btu/hr	23542.28	23554.57	23589.87
Water Side Capacity:	Btu/hr	22504.23	22516.00	22572.32
Heat Balance:	%	4.41	4.41	4.31
Log Mean Temp	°C	30.12	30.11	30.15

APPENDIX B-13

Wilson Plot Experiment Data

		850CFM & 0.80 m^3/hr			850CFM & 0.90 m^3/hr		
Parameter	Unit	Average 1	Average 2	Average 3	Average 1	Average 2	Average 3
Ta,in DB :	°C	20.02	19.99	20.03	19.99	20.02	19.99
Ta,in WB :	°C	13.81	13.88	13.82	15.58	13.71	13.74
Ta,out DB :	°C	35.59	35.61	35.62	36.00	35.98	35.97
Ta,out WB :	°C	19.52	19.64	19.56	21.01	19.51	19.56
Taout WB Calc:	°C	19.52	19.64	19.56	21.01	19.51	19.56
Tw,in :	°C	49.98	50.01	49.98	50.01	49.96	49.96
Tw,out :	°C	42.45	42.46	42.46	43.14	43.11	43.11
Water Flow Rate :	m^3/hr	0.80	0.80	0.80	0.90	0.90	0.90
P Barometric :	inHg	29.58	29.58	29.56	29.64	29.58	29.58
DP Nozzle :	mmAq	33.16	33.17	33.13	33.16	33.13	33.13
PS before Nozzle :	mmAq	-23.06	-23.10	-22.97	-22.94	-23.00	-23.01
DP Coil :	mmAq	4.85	4.83	4.87	4.87	4.86	4.85
T before Nozzle :	°C	35.10	35.10	35.15	35.50	35.43	35.42
Air Flow	CFM	849.95	850.04	849.99	850.03	849.96	849.98
Air Side Capacity:	Btu/hr	24429.33	24512.53	24433.56	25181.15	25013.88	25042.35
Water Side Capacity:	Btu/hr	23729.25	23780.83	23698.88	24343.05	24255.71	24283.27
Heat Balance:	%	2.87	2.99	3.01	3.33	3.03	3.03
Log Mean Temp	°C	28.10	28.10	28.12	28.38	28.38	28.36

APPENDIX B-14

Wilson Plot Experiment Data

		850CFM & 1.00 m³/hr			850CFM & 1.10 m³/hr		
Parameter	Unit	Average 1	Average 2	Average 3	Average 1	Average 2	Average 3
Ta,in DB :	°C	20.05	20.12	20.02	20.02	20.02	20.05
Ta,in WB :	°C	13.54	14.40	15.07	13.77	13.75	13.75
Ta,out DB :	°C	36.43	36.47	36.36	36.68	36.65	36.71
Ta,out WB :	°C	19.42	20.08	20.59	19.79	19.76	19.75
Taout WB Calc:	°C	19.42	20.08	20.59	19.79	19.76	19.75
Tw,in :	°C	50.01	50.05	49.92	49.99	49.97	50.05
Tw,out :	°C	43.77	43.80	43.68	44.24	44.22	44.29
Water Flow Rate :	m^3/hr	1.00	1.00	1.00	1.10	1.10	1.10
P Barometric :	inHg	29.53	29.53	29.55	29.53	29.52	29.52
DP Nozzle :	mmAq	33.03	33.01	33.02	33.01	33.00	32.99
PS before Nozzle :	mmAq	-22.76	-22.75	-22.73	-22.81	-22.79	-22.77
DP Coil :	mmAq	4.89	4.89	4.90	4.90	4.90	4.91
T before Nozzle :	°C	35.90	35.96	35.90	36.10	36.08	36.10
Air Flow	CFM	849.94	849.96	849.98	849.99	850.02	849.97
Air Side Capacity:	Btu/hr	25579.12	25550.32	25582.53	26000.81	25953.52	25981.19
Water Side Capacity:	Btu/hr	24624.93	24602.52	24589.56	24931.11	24932.98	24968.24
Heat Balance:	%	3.73	3.71	3.88	4.11	3.93	3.90
Log Mean Temp	°C	28.71	28.76	28.66	28.89	28.87	28.92

APPENDIX B-15

Wilson Plot Experiment Data

		850CFM & 1.20 m^3/hr		
Parameter	Unit	Average 1	Average 2	Average 3
Ta,in DB :	°C	20.01	19.99	19.98
Ta,in WB :	°C	15.38	15.75	15.75
Ta,out DB :	°C	36.88	36.84	36.86
Ta,out WB :	°C	20.98	21.28	21.29
Taout WB Calc:	°C	20.98	21.28	21.29
Tw,in :	°C	50.01	49.99	49.97
Tw,out :	°C	44.67	44.64	44.64
Water Flow Rate :	m^3/hr	1.20	1.20	1.20
P Barometric :	inHg	29.64	29.61	29.57
DP Nozzle :	mmAq	33.07	33.04	32.99
PS before Nozzle :	mmAq	-22.83	-22.93	-22.89
DP Coil :	mmAq	4.89	4.85	4.84
T before Nozzle :	°C	36.29	36.22	36.30
Air Flow	CFM	850.01	849.98	850.04
Air Side Capacity:	Btu/hr	26467.21	26439.14	26435.19
Water Side Capacity:	Btu/hr	25287.62	25303.62	25246.97
Heat Balance:	%	4.46	4.29	4.49
Log Mean Temp	°C	29.04	29.01	29.03

APPENDIX C-1

No of Passes	No	Tube Pass Ratio	Total Pressure Drop, kPa (Friedel 2-Ph)	Q_t, kW (Shah 2-Ph)	$Q_t/dP.V_r$ (Shah 2-Ph)x10^{-4}	Q_t, kW (Traviss 2-Ph)	$Q_t/dP.V_r$ (Traviss 2-Ph)10^{-4}	Q_t, kW (Dob. & Chato 2-Ph)	$Q_t/dP.V_r$ (Dob. & Chato 2-Ph)10^{-4}
2-Pass	1	95-5	10.92	3.47	0.586	3.47	0.586	3.48	0.589
	2	90-10	9.09	3.67	0.745	3.49	0.709	3.61	0.732
	3	85-15	8.45	3.65	0.796	3.65	0.796	3.63	0.792
	4	80-20	9.99	3.64	0.671	3.64	0.672	3.63	0.669
	5	75-25	9.89	3.63	0.677	3.55	0.663	3.63	0.677
	6	70-30	10.22	3.59	0.649	3.59	0.648	3.66	0.661
	7	60-40	11.19	3.59	0.591	3.62	0.597	3.63	0.598
	8	50-50	12.47	3.54	0.523	3.46	0.512	3.60	0.533
3-Pass	9	33-33-33	15.96	3.58	0.414	3.63	0.420	3.61	0.418
	10	40-30-30	13.40	3.63	0.500	3.67	0.505	3.67	0.506
	11	50-30-20	12.22	3.70	0.559	3.69	0.557	3.74	0.564
	12	70-20-10	11.50	3.85	0.617	3.79	0.608	3.77	0.604
	13	60-30-10	13.07	3.80	0.536	3.84	0.542	3.83	0.540
	14	55-30-15	13.50	3.77	0.516	3.81	0.521	3.80	0.520

APPENDIX C-2

No of Passes	No	Tube Pass Ratio	Total Pressure Drop, kPa (Friedel 2-Ph)	Q_t, kW (Shah 2-Ph)	$Q_t/dP.V_r$ (Shah 2-Ph)x10^{-4}	Q_t, kW (Traviss 2-Ph)	$Q_t/dP.V_r$ (Traviss 2-Ph)10^{-4}	Q_t, kW (Dob. & Chato 2-Ph)	$Q_t/dP.V_r$ (Dob. & Chato 2-Ph)10^{-4}
4-Pass	15	25-25-25-25	22.33	3.59	0.297	3.61	0.298	3.61	0.298
	16	45-25-18-12	20.87	3.79	0.335	3.81	0.337	3.81	0.337
	17	40-30-20-10	21.76	3.68	0.312	3.69	0.313	3.72	0.316

APPENDIX C-3

No of Passes	No	Tube Pass Ratio	Total Pressure Drop, kPa (Caval. 2-Ph)	Q_t, kW (Shah 2-Ph)	$Q_t/dP.V_r$ (Shah 2-Ph)x10^{-4}	Q_t, kW (Traviss 2-Ph)	$Q_t/dP.V_r$ (Traviss 2-Ph)10^{-4}	Q_t , kW (Dob. & Chato 2-Ph)	$Q_t/dP.V_r$ (Dob. & Chato 2-Ph)10^{-4}
2-Pass	1	95-5	13.56	3.47	0.471	3.47	0.472	3.48	0.474
	2	90-10	11.76	3.67	0.575	3.49	0.548	3.61	0.566
	3	85-15	11.11	3.65	0.605	3.65	0.605	3.63	0.602
	4	80-20	14.18	3.64	0.473	3.64	0.473	3.63	0.472
	5	75-25	14.07	3.63	0.476	3.55	0.466	3.63	0.476
	6	70-30	14.52	3.59	0.456	3.59	0.456	3.66	0.465
	7	60-40	15.56	3.59	0.425	3.62	0.430	3.63	0.431
	8	50-50	17.01	3.54	0.384	3.46	0.375	3.60	0.391
3-Pass	9	33-33-33	19.36	3.58	0.341	3.63	0.346	3.61	0.344
	10	40-30-30	16.55	3.63	0.405	3.67	0.409	3.67	0.409
	11	50-30-20	15.18	3.70	0.450	3.69	0.448	3.74	0.455
	12	70-20-10	14.34	3.85	0.495	3.79	0.487	3.77	0.484
	13	60-30-10	15.93	3.80	0.440	3.84	0.444	3.83	0.443
	14	55-30-15	16.40	3.77	0.425	3.81	0.429	3.80	0.428

APPENDIX C-4

No of Passes	No	Tube Pass Ratio	Total Pressure Drop, kPa (Caval. 2-Ph)	Q_t, kW (Shah 2-Ph)	$Q_t/dP.V_r$ (Shah 2-Ph)x10^{-4}	Q_t, kW (Traviss 2-Ph)	$Q_t/dP.V_r$ (Traviss 2-Ph)10^{-4}	Q_t , kW (Dob. & Chato 2-Ph)	$Q_t/dP.V_r$ (Dob. & Chato 2-Ph)10^{-4}
4-Pass	15	25-25-25-25	28.06	3.59	0.236	3.61	0.237	3.61	0.237
	16	45-25-18-12	23.79	3.79	0.294	3.81	0.296	3.81	0.296
	17	40-30-20-10	24.15	3.68	0.281	3.69	0.282	3.72	0.284

APPENDIX D
REFERENCES

[1] U.S. Energy Information Administration. (2009, September). Country Analysis Briefs: Malaysia. [Online]. Available: http://www.eia.doe.gov/emeu/cabs/Malaysia/Full.html

[2] A. Zain-Ahmed. Contemporary Issues in Energy and Buildings in Malaysia: Focus on R&D and Policies, presented at *SENVAR +ISESEE 2008*. [Online]. Available: http://www.scribd.com/doc/13455256/CONTEMPORARY-ISSUES-IN-ENERGY-AND-BUILDINGS-IN-MALAYSIA-FOCUS-ON-RD-AND-POLICIES

[3] L. Perez-Lombard, J. Ortiz, C. Pout, "A Review on Buildings Energy Consumption Information," *Energy & Buildings*, vol. 40, pp. 394-398, 2008

[4] J. H. Wood, G. R. Long, D. F. Morehouse, U.S. Energy Information Administration. (2004, August). Long-term World Oil Supply Scenarios: The Future is neither as Bleak or Rosy as Some Assert. [Online]. Available: http://www.eia.doe.gov/pub/oil_gas/petroleum/feature_articles/2004/worldoilsupply/oilsupply04.html

[5] U.S. Energy Information Administration. (2009, September). NYMEX Futures Prices. [Online]. Available: http://tonto.eia.doe.gov/dnav/pet/pet_pri_fut_s1_d.htm

[6] EUR-Lex. (1992, September). Council Directive 92/75/EEC on the Indication by Labelling and Standard Product Information of the Consumption of Energy and Other Resources by Household Appliances. [Online]. Available: http://eur-lex.europa.eu/LexUriServ/LexUriServ.do?uri=CELEX:31992L0075:EN:NOT

[7] Department of Climate Change and Energy Efficiency, Australia. (2009, October). Requirements for Air Conditioners - Program Overview and Test Procedures. [Online]. Available: http://www.energyrating.gov.au/rac1.html

[8] Asia-Pacific Economic Corporation, Energy Standard Information System. (2010, July). The Hong Kong Mandatory Energy Efficiency Labelling Scheme (EELS) for Room Air-conditioners. [Online]. Available: http://www.apec-esis.org/

[9] Government of Singapore. (2008, January). Environmental Protection and Management Act (Chapter 94A, Section 77), Environmental Protection and Management (Energy Conservation) Regulation. [Online]. Available: http://app2.nea.gov.sg/data/cmsresource/20090316653072840750.pdf

[10] Malaysian Green Technology Corporation. (2010). Energy Rating & Labelling. [Online]. Available:
http://www.ptm.org.my/index.php/energy/energy-efficiency/energy-rating-labelling.html

[11] R. L. Webb, K. Ermis, "Effect of Hydraulic Diameter on Condensation of R-134A in Flat Extruded Aluminium Tubes," *J. Enhancement Heat Trans.*, vol. 8, no. 2, pp.7–90, 2001.

[12] R. L. Webb, H. Lee, "Brazed Aluminum Condensers for Residential Air Conditioning", *J. Enhancement Heat Trans.*, vol. 8, no. 1, pp. 1–13, 2001.

[13] Y. Jiang, S. Garimella, "Compact Air-Coupled and Hydronically Coupled Micro-channel Heat Pumps," *ASME International Mechanical Engineering Congress and Exposition, November 11–16, NewYork, NY, USA*, American Society of Mechanical Engineers, pp. 227–239, 2001.

[14] M. H . Kim, C. W. Bullard, "Performance Evaluation of a Window Room Air Conditioner with Micro-channel Condensers," *J. Energy Resources Tech., Trans. of the ASME,* vol. 124, no. 1, pp. 47-55, 2002.

[15] T. T. Dang, J. T. Teng, J. C. Chu, "A Study on the Simulation and Experiment of a Micro-channel Counter-Flow Heat Exchanger," *Appl. Therm. Eng.*, vol. 30, pp. 2163–2172, 2010.

[16] S. G. Kandlikar, "A Roadmap for Implementing Mini-channel in Refrigeration and Air-Conditioning Systems – Current Status and Future Directions," *Heat Trans. Eng.*, vol. 28, no. 12, pp. 979-985, 2007.

[17] S. G. Kandlikar, W. J. Grande, "Evolution of Micro-channel Flow Passages-Thermohydraulic Performance and Fabrication Technology," *Heat Trans. Eng.*, vol. 24, no. 1, pp. 3-17, 2003.

[18] A. Cavallini, G. Censi, D. D. Col, L. Dorettti, "Experimental Investigation on Condensation Heat Transfer and Pressure Drop of New HFC Refrigerants," *Int. J. Refrig.*, vol. 24, no. 1, pp. 73- 87, 2001.

[19] D. D. Col, S. Bortolin, A. Cavallini, M. Matkovic, "Effect of Cross Sectional Shape during Condensation in a Single Square Mini-Channel," *Int. J. Heat and Mass Trans.*, vol. 54, pp. 3909-3920, 2011.

[20] S. G. Kandlikar, D. Schmitt, A. L. Carrano, J. B. Taylor, "Characterization of Surface Roughness Effects on Pressure Drop in Single-Phase Flow in Mini-channels," *Physics of Fluids* vol. 17, Article no. 100606, 2005.

[21] T. P. Brackbill, S. G. Kandlikar, "Effect of Sawrooth Roughness on Pressure Drop and Turbulent Transition in Micro-channels," *Heat Trans. Eng.,* vol. 28, no. 8-9, pp. 662-669, 2007.

[22] V. Subramaniam, S. Garimella, "Design of Air-Cooled R-410A Micro-chanel Condensers," *ASHRAE Transac.*, vol. 111, no. 1, pp. 471-486, 2005.

[23] C. Y. Yang, R. L. Webb, "Condensation of R-12 in Small Hydraulic Diameter Extruded Aluminum Tubes with and without Micro-Fins," *Int. J. Heat Mass Trans.*, vol. 39, no. 4, pp. 791–800, 1996.

[24] C. Y. Yang, R. L. Webb, "Predictive Model for Condensation in Small Hydraulic Diameter Tubes having Axial Micro-Fins," *J. Heat Trans., Transac. ASME*, vol. 119, no. 4, pp. 776–782, 1997.

[25] N. H. Kim, J. P. Cho, J. O. Kim, B. Youn, "Condensation Heat Transfer of R-22 and R-410A in Flat Aluminum Multi-Channel Tubes with or without Micro-Fins," *Int. J. Refrig.*, vol. 26, no. 7, pp. 830–839, 2003.

[26] T. C. Carnavos, "Cooling Air in Turbulent Flow with Internally Finned Tubes," *Heat Transfer Engineering,* vol. 1, no. 2, pp. 41–46, 1979.

[27] T. C. Carnavos, "Heat Transfer Performance of Internally Finned Tubes in Turbulent Flow," *Heat Transfer Engineering,* vol. 1, no. 4, pp. 32-37, 1980.

[28] W. W. W. Wang, T. D. Radcliff, R. N. Christensen, "A Condensation Heat Transfer Correlation for Millimeter-Scale Tubing with Flow Regime Transition," *Exp. Therm. Fluid Sci.*, vol. 26, no. 5, pp. 473–485, 2002.

[29] S. Koyama, K. Kuwahara, K. Nakashita, K. Yamamoto, "An Experimental Study on Condensation of Refrigerant R134a in Multi-Port Extruded Tube," *Int. J. Refrig.*, vol. 26, no. 4, pp. 425–432, 2003

[30] H. S. Wang, J. W. Rose, "Film Condensation in Horizontal Triangular Section Micro-Channels: A Theoretical Model," *Proceedings of the Second International Conference on Micro-channels and Mini-channels (ICMM2004)*, June 17–19 2004, Rochester, NY, USA, American Society of Mechanical Engineers, NewYork, NY 10016-5990, USA, 661–666, 2004.

[31] H. S. Wang, J. W. Rose, "A Theory of Condensation in Horizontal Non-Circular Micro-channels, *ASME J. Heat Trans.*, vol. 127, no. 10, pp. 1096-1105, 2005.

[32] H. S. Wang, J. W. Rose, H. Honda, "A Theoretical Model of Film Condensation in Square Section Horizontal Micro-channels, *Chem. Eng. Res. Des.*, vol. 82, no. 4, pp. 430–434, 2004.

[33] L. Friedel, "Improved Friction Pressure Drop Correlations for Horizontal and Vertical Two Phase Pipe Flow," *European Two Phase Flow Group Meeting, Ispra, Italy,* paper E2, 1979.

[34] M. Zhang, R. L. Webb, "Correlation of Two-Phase Friction for Refrigerants in Small Diameter Tubes, *Exp. Therm. Fluid Sci.*, vol. 25, no.3–4, pp. 131–139, 2001.

[35] K. Mishima, T. Hibiki, "Some Characteristics of Air–Water Two-Phase Flow in Small Diameter Vertical Tubes, *Int. J. Multiphase Flow*, vol. 22, no. 4, pp. 703–712, 1996.

[36] H. Muller-Steinhagen, K. Heck, "A Simple Friction Pressure Drop Correlation for Two-Phase Flow in Pipes, *Chem. Eng. Proces.*, vol. 20, no.6, pp. 297–308, 1986.

[37] J.S. Shin, M.H. Kim, "An Experimental Study of Flow Condensation Heat Transfer Inside Circular and Rectangular Mini-Channels, *Heat Trans. Eng.*, vol. 26, no. 3, pp. 36–44, 2005.

[38] W. W. Akers, H. A. Deans, O. K. Crosser, "Condensation Heat Transfer within Horizontal Tubes, *Chem. Eng. Prog. Symp. Series*, vol. 55, no. 29, pp. 171–176, 1959.

[39] H. M. Soliman, J. R. Schuster, P. J. Berenson, "A General Heat Transfer Correlation for Annular Flow Condensation, *J. Heat Trans.*, vol. 90, pp. 267–276, 1968

[40] D. P. Traviss, W. M. Rohsenow, A. B. Baron, "Forced-Convection Condensation Inside Tubes: a Heat Transfer Equation for Condenser Design, *ASHRAE Transac.*, vol. 79, no. 1, pp. 157–165, 1973.

[41] A. Cavallini, R. Zecchin, "Dimensionless Correlation for Heat Transfer in Forced Convection Condensation," *Int. Heat Trans. Conf.*, 5th. Proceeding, pp. 309–313, 1974.

[42] M. M. Shah, "A General Correlation for Heat Transfer During Film Condensation Inside Pipes," *Int. J. Heat Mass Trans.*, vol. 22, no. 4, pp. 547–556, 1979.

[43] M. K. Dobson, "Heat Transfer and Flow Regimes during Condensation in Horizontal Tubes," PhD Thesis, Mechanical and Industrial Engineering, University of Illinois at Urbana-Champaign, Urbana-Champaign, IL, 1994.

[44] K. W. Moser, R. L. Webb, B. Na, "A New Equivalent Reynolds Number Model for Condensation in Smooth Tubes," *Transac. ASME, J. Heat Trans.*, vol. 120, no. 2, pp. 410–417, 1998.

[45] H. M. Soliman, "Mist–Annular Transition during Condensation and its Influence on the Heat Transfer Mechanism," *Int. J. Multiphase Flow*, vol. 12, no. 2, pp. 277–288, 1986.

[46] M. S. Chitti, N. K. Anand, "An Analytical Model for Local Heat Transfer Coefficients for Forced Convective Condensation inside Smooth Horizontal Tubes," *Int. J. Heat MassTrans.*, vol. 38, no. 4, pp. 615–627, 1995.

[47] M. S. Chitti, N. K. Anand, "Condensation Heat Transfer inside Smooth Horizontal Tubes for R- 22 and R-32/125 Mixture," *HVAC&R Res.*, vol. 2, no. 1, pp. 79–101, 1996.

[48] Y. Hwang, D. Jin, R. Radermacher, "Refrigerant Distribution in Mini-channel Evaporator Manifolds," *ASHRAE HVAC&R*, vol. 13, no. 4, pp. 543-555, 2007.

[49] W. M. Chin, V. R. Raghavan, "On the Adverse Influence of Higher Statistical Moments of Flow Mal-distribution on the Performance of a Heat Exchanger," *Int. J. Thermal Sciences*, vol. 50, pp. 581-591, 2011.

[50] B. P. Rao, P. K. Kumar, S. K. Das, "Effect of Flow Distribution to the Channels on the Thermal Performance of a Plate Heat Exchanger," *Chem. Eng. and Processing*, vol. 41, no. 1, pp. 49-58, 2002.

[51] R. W. Lockhart, R.C. Martinelli, "Proposed Correlation of Data for Isothermal Two-Phase, Two-Component Flow in Pipes," *Chem. Eng. Prog.*, vol. 45, no. 1, pp. 39–45, 1949.

[52] D. Chisholm, "Pressure Gradients due to Friction during the Flow of Evaporating Two-Phase Mixtures in Smooth Tubes and Channels, *Int. J. Heat Mass Trans.*, vol. 16, no. 2, pp. 347–358, 1973.

[53] L Friedel, "Pressure Drop during Gas/Vapor–Liquid Flow in Pipes," *Int. Chem. Eng.*, vol. 20, no. 3, pp. 352 367, 1980.

[54] D. Chisholm, "A Theoretical Basis for the Lockhart–Martinelli Correlation for Two-Phase Flow," *Int. J.Heat Mass Trans.*, vol. 10, no. 12, pp. 1767–1778, 1967.

[55] C. J. Baroczy, "Systematic Correlation for Two-Phase Pressure Drop," *Chem. Eng. Prog. Symp. Series*, vol. 62, no. 64, pp. 232–249, 1966.

[56] C. J. Baroczy, V. D. Sanders, "Pressure Drop for Flowing Vapors Condensing in Straight Horizontal Tube," *ASME MeetingWA-257*, November 26–December 1 1961, American Society of Mechanical Engineers (ASME), NewYork, NY, USA, 16, 1961.

[57] G. F. Hewitt, G. L. Shires, T. R. Bott, "*Process Heat Transfer,*" *Boca Raton: CRC Press, Begell House*, 1994.

[58] G. Hetsroni, *Handbook of Multiphase Systems, NewYork: Hemisphere*, 1982.

[59] S. Garimella, J. D. Killion, J. W. Coleman, "An Experimentally Validated Model for Two-Phase Pressure Drop in the Intermittent Flow Regime for Circular Micro-channels," *J. Fluid. Eng.*, vol. 124, no. 1, pp. 205–214, 2002.

[60] S. Garimella, J.D. Killion, and J.W. Coleman, "An Experimentally Validated Model for Two-Phase Pressure Drop in the Intermittent Flow Regime for Noncircular Micro-channels," *J. Fluid. Eng.*, vol. 125, no. 5, pp. 887–894, 2003.

[61] S. Garimella, A. Agarwal, J. W. Coleman, "Two-Phase Pressure Drops in the Annular Flow Regime in Circular Micro-channels," *21st IIR International Congress of Refrigeration*, Washington, DC, International Institute of Refrigeration, 2003.

[62] S. Garimella, "Condensation Flow Mechanisms, Pressure Drop and Heat Transfer in Micro-channels," *Micro-scale Heat Transfer Fundamental and Applications*, S. Kakac, L. L.Vasiliev, Y. Bayazitoglu, Y. Yener eds., The Netherlands: Kluwer Academic Publishers, 2005.

[63] S. W. Churchill, "Friction-Factor Equation spans all Fluid-Flow Regimes," *Chem. Eng. Prog.*, vol. 84, no. 24, pp. 91–92, 1977.

[64] E.E. Wilson, "A Basis of Rational Design of Heat Transfer Apparatus," *ASME Journal of Heat Transfer*, vol. 37, pp. 47–70, 1915.

[65] R.B. Williams, D.L. Katz, "Performance of Finned Tubes in Shell and Tube Heat Exchangers," Engineering Research Institute, University of Michigan, 1951.

[66] F. Hasim, M. Yoshida, H. Miyashita, "Compound Heat Transfer Enhancement by a Combination of Ribbed Tubes with Coil inserts," *Journal of Chemical Engineering of Japan,* vol. 36, pp. 647–654, 2003.

[67] F. Hasim, M. Yoshida, H. Miyashita, "Compound Heat Transfer Enhancement by a Combination of a Helically Ribbed Tube with Twisted Tape inserts," *Journal of Chemical Engineering of Japan*, vol. 36, pp. 1116–1122, 2003.

[68] E. H. Young, J. R. Wall, "Development of an Apparatus for the Measurement of Low Bond Resistance in Finned and Bare Duplex Tubing", University of Michigan, Ann Arbor, Report no. 48, 1957.

[69] G. Ribatski, J. R. Thome, "Nucleate Boiling Heat Transfer of R134a on Enhanced Tubes," *Applied Thermal Engineering*, vol. 26, pp. 1018–1031, 2006.

[70] D. E. Briggs, E. H. Young, "Modified Wilson Plot Techniques for Obtaining Heat Transfer Correlation for Shell and Tube Heat Exchangers," *Journal of Heat Transfer*, vol. 5, pp. 51–56, 1969.

[71] H. F. Khartabil, R. N. Christensen, D. E. Richards, "A Modified Wilson Plot Technique for Determining Heat Transfer Correlations," *Proceedings of the Second UK National Conference on Heat Transfer*, vol. 11, pp.1331–1357, 1988.

[72] K. Jambunathan, S. L. Hartle, S. Ashforth-Frost, V. N. Fontama, "Evaluating Convective Heat Transfer Coeffcients using Neural Networks," *International Journal of Heat and Mass Transfer*, vol. 39, no. 11, pp. 2329-2332, 1996.

[73] E. Alvarez, J. M. Correa, C. Riverol, J. M. Navaza, "Model Based in Neural Networks for the Prediction of the Mass Transfer Coefficients in Bubble Columns-Study in Newtonian and Non-Newtonian Fluids," *International Communications of Heat and Mass Transfer*, vol. 27, no. 1, pp. 93-98, 2000.

[74] A. Mazzola, "Integrating Artificial Neural Networks and Empirical Correlations for the Prediction of Water-Subcooled Critical Heat Flux," *Revue Generale de Thermique*, vol. 36, no. 11, pp. 799-806, 1997.

[75] M. M. Fowler, D. E. Klett, J. B. Moreno, P. D. Heermann, "Using Articial Neural Networks to Predict the Performance of a Liquid Sodium Reflux Pool Boiler Solar Receiver," in *Proceedings of the International Solar Energy Conference*, pp. 93-104, 1997.

[76] S.A. Kalogirou, S. Panteliou, A. Dentsoras, "Artificial Neural Networks used for the Performance Prediction of a Thermosyphon Solar Water Heater," *Renewable Energy*, vol. 18, no. 1, pp. 87-99, 1999.

[77] S. I. Mistry, S. S. Nair, "Nonlinear HVAC Computations using Artificial Neural Networks," *ASHRAE Transactions*, vol. 99, part 1, pp. 775-784, 1993.

[78] X. Zhao, "Performance of a Single-Row Heat Exchanger at Low In-Tube Flow Rates," M.S. Thesis, *Department of Aerospace and Mechanical Engineering, University of Notre Dame*, Notre Dame, Indiana, 1995.

[79] G. Diaz, M. Sen, K. T. Yang, R. L. McClain, "Simulation of Heat Exchanger Performance by Artificial Neural Networks," *International Journal of HVAC & R Research*, vol. 5, no. 3, pp. 195-208, 1999.

[80] E. Jeannette, K. Assawamartbunlue, P. S. Curtiss, J. F. Kreider, "Experimental Results of a Predictive Neural Network HVAC controller," *ASHRAE Transactions*, vol. 104, part 2, pp. 192-197, 1998.

[81] G. Diaz, "Simulation and Control of Heat Exchangers Using Artificial Neural Networks," Ph.D. Thesis, *Department of Aerospace and Mechanical Engineering, University of Notre Dame*, Notre Dame, Indiana, 2000.

[82] J. von Wolfersdorf, E. Achermann, B. Weigand, "Shape Optimization of Cooling Channels using Genetic Algorithms," *Journal of Heat Transfer*, vol. 119, no. 2, pp. 380-388, 1997.

[83] G. Fabbri, "A Genetic Algorithm for Fin Profile Optimization," *International Journal of Heat and Mass Transfer*, vol. 40, no. 9, pp. 2165-2172, 1997.

[84] A. Castrogiovanni, P. M. Sforza, "A Genetic Algorithm Model for High Heat Flux Flow Boiling," *Experimental Thermal and Fluid Science*, vol. 15, no. 3, pp. 193-201, 1997.

[85] M. Raudensky, K. A. Woodbury, T. Brezina, "Genetic Algorithm in Solution of Inverse Heat Conduction Problems," *Numerical Heat Transfer. Part B, Fundamentals*, vol. 28, no. 3, pp. 293-306, 1995.

[86] K. Okamoto, D. Tsuru, M. Fumizawa, "Reconstruction of Three Dimensional Density Distribution from the Limited Projection Images with Genetic Algorithm," *Journal of Flow Visualization and Image Processing*, vol. 3, no. 4, pp. 253-263, 1996.

[87] H. Y. Li, C. Y. Yang, "A Genetic Algorithm for Inverse Radiation Problems," *International Journal of Heat and Mass Transfer*, vol. 40, no. 7, pp 1545-1549, 1997.

[88] R. V. Davalos, B. Rubinsky, "An Evolutionary-Genetic Approach to Heat Transfer Analysis," *Journal of Heat Transfer*, vol. 118, no. 3, pp. 528-531, 1996.

[89] T. S. Schmit, A. K. Dhin gra, F. L andis, G. Kojasoy, "A Genetic Algorithm Optimization Technique for Compact High Intensity Cooler Design," *Journal of Enhanced Heat Transfer*, vol. 3, no. 4, pp. 281-290, 1996.

[90] M. C. Tayal, Y. Fu, U. M. Diwekar, "Optimal Design of Heat Exchangers: A Genetic Algorithm Framework," *Industrial and Engineering Chemistry Research*, vol. 38, no. 2, pp. 456-467, 1999.

[91] P. V. Arturo, S. Mihir, K.T. Yang, "Simultaneous Determination of In- and Over-Tube Heat Transfer Correlations in Heat Exchangers by Global Regression," *Int J. Heat and Mass Transfer*, vol. 46, pp. 1029-1040, 2003.

[92] *Standard Method for Temperature Measurement*, ANSI/ASHRAE 41.1-1986 (RA 2006), 2006.

[93] *Methods of Testing Forced Circulation Air Cooling and Air Heating Coils*, ASHRAE 33-2000, 2000.

[94] *Methods of Testing for Rating Heat-Operated Unitary Air-conditioning Equipment for Cooling*, ANSI/ASHRAE 40-2002, 2002.

[95] *Methods of Testing for Rating Unitary Air Conditioning & Heat Pump Equipment*, ANSI/ASHRAE 37-2009, 2009.

[96] V. Subramaniam, "Design of Air-Cooled Micro-channel Condensers for Mal-distributed Air Flow Conditions", *Georgia Institute of Technology*, pp.15-55, 2004.

[97] M. S. Bhatti, R. K. Shah, "Turbulent and Transition Flow Convective Heat Transfer in Ducts Handbook of Single Phase Convective Heat Transfer," *S. Kakac, R.K. Shah and W. Aung, Wiley-Interscience*, 4.1-4.166, 1987.

[98] H. F. P. Purday, "An Introduction to the Mechanics of Viscous Flow, Film Lubrication, the Flow of Heat by Conduction and Heat Transfer by Convection", New York, Dover, 1949.

[99] N. M. Natarajan, Lakshmanan (1972), "Laminar Flow in Rectangular Ducts: Prediction of Velocity Profiles and Friction Factor," *Indian Journal of Technology*, 10(12): 435-438

[100] M. K. Dobson, J. C. Chato, "Condensation in Smooth Horizontal Tubes," *J. Heat Trans., Transac. ASME*, vol. 120, no. 1, pp. 193–213, 1998.

[101] R. K. Shah, A. L. London, "Laminar Flow Forced Convection in Ducts: A Source Book for Compact Heat Exchanger Analytical Data." *New York, Academic Press*, 1978.

[102] D. Butterworth, "A Comparison of some Void-Fraction Relationships for Co-Current Gas-Liquid Flow," *International Journal of Multiphase Flow*, vol. 1, no. 6, pp. 845-50, 1975.

[103] A. Cavallini, G. Censi, D. Del Col, L. Doretti, G.A. Longo, L. Rossetto, "Condensation of Halogenated Refrigerants inside Smooth Tubes," *HVAC and R Research*, vol. 8, no. 4, pp. 429–451, 2002.

[104] A. Cavallini, G. Censi, D. Del Col, L. Doretti, G. A. Longo, L. Rossetto, G. D. Mathur, "In-Tube Condensation of Halogenated Refrigerants," *2002 ASHRAE Winter Meeting*, January 13–16 2002, Atlantic City, NJ, Amer. Soc. Heating, Ref. Air-Conditioning Eng. Inc., 146–161, 2002.

LIST OF PUBLICATIONS

Journal paper

[1] K. K. Thoo, W. M. Chin, R. H. Morgan, "Determination of Air Side Heat Transfer Coefficient in a Mini-Channel Heat Exchanger using Wilson Plot Method," *International Conference on Mechanical Engineering Research 2013*, Gambang, Kuantan, Pahang, 1-3 July 2013, indexed by Scopus, to be published by IOP Conference series: Material Science & Engineering Journal.

Conference paper

[1] K. K. Thoo, W. M. Chin, R. H. Morgan, "Effect of Tube Pass Ratios and Flow Pass Configurations on the Thermal and Hydraulic Performance of the Aluminium Mini-Channel Heat Exchanger," *Annual Postgraduate Conference 2013, University Teknologi Petronas.*